

SEISMIC CHARACTERIZATION OF FRACTURED ROCK FABRIC IN  
MISSISSIPPIAN LIMESTONE, PAYNE COUNTY OKLAHOMA

By

ROBERT HOLMAN

Bachelor of Science in Geology

Brigham Young University-Idaho

Rexburg, Idaho

2011

Submitted to the Faculty of the  
Graduate College of the  
Oklahoma State University  
in partial fulfillment of  
the requirements for  
the Degree of  
MASTER OF SCIENCE  
August, 2014

SEISMIC CHARACTERIZATION OF FRACTURED ROCK FABRIC IN  
MISSISSIPPIAN LIMESTONE, PAYNE COUNTY OKLAHOMA

Thesis Approved:

Dr. Priyank Jaiswal

---

Thesis Adviser

Dr. Michael Grammer

---

Dr. James Puckette

---

Name: ROBERT HOLMAN

Date of Degree: AUGUST, 2014

Title of Study: SEISMIC CHARACTERIZATION OF FRACTURED ROCK FABRIC IN MISSISSIPPIAN LIMESTONE, PAYNE COUNTY OKLAHOMA

Major Field: GEOLOGY

Abstract

Fractures are pre-existing planes of weaknesses. They play a critical role in determining the production potential of reservoirs that are developed through lateral drilling and fracture stimulation, such as the Mid-Continent Mississippian limestone. Estimation of fracture density using geophysical methods, such as seismic, is desirable, but extremely challenging at the same time. Conventionally, a single seismic attribute such as amplitude or coherency has been proxy for fractures with limited success. This thesis demonstrates that multiple seismic attributes can be combined using statistical methods to yield a reliable fracture density map.

## TABLE OF CONTENTS

Chapter	Page
I. INTRODUCTION .....	1
II. BACKGROUND.....	5
2.1: Study Area.....	5
2.2: Dataset description .....	7
2.2.1: Seismic .....	7
2.2.2: Well Logs .....	8
III. METHODOLOGY .....	10
3.1: Well to seismic tie.....	10
3.2: Geostatistical Modeling .....	12
3.3: Wedge Modeling.....	16
3.4: Seismic Attributes .....	16
3.5: Cluster Analysis .....	18
3.6: Multivariate Non-linear Regression.....	19
IV. APPLICATION AND RESULTS .....	21
4.1: Well to seismic tie.....	21
4.2: Geostatistics .....	22
4.2.1: Depth conversion.....	23
4.2.2: Isopach.....	24
4.3: Wedge Modeling.....	26
4.4: Attributes.....	28
4.4.1: Instantaneous Amplitude.....	28
4.4.2: Instantaneous Frequency .....	29
4.4.3: Curvature .....	30
4.4.4: Coherency.....	31

Chapter	Page
4.5: Clustering and classification .....	32
4.5.1 Horizontal Classification .....	32
4.5.2: Vertical Classification .....	33
4.6: Fracture density prediction from Multivariate Non-Linear Regression.....	35
V. DISCUSSION .....	38
5.1: Fracture Density Prediction.....	38
5.2: Multivariate Non-Linear Regression .....	40
5.3: Cluster analysis .....	42
5.4: Seismic Attributes .....	43
5.5: Kriging and Cokriging .....	45
5.6: Synthetic Seismogram.....	47
5.7: Acquisition/Processing.....	47
5.7: Play types .....	49
IV. CONCLUSION.....	51
6.1: Recommendations .....	53
LIST OF TABLES .....	61
LIST OF FIGURES .....	62
APPENDIX A: SEISMIC ACQUISITION .....	111
APPENDIX B: SURVEY MISTIES .....	113
APPENDIX C: DETUNING AMPLITUDES .....	116
APPENDIX D: MCMURTRY 1-22H VALIDATION .....	121

## LIST OF TABLES

Table	Page
1: Attribute cross correlation Table .....	61

## LIST OF FIGURES

Figure	Page
1: Mississippian Play .....	62
2: Paleogeography during the Mississippian .....	63
3: Base map.....	64
4: Stratigraphic column.....	65
5: Frequency spectrum for the LMM (a), LCBm (b) and LCB (c) surveys.....	66
6: The LMM survey fold map.....	67
7: The LCBm survey fold map .....	68
8: The LCB survey fold map .....	69
9: Well log interpretation.....	70
10: Fracture density from Blair 1-24H 1-24H FMI.....	71
11: Ruark 1-29 SWD well synthetic seismogram.....	71
12: Geostatistical mapping cartoon.....	72
13: Kriging and cokriging flow chart.....	73
14: Wedge model response .....	74
15: Well to seismic tie at Ruark location .....	75
16: Synthetic tie to seismic .....	76
17: Mississippian time surface.....	77
18: Geostatistical models .....	78
19: Subsea depth structure maps.....	79
20: Model validation-structure.....	80
21: Cross plot-Mississippian top time-vs-depth .....	81
22: Semivariogram model for kriging isopach .....	82
23: Mississippian isopach map .....	83
24: Model validation-isopach .....	84
25: Mississippian isopach-vs-isochron .....	85
26: LCB frequency and wavelet .....	86
27: Mississippian wedge model in depth.....	87
28: Mississippian wedge model in time.....	88
29: Instantaneous amplitude attribute map .....	89
30: Instantaneous frequency attribute map .....	90
31: Positive curvature attribute map .....	91
32: Negative curvature attribute map.....	92
33: Combined positive and negative curvature attribute map .....	93
34: Coherency attribute map.....	94
35: Cross plot- amplitude-vs-negative curvature.....	95
36: Horizontal classification map .....	96

Figure	Page
37: Volume prism .....	97
38: Vertical classification .....	98
39: Mississippian depth structure map on the LMM survey.....	99
40: FMI upscaling techniques.....	100
41: Blair 1-24H multivariate model inputs .....	101
42: Blair 1-24H multivariate model output.....	102
43: Blair 1-24H fracture density comparison: along-trajectory view .....	103
44: Dip projection .....	104
45: Blair 1-24H fracture density re-comparison: along-trajectory view.....	105
46: Predicted fracture density map at the Mississippian Top .....	106
47: McMurtry 1-21H fracture density comparison: along-trajectory .....	107
48: McMurtry 1-21H fracture density re-comparison: along-trajectory.....	108
49: Lake acquisition seismic line.....	109
50: Lady Fern analog. ....	110
A 1: LCB Acquisition setup.....	111
A 2: LCB nearest offset map .....	112
B 1: Mistie analysis of the LCBm to LCB.....	114
B 2: Mistie analysis of the LCBm to LMM.....	115
C 1: LCB amplitude map .....	117
C 2: Cross plot isopach and amplitude (a) Tuned, (b) Detuned method and (c) Detuned model .....	119
C 3: Detuned amplitudes.....	120
D 1: McMurtry 1-22H fracture density comparison: along-trajectory .....	122
D 2: McMurtry 1-22H fracture density re-comparison: along-trajectory.....	122



## CHAPTER I

### INTRODUCTION

The Mississippian age limestone, with an estimated 8 billion barrels of oil equivalent in-place, extends from present day northern Oklahoma to southern Kansas and presents approximately 30 million acres for potential drilling and resource development within the Anadarko Basin (Redden 2013, Durham, 2013) (Figure 1). The Mississippian play is attractive due to a high ultimate recovery (EUR) potential at relatively low drilling costs. For example, the cost of a typical well in the Mississippian, spud to completion, is ~\$3.5 million (Redden, 2013), which is significantly less than comparable wells in other unconventional plays such as the Bakken in North Dakota, where a typical well costs ~\$11 million (Redden, 2013).

MS Sandridge Inc, who holds the maximum acreage (~1.7 million acres) in the Mississippian play, estimated ~204,000 barrels of crude oil and ~1.5 billion cubic feet (bcf) EUR for their individual wells in 2012 making the overall EUR for their drilling program as ~456 million barrels of oil equivalent (Pickett,2012). At a nominal price of \$85 per barrel of crude oil and \$3 per thousand cubic feet (mcf) of gas, a typical well was estimated to have ~500% return. However, it is common knowledge that not every well completed in the Mississippian limestone is economic. The complex reservoir architecture and drilling challenges typical of a carbonate play determine the rate of economic returns for a given well or project. A general consensus among operators, is that the poor understanding of depositional facies and inadequately constrained rock-properties make the Mississippian play a high-risk, high-return venture, and one in which being able to predict the rock fabric ahead of the drill bit appear to be the key to

economic success.

Traditionally the Mississippian play was developed through vertical drilling which targeted the highly altered zones with 35-48% secondary porosity (Matson, 2013). Outside the altered zone, the hydrocarbon drainage area for a typical vertical well averages less than 15 acres (Dick, 2011). Poor volumetrics or the amount of reservoir drainage per well is the result of the extremely low permeability of the host rock. The highly productive target interval within the Mississippian unit, commonly known as the “chat” (or formally as the tripolite), is a thin siliceous zone close to the top of the unit drilled in Kansas (Mazzullo, 2009). Other targets within the formation include cherty and spiculitic intervals with relatively lower porosity being 5%-21% (Mazzullo, 2009).

With the advent of horizontal drilling and hydraulic fracturing, it is now possible not only to tap multiple zones of secondary porosity with a single well but also induce new fractures in the host rock to enhance its permeability. Mississippian intervals that were once not prospective, with only 2-5% porosity, can now be hydraulically stimulated to increase permeability around the wellbore, thereby improving the economic returns of the well (Matson, 2013). However, multitude development challenges still remain, even with horizontal drilling, mainly due to the rapidly varying reservoir properties such as permeability, porosity, water saturation and the lack of reliable a-priori information on the reservoir rock fabric prior to the well placement (Durham, 2013). The most critical factor in determining the effectiveness of the hydraulic stimulation process are the pre-existing fracture planes that serve as stress guides. The orientation and density of fracture can severely affect the fate of fracking. As present, there are no surface geophysical tools that can reliably image fracture density in carbonate reservoirs.

Paleogeographic information such as deposition environment and facies architecture of the Mississippian reservoir (Rogers, 2001) is known through well control. For example, it is known that the Mississippian carbonates vary in thickness from 200-300 ft, but are locally absent where removed by erosion (Clarke, 1963). However, well information is relatively sparse compared to rock volume and one-

dimensional (1D) in nature, which limits the interpretation of Mississippian reservoir architecture and quality (mineralogy, fluid type and saturation, porosity, permeability, etc.). Information from wells, such as rock properties, can be in principle, extrapolated in three-dimensional (3D) using high-resolution seismic data provided the seismic volume is properly calibrated to wells (Mitchum, 1977). Such seismic-to-rock-property transforms have been routinely done in clean sandstones (Sharma, 2013; Fatti, 1994; Quijada, 2007; Soubotcheva, 2005). In carbonates such, applications remain fairly uncommon. Possible reasons include the high velocity of carbonates, which does not allow for a large move-out, sharp velocity contrast from rapidly changing facies that violate ray hyperbolic assumption, and high impedance contrast across the top and base of the formation that overshadows subtle amplitude changes related to fracturing and diagenetic alterations.

A multitude of challenges in seismic application in carbonate settings often call for creative solutions. The most generic use of seismic data is in mapping structures which typically reveal only large-scale plays (circa 1930-1960). More subtle plays are often detected using an attribute i.e, properties related to arrival times, amplitudes, frequency, etc., of the seismic data. Examples include Mukerji (1998) integrating elastic velocity ratio into rock physics models to map lithofacies and pore fluid in an alternating sand-shale turbidite facies; Hasanusi (2007) using sparse-spike inversion of acoustic impedance to create facies and porosity maps in the Tiaka carbonate reservoir in Sulawesi, Indonesia; Harilal (2006) using well-log based relation between porosity and seismic impedance to identify reservoir faces within a mixed carbonate-siliciclastic sequence in Bombay offshore basin, India; Wang (2008) developing a local relationship between porosity and inverted Lames' constants to show that high porosity intervals are likely associated with karst features; Mitchell (2009) using the "negative curvature" and "similarity" attributes in the Ellenburger Formation immediately underlying the Barnett Shale in Texas to identify fluid conduit hazards; and Ogiesoba (2014) showing that the curvature attribute could be illuminating faults and fractures that are associated with producing zones within the Austin Chalk Formation.

In the case of Mid-Continent Mississippian carbonate plays, the key to a successful well development is being able to predict zones of high permeability, which in turn are generally related to high fracture density. In this thesis, multiple attributes from a 3D seismic volume are combined to create a fracture density map in a series of sequential steps. The first step was to tie the volume to a well located within the survey using synthetic seismograms to identify geological horizons in the seismic volume. Next, the Mississippian time horizon was interpreted and converted to depth. In this case, since the processing velocities may not adequately represent the heterogeneous nature of the overburden sediments, instead of depth migration geostatistical methods were used to generate the “Mississippian top” depth map and an isopach map. The next step involved identifying potential biases in the seismic data that may cause attributes to not be representative of the reservoir characteristics. After identifying the biases an appropriate location for attribute extraction was chosen and a multitude of extracted attributes were combined using non-linear regression to generate a fracture density map. Finally, the map was validated using existing Fracture Microimage (FMI) logs. As a dual goal, after identifying the biases in the data the attributes were translated to geomorphological features by cluster analysis.

## CHAPTER II

### BACKGROUND

#### *2.1: Study Area*

During the Mississippian subsystem, which spans from 356 to 318 Ma, present day Oklahoma and Kansas were situated close to the equator (Figure 2). Extensive Mississippian carbonate sediment were deposited, resulting in a large volume of mostly limestone is stratigraphically above the Devonian-Mississippian Woodford Shale (Elebiju, 2011; Rogers, 2001). Mississippian carbonate deposition ended with a period of uplift and erosion in the late Mississippian with collision between Gondwana with Euramerica, which began to build the Appalachian and Variscan Mountains. Base level changes due to both higher-order eustatics and tectonism controlled the depositional patterns as well as sediment types in the Mississippian, which resulted in section that ranges from chert- to limestone dominated. Finally the Pennsylvanian transgression enveloped the carbonate shelf and the Mississippian carbonates were succeeded by a shale-dominated interval. The Pennsylvanian shale forms the regional seal for the Mississippian petroleum system. Extensive erosion preceded Pennsylvanian deposition and the Mississippian – Pennsylvanian contact is marked by a regional scale unconformity.

Significant to the Mississippian play is the late Mississippian or early Pennsylvanian Nemaha Uplift in central of Oklahoma, which created favorable traps (Dolton, 1989). The Nemaha Ridge, which is of particular relevance to this thesis, is a result of episodic right-lateral, transpressional stress which initiated in the Middle Ordovician during the Taconic orogeny and continued through the mid-Cretaceous (Burchett, 1985; McBee, 2003). The resulting strike-slip movement ultimately resulted in pop-horst

blocks and pull-apart grabens (Crowell, 1974), that locally controlled the Mississippian reservoir architecture. Fault surfaces associated with the Nemaha Ridge can be near vertical with some segments displaying reversed throw such as the Garber structure in Garfield County, Oklahoma (McBee, 2003). These deep seated faults also serve as fluid migration pathways (Gregg, 2012; Garven, 1995).

This study area is located in Payne County, Oklahoma (Figure 3). A generalized stratigraphic column shows the formations within the study area (Figure 4). The Mississippian play unconformably resides atop the black, organic-rich shale Woodford Shale, which is also the main source rock for the Mississippian petroleum systems (Ball, 1991; Remero, 2012). Woodford sediment was deposited in the Late Devonian Early Mississippian (Johnson, 1995) in a mostly anoxic, deep water environment (Kirkland, 1992). Total organic carbon (TOC) in the Woodford is fairly high (5-14%; Romero, 2012). The hydrogen (HI) and oxygen (OI) indices further suggest that the kerogen in the Woodford Shale is Type II, i.e., it is marine sourced. It is commonly accepted that the Woodford Shale hydrocarbon generation and up-dip migration to the north occurred during the late Triassic within the Anadarko and Arkoma basins (Cardott, 2012).

The structure of the Mississippian reservoir is complex. Uplift associated with Nemaha Ridge created low-lying, fault-blocked mountain ranges that caused thinning on horst blocks and preservation in grabens of Mississippian strata (Johnson, 1995). Along the flanks of the uplift, reworked Mississippian strata can create pinch-outs. At present, the Mississippian thickness varies from absent on upthrown fault blocks, to an average of 250 feet on downthrown fault blocks (Shelton, 1985). The later-stage Mississippian uplift also created the primary reservoirs. The Osagean cherty limestone underwent diagenesis during this period forming tripolite, which is a facies with high secondary porosity but low permeability (Roger 2001), forming an ideal target for fracking. In the well logs, the tripolitic facies can be identified by low resistivity and low density within the background tight, nonporous chert (Elebiju, 2011). The thick marine or deltaic shale interfingering with sandstone, limestone, and coals of the Pennsylvanian (Johnson, 1995), serve as the seal for the Mississippian petroleum systems.

It is notable that in Payne County the Mississippian carbonate is locally absent on structural anticlines responsible for oil fields such as the Cushing Field (it's western flank is in eastern Payne County), the Ramsey field and the Orlando field (Shelton, 1985). Traps in the study area were most likely charged by the underlying Woodford Shale (Shelton, 1985). In northwestern Payne County an east-west striking fault, downthrown to the north has been documented in association with the Nemaha Ridge (Gay, 2003). The surface expression of the fault is hidden by the present day Lake Carl Blackwell. Thus, the study area has strong hydrocarbon potential in the Mississippian play with plausibility charging from the Woodford Shale, structural and stratigraphic traps created by the Nemaha Ridge system, and sealing by Pennsylvanian shale.

## *2.2: Dataset description*

In this thesis, three 3D seismic volumes (courtesy of Red Fork Energy) were analyzed with the help of three well-logs (one vertical and two lateral; Figure 3). The seismic volumes are hereafter referred to as the Lake Carl Blackwell (LBC; red fill; Figure 3), Lake Carl Blackwell mini (LCBm; orange fill; Figure 3), and Lake McMurry (LMM; green fill; Figure 3) survey. The seismic surveys cover portions of northwestern Payne County and southern Noble County around Lake Carl Blackwell and Lake McMurry.

### *2.2.1: Seismic*

Three different types of source were used in the seismic surveys depending on the terrain, they include vibroseis and dynamite on the land and airgun in the lake. The vibroseis sources were IVI type and simultaneously performed 4 linear 10 – 100 Hz sweeps each 12s long with a start and end taper of .3s and a peak ground force of 70% of the weight of the vibroseis. Vibroseis source parameters for this shoot deliberately filter out frequencies lower than 10Hz to reduce source created noise such as the ground roll (Martin, 1994). In areas that were inaccessible to the vibroseis, 2.2lbs of dynamite placed in 40 feet holes were used as sources. For the water portion of the survey, an airgun source was used with hydrophones placed across the bottom of the lake. A mixture of source types presents potential challenges in

normalizing the data amplitude spectrum in processing, which can potentially interfere with interpretation of data-derived attributes.

In all the surveys, the receiver type used was a SM24 10Hz resonance frequency geophone. This particular type of geophone only recorded vertical ground motion and field filters frequencies less than 10Hz. The purpose of this design is to reduce low frequency noise created by movement of both the suspended mass and the geophone housing during recording. The suspended mass and geophone housing move in tandem when velocities lower than resonance frequency arrive at the geophone, resulting in noisy field records. For frequencies above 10Hz, the mass remains stationary while the housing moves, decreasing the noise (Dams, 2009).

In the LCB survey the receiver lines were spaced 660 feet apart, and oriented east-west with individual channels (group of geophones) at a 220 foot interval. The source line spacing was 1,320 feet with individual sources being fired at 220 foot intervals. In the LMM survey the receiver lines were spaced 880 feet apart, they were orientated EW with individual channels (group of geophones) at a 220 foot interval. The source line spacing was 1,760 feet with individual sources being fired at every 220 foot intervals. The source lines for these two surveys were orientated diagonally (45°; NE-SW) to the receiver line to reduce acquisition footprint. Dominant frequency in the LMM is approximately 50Hz (Figure 5a), LCBm 40Hz (Figure 5b) and LCB 55Hz (Figure 5c). The maximum fold in the LMM survey was 91 (Figure 6), LCBm 70 (Figure 7), and LCB 47 (Figure 8) (Appendix A).

### *2.2.2: Well Logs*

The study area contained one vertical well, the Ruark salt water disposal (SWD), in the LCBm survey. The well was logged with sonic, density, gamma-ray and resistivity logs. A vertical well calibrates seismic data by helping identify the corresponding depth markers of a horizon in the 3D volume. A nominal procedure for tying the well logs to seismic data was followed. Ruark well data were first interpreted for the key geological horizons (Figure 9). Identifying the Mississippian unit in the Ruark



well was straightforward as the expected signature of a limestone that is underlain and succeeded by shale. Mississippian carbonates have a low gamma-ray (15-50 API) signature, higher density (2.55-2.73 g/cc) and low transit time (50-60 usec/ft). For comparison, the underlying Woodford Shale radioactive with a high gamma-ray value (>300 API), lower density (2.49-2.51 g/cc) and longer transit time (80-90 usec/ft). The Pennsylvanian section is mostly shale and similar to Woodford Shale, except that Pennsylvanian shale gamma-ray values are lower (90-105 API). In the study area, Mississippian top depths were also available from 350 other wells of older vintages. These wells were logged but were not useful for calibrating seismic parameters, however well top information was suitable for geostatistics.

The study area also contained two lateral wells, the Blair 1-24H and McMurtry 1-21H. These wells in the LMM survey were logged using Fracture Microimager (FMI) equipment (Figure 10). A FMI log is a high-definition wireline resistivity imaging tool (Ekstrom, 1987), with a vertical resolution of 0.2", vertical sampling 0.1" and depth of investigation of 30" (Gaillot, 2007). Once processed, the resistivity measurements create a 360° electric image of the borehole highlighting variations in mineralogy, porosity, and fluid content. These electrical images are then interpreted to relate information about rock fabric such as fractures, karstic carbonates, and laminated sandstone/shale sequences (Gaillot, 2007). In this study, the FMI logs were interpreted for dip, azimuth, and fracture density (personal communication, Miller, 2014).

## CHAPTER III

### METHODOLOGY

#### *3.1: Well to seismic tie*

Although the seismic methods are capable of imaging spatial variability in the subsurface, the reconstructed physical properties are actually an average over a finite volume (the Fresnel's volume). The lower the dominant frequency, the larger is the volume. In a typical survey where the dominant frequency ( $f$ ) ranges from 30 – 80 Hz, the resolution, which is  $\frac{1}{4}$  of the dominant wavelength ( $\lambda$ ), varies from 5 – 50 m depending on the formation velocity ( $v = \lambda * f$ ). For example, in the Mississippian carbonate play, where the average interval velocity is 4.5 km/s and dominant seismic frequency is 60 Hz, the maximum expected vertical resolution is 18.75m. Although this resolution is low, it is notable that it is being achieved by sources and receivers at the surface which is ~3500m above the target horizons. The other end of the spectrum is imaging through well logs where the dominant frequency is in the MHz range, the spatial resolution is 6 inches, but investigation is also within 10 inches of the borehole making the information essentially 1D.

To obtain 2D and 3D information on the reservoir architecture, log data have to be reconciled with seismic after which the interpretation is extended outwards from the borehole. Reconciling well and seismic data is a multi-step process and involves several simplistic assumptions. The foremost is the convolution model which assumes that a seismic trace is a convolution between the source wavelet and the reflectivity series (Yilmaz, 1987). The second assumption is the stationary nature of the source wavelet, i.e., the wavelet does not change its frequency spectrum in time. Third, the seismic trace only

comprises primary reflections, i.e., no multiples or mode-converted energy. Fourth, the noise is random and is weaker than the strength of the weakest reflection of interest; and finally, that the raypaths are vertical (Yilmaz, 1987).

The first step in reconciling well and seismic data is to generate a reflectivity series using the sonic and density logs (Figure 11). The reflectivity coefficient ( $R_0$ ) corresponding to the interface between any two rock units is determined from their impedance contrast, impedance being the product of velocity ( $v$ ) and/or density ( $\rho$ ).

$$R_0 = \frac{(\rho_2 v_2 - \rho_1 v_1)}{(\rho_2 v_2 + \rho_1 v_1)} \quad (1)$$

In Equation 1 (Sheriff, 1982) subscripts 1 and 2 respectively represent the over- and underlying layer. It follows from Equation 1 that greater impedance differences between the layers will generate a higher reflectivity. In the case of the Ruark well, the Mississippian carbonate reservoir has an  $\rho$  of 2.64 g/cc and  $v$  of 17000 ft/sec, which equates to an acoustic impedance (AI) of 44880 g·ft/cm<sup>3</sup>·sec. In comparison, the underlying Woodford Shale has  $\rho$  of 2.5 g/cc and  $v$  of 12500 ft/sec yielding an AI of 31250 g·ft/cm<sup>3</sup>·sec. The  $R_0$  for the Mississippian base is -0.179. The standard convention in seismic displays is to have a trough for a negative reflection coefficient and peak for a positive. As a result, the Mississippian top appears as a peak in the seismic volume and the Mississippian-Woodford interface appears as a trough.

The strength of the individual reflectivity coefficients in the reflectivity series depend on lithologies samples by the well log. Well log data has a relatively high sample rate of .5 ft in comparison to seismic vertical resolution. Calculating reflectivity coefficients at well log resolution is not necessary. The interpreter can choose to upscale the log such that it contains reflections corresponding to only the key formations under investigation. The upscaled reflectivity series is then convolved with a wavelet which is representative of the seismic source. In the land survey, it is difficult to record the source wavelet. As a result the convolution wavelet can be synthetically generated as a “best guess” by using a Butterworth or Ormsby wavelet or, as in this study, extracted from the seismic volume near the wellbore.

If the seismic data are properly processed using correct interval velocities, it is expected that the synthetic trace from convolution will show a good visual correlation with the seismic trace at the well location. When the correlation is not apparent, a match can be achieved in an interpretive manner by “stretching” and “squeezing” the individual wavelets in the seismic trace and/or bulk shifting it. The matching process modifies the time-depth relationship (velocity) at the wellbore. A quality control step is to ensure that the velocity remains generally increasing with depth. Once completed, a time-depth chart can be used to determine which horizons in the seismic volume correspond to which formation tops/bases interpreted in the log. Relevant horizons can then be propagated in the seismic volume outwards from the wellbore.

### *3.2: Geostatistical Modeling*

The biggest challenge in depth-converting a seismic horizon interpreted in time is availability of an accurate interval velocity model. In rather homogenous layer-cake geology, stacking velocity analysis can yield reasonable interval velocities. In more complex environments, tomographic methods using long offset data have to be used (Woodward, 2008). In absence of long-offset data, but with the presence of a large number of wells, such as this dataset, a statistical relationship between time and depth can be defined with variography without actually estimating a velocity model. The statistical approach, generally referred to as geostatistics, has been successfully applied in many reservoirs throughout the world (Abrahamsen, 1996; Olabode, 2008; Clapgood, 2011).

The underlying assumption of variography is that variation in data between a location pair is dependent on their mutual separation rather than their spatial location (Figure 12). Generally, variation in data between any two data-pairs increases as the separation between the pairs, referred to as the lag, increases. A model that describes variation for all possible data pairs in a given dataset with respect to lag is known as a variogram. The process of interpolating or extrapolating data using a variogram is known as kriging. In the study area, besides the Ruark SWD, the Mississippian tops have been interpreted at 350 other location in wells of different exploration vintages. The numbers of data points representing the

contact between the Pennsylvanian and Mississippian strata are adequate to estimate a continuous “Mississippian Top” depth surface in the study area through Kriging.

The first step in interpolation through variography or Kriging is to construct a semivariogram by computing variance,  $\gamma$ , as a function of lag as follows:

$$\gamma(s_i, s_j) = \frac{1}{2} * \text{var}(Z(s_i) - Z(s_j))^2 \quad (3)$$

Where  $s$  is the data to be interpolated,  $s_i$  and  $s_j$  are data at two locations, and  $Z$  is their magnitude. When  $s_i$  and  $s_j$  are closer,  $Z(s_i)-Z(s_j)$  is smaller. As the spatial location of  $s_i$  and  $s_j$  increases, they become less similar, thus the difference in their values,  $Z(s_i)-Z(s_j)$ , will become larger. A plot of  $\gamma$  with respect to the lag generally creates an arcuate shaped point-cloud; the best fit line to this point cloud is the model used for data prediction, e.g., prediction of “Mississippian Top” depth surface in between the well locations. Besides being the best fit, the other model character includes nugget, range, and sill. The nugget represents data variation at zero lag, meaning inherent error or micro variation in the data. Although zero lag may not physically exist in the dataset, the nugget represents a threshold below which the variations cannot be modeled by the variogram. The range is the distance beyond which data variations are independent of lag distance. Generally data are not predicted beyond the range. The sill is the variance corresponding to the range.

The semivariogram model only provides variance for a given lag distance. For interpolation through kriging, a model-based weighted average technique is used where the weights depend on distances to other data locations. The magnitude of the data  $Z$  at an interpolated location  $s_0$  is:

$$Z_0 = \sum_{i=1}^N \lambda_i Z_i \quad (2)$$

In Equation 2,  $Z_0$  is the predicted value,  $Z_i$  is the data value at the  $i^{\text{th}}$  location,  $\lambda_i$  is the corresponding weight and  $N$  is the number of data used for computing the prediction.

The biggest limitation of kriging is the inherent assumption of stationarity, i.e. all spatial trends

that are present in the region where the interpolation is being sought can be reconstructed using a finite amount of data. This assumption is rarely true as the variability cloud may not reflect the local, high-frequency disparities, i.e, kriging cannot predict trends that have not been sufficiently sampled. The stationarity can be overcome to some extent by using a secondary variable, with a reasonably high spatial density, as an aid in interpolation of the primary variable; the method is known as cokriging (Journel, 1989). As intuitively expected, a valid secondary variable needs to have reasonable cross-correlation with the primary variable.

In cokriging interpolation methods, estimates  $Z_0^*$  as a linear combination of N values of two variables described as:

$$Z_0^* = \sum_{i=1}^N \lambda_i Z_i + \sum_{j=1}^N \beta_j T_j \quad (3)$$

Where  $Z_0^*$  is the prediction,  $\lambda_i$  is the undetermined weight assigned to the primary variable  $Z_i$ ,  $\beta_j$  is the undetermined weight assigned to the secondary variable  $T_j$ . Similar to kriging, cokriging also uses variography. Interpolation of  $Z_i$  using  $T_j$  is done through a covariance model, which is built in two steps. Semivariogram models for primary and secondary variables are first constructed independently followed by their cross-correlation, which creates the covariance model. The nuggets in both models are incorporated into a cumulative nugget in the covariance model. This can also result in a higher potential modeling error. The more linear relation the primary and secondary variable exhibit, the more effective the cokriging.

The general work flow for kriging is as follows: detrending, variogram modeling, neighborhood search, and reincorporation of the trend (Figure 13). Data for kriging have to be preconditioned to achieve a normal distribution (Journel, 1986) which can be achieved by detrending or extraction of the “background” trend from the data. Detrending also makes the data spatially isotropic, i.e., the data variance becomes independent of azimuths. The background trend is a user-defined, first or second order, exponential function. The residual data after detrending is used for creating a semivariogram.

The semivariogram model, or the best fitting line to the variance cloud, is generally a spherical, exponential, Gaussian, or stable function. In this thesis a stable model is used. This function has a monoclinial shape, meaning low variance at near distances and a sharp rise in variance that levels off at the range distance. The function is expressed as:

$$\gamma(h; \theta) = \theta_s \left[ 1 - \exp \left( -3 \left( \frac{\|h\|}{\theta_r} \right)^{\theta_e} \right) \right] \text{ for all } h, \quad (6)$$

where  $\theta_s \geq 0$  and  $0 \leq \theta_e \leq 2$

Where  $\lambda(h; \theta)$  is the stable function,  $h$  is the spatial vector,  $\theta_s$  is the partial sill,  $\theta_r$  is the range, and  $\theta_e$  is the nugget.

After the model is established, limitation on the distance of the model influence can be restricted using a search neighborhood. As measured values get further away from the predicted location, they have less spatial significance with the predicted location. These measured points will have little to no effect on the predicted value, so they can be eliminated from the weight calculation. Search neighborhood can also be used to optimize computational time with large datasets without significantly effecting the results. A multitude of criteria exist for determining the search neighborhood, its shape being the most important. It can be isotropic or anisotropic depending on the azimuthal behavior of the data. Further criteria include dividing the shape into sectors and choosing number of data points within individual sectors.

Conceptually, cokriging has a similar workflow to kriging with two exceptions, linearity between the variables needs to be established and no detrending is necessary. Prior to cokriging, it is necessary to determine the degree of correlation of the primary and secondary variable. High cross-correlation is expected if the background trend is the same in both primary and secondary datasets. After constructing the covariance model, a search neighborhood is defined similar to the kriging.

Post-kriging and cokriging cross-plots are used to validate the model by comparing the predicted and measured values. The model is made to predict data even at locations where the values are known from direct measurements. Robust models will have a near 1:1 relationship. Another way of visualization is through errors, where the error is equal to the difference between the predicted and measured data. Robust models will have a difference close to zero. This plot is helpful with determining if the interpolation was biased, i.e., the model as a whole is over or under predicting the measured values.

### *3.3: Wedge Modeling*

Wedge models are created to understand lateral variability in the seismic amplitude response as a composite function of formation thickness and source wavelet (Widess, 1973; Cooper, 2007). In this context, tuning thickness is defined as the formation thickness at which there is constructive or destructive interference between the top and base of a formation (Figure 14). In this case, a wedge model is needed to properly evaluate the fidelity of the instantaneous amplitude attribute map.

The wedge model in this case could be built in two ways. First by squeezing the Ruark acoustic logs such that even if the thickness changes, the log character stays the same. Second, by assigning a constant velocity to the whole wedge. The former method may influence the reflectivity by introducing unnecessary internal character of the Mississippian. The second way and the one used here is to build the model by averaging the sonic log velocities to gain a constant average velocity (17,000 ft/s). The wedge model, which is created in terms of velocity, can be transformed into reflectively coefficients at regular spatial intervals and convolved with a wavelet, similar to how a synthetic seismogram is made. The resulting traces show how reflection amplitudes of the top and base of the Mississippian carbonate section change as it thins.

### *3.4: Seismic Attributes*

Besides reflectivity, other attributes of the seismic wavelet such as amplitude, phase and frequency also provide additional information about the reservoir including fluid type and saturation



(Taner, 2001; Pennington, 2002; Ogiesoba, 2010; Rotimi, 2014). In their pioneering work, Taner et al. (1979) classified attributes into two categories: geometrical and physical. Geometrical attributes examine continuity/discontinuity of traces over a given time/space window and have been routinely used to illuminate subtle faults and fractures, karsts, sinkholes and fluvial systems. Physical attributes, also referred to as complex traces attributes, are a rather abstract mathematical concept but provide important rock and fluid information.

The most commonly used geometrical attribute is coherency which measures trace-to-trace discontinuity by evaluating local changes in the amplitude. By calculating localized waveform similarity in the in-line and cross-line direction, estimation of three-dimensional seismic coherency is obtained (Bahorich, 1995). Regions of seismic data that are highlighted using the coherency algorithm that shows low coherency coefficients, illustrate spots in the data where traces are discontinuous. Structural examples that can create discontinuities in the traces are faults or fractures. In addition to structural discontinuities, coherency can also show stratigraphic features that have sharp differing lateral impedance such as channels (Urgeles, 2011), karst (Zheng, 2011), and reef build-ups (Skirius, 1999) (Chopra, 2001). The coherency seismic volume is a powerful interpretation tool because it can numerically separate data that is laterally inconsistent (Bahorich, 1995)(Ogiesoba, 2014).

The next most commonly used geometric attribute is curvature, which extends the measurement of discontinuity in 3D to examine local shape change within a cluster of traces. The underlying assumption behind curvature is that a rugged surface can be decomposed into multiple synclines and anticlines. The synclines and anticlines can be visualized as forming arcs of a circle with varying radii. Curvature is defined as the inverse of this radius. As radius approaches infinity, or the curvature becomes zero, the shape of the interface changes from rugged to flat (Roberts, 2001). Conventionally, K1 symbolizes the most-positive curvature representing the direction and magnitude of concave-down, anticlinal, features. K2 symbolizes the most-negative curvature representing the direction and magnitude of concave-up, synclinal, features (Mai, 2009).

The underlying assumption of physical attributes is that the recorder trace (also referred to as the “real” trace) is a projection (the real component) of a 3D helical trace. The helical trace,  $Z(t)$ , is constructed by first computing the imaginary part,  $Y(t)$ , using the Hilbert Transform of the real trace,  $X(t)$ , and then adding both of them together (Taner, 1979; Hardager, 2010):

$$Z(t) = X(t) + iY(t) \quad (7)$$

The helical trace can be imagined as a spiral traced by the tip of a vector that constantly progresses in time and rotates about the time axis. The instantaneous amplitude,  $a(t)$ , is the magnitude of the vector and can be computed as:

$$a(t) = \sqrt{x^2(t) + y^2(t)} \quad (8)$$

In equation (8),  $x(t)$  is the real seismic trace and  $y(t)$  is the imaginary trace. The instantaneous phase,  $\theta(t)$ , is the angle between the amplitude vector  $a(t)$  and the horizontal plane (which contains the real trace) and is computed as:

$$\theta(t) = \tan^{-1} \frac{y(t)}{x(t)} \quad (9)$$

The instantaneous frequency,  $\omega(t)$ , is defined as the rate of change of the phase angle:

$$\omega(t) = \frac{d\theta(t)}{d(t)} \quad (10)$$

### 3.5: Cluster Analysis

Much like attribute analysis that tends to isolate zones with different elastic properties, data clustering involves creating sub-groups based on data character that meets specified criteria. In this case two criteria were used. The first is based on attributes extracted along a horizon which is referred to as “horizontal.” Second is based on the appearance of a seismic trace within the time-interval of interest which is referred to as “vertical.” Horizontal classification is based on an attribute cross plot where the classification algorithm groups the data into a predefined number of distinct clusters through a five step process:

1. Selecting the number of classes or centroids desired in the model.
2. Placing the centroids into the space representing the data to be clustered
3. Assigning each data point to the closest centroid
4. Recalculating centroids after all data points are initially clustered.
5. Repeat steps 3 and 4 until recalculation does not move the centroids any more.

Mathematically, the clusters,  $W(C)$ , can be expressed as follows:

$$W(C) = \sum_{k=1}^k N_k \sum_{C(i)=k} \|x_i - m_k\|^2 \quad (11)$$

In equation 11,  $W(C)$  are clusters within the scatter,  $N_k$  is the number of observations in the  $k^{\text{th}}$  cluster,  $C(i)$  denotes the cluster number for the  $i^{\text{th}}$  observation,  $x_i$  are the number of observation points and  $m_k$  is the mean vector of the  $k^{\text{th}}$  cluster (Bock, 2008; Hans-Hermann, 2008).

### 3.6: Multivariate Non-linear Regression

Multivariate statistics is a technique for analyzing multi-variable dependencies for identifying patterns and relationships. Relations between the response and predictor variables are linear when change in one variable brings a proportional change in the other. The relation is non-linear when change is not proportional. In presence of noise, a mildly non-linear relation cannot be distinguished from a linear relation. In such cases it is common to regress, i.e, identify a best-fit-line to the data through minimizing the sum of the squares distances of the data to a line. Non-linear regression, as the name suggests, finds the best fitting function instead of the best fitting trend line. In multivariate linear regression it is assumed that in order to estimate the response variable with higher a confidence, multiple unique predictor variables with a linear relationship to the response variable are combined. Similarly, multivariate non-linear regression uses the combination of the predictor variables except uses the non-linear relationships to the response variable in increase the correlation. Multivariate non-linear regression, relationships can be expressed as:

$$\theta(Y) = \sum_{i=1}^p \varphi_i(X_i) + \varepsilon \quad (12)$$

In Equation 12,  $\theta$  is a function of the response variable,  $Y$ ,  $\varphi_i$  is a function of the predictor  $X_i$ ,  $i=1, \dots, p$  is the number of predictors and  $\varepsilon$  is error. Typically  $\varphi_i$  has generic behavior such as positive and negative monotonic, multi-order polynomial, or periodic. Both variables  $Y$  and  $X_i$ , instead of being single valued, can be attribute maps. A combination of functions  $\varphi_i$  and constants is known as the model.

Model validation in multivariate statistics is not straightforward. An effective way is to use the model for predicting a variable that is already determined from direct sampling. This is generally done through cross-plotting the predicted and measured value of the variable. Validation also requires a plausible physical relationship to exist between the response and the predictor variables. For example, natural microfractures in low porosity, crystalline rocks, show a log-linear decrease in fracture density with perpendicular distance from the fault core (Mitchell, 2012). To predict fractures as a function of distance, a negative monotonic function can be used. If the result from a multivariate analysis shows a reversed correlation (changing from negative to a positive correlation), then the model is not realistic or needs geological justification.

## CHAPTER IV:

### APPLICATION AND RESULTS

#### *4.1: Well to seismic tie*

The well-to-seismic tie with was accomplished using the Ruark 1-29, a salt-water disposal (SWD) well with a sonic and density log. These logs are necessary to create the synthetic seismogram required to tie the well to the seismic data. Unfortunately the density log in Ruark 1-29 SWD was run over only half of the Mississippian section. Acoustic impedance (AI) however is dominated by velocity rather than density. Therefore it is reasonable to assume a constant (average) density value where the density log is absent. To create the AI log the sonic and density logs are multiple together. This can then be used to create the reflectivity spike series (Sheriff, 1982). The reflectivity series is then convolved with a wavelet extracted close to the wellbore from the LCBm survey to create a synthetic seismogram. A minor adjustment of the synthetic led to a reasonable alignment of similar looking waveforms. The final well-to-seismic tie had a correlation coefficient of 0.79 between the seismic survey and the synthetic at the Ruark 1-29 SWD, which is a sufficient to allow the transfer of geological markers identified in the log on to the seismic volume (Figure 15). In the following sections, “peak” and “trough” respectively refers to positive and negative impedance contrast with corresponding amplitudes shaded in black and red (Figure 16).

After the well-to-seismic tie, the wavetrain that covers the Mississippian section at the Ruark well can be described as follows: a large peak marks the Mississippian-Pennsylvanian contact indicating strong impedance contrast; it is followed by a weak trough and another weak peak which could represent the internal litho-stratigraphy of the Mississippian unit; and finally a large trough marks the Mississippian-

Woodford interface also indicating a strong impedance contrast. Using the synthetic seismogram at the Ruark SWD well, it was possible to confidently interpret four formations tops – Mississippian, Woodford, Viola, and Arbuckle – as well as two sub-horizons within the Mississippian where the section was thicker in the LCBm survey. After tying the LCM and LMM surveys to the LCBm survey (Appendix B) it was also possible to extend the Mississippian top interpretation across the whole study with confidence (Figure 17).

Once interpreted, the time horizon reveals that there is a large east-west fault with approximately 200' of throw with the downthrown-side to the north bisecting the LCB survey. This structure is interpreted as being associated with the Nemaha fault zone (Burchett, 1985; McBee, 2003). Along strike of the fault the degree of throw decreases to the east, showing little displacement at position  $x=9$  and  $y=6$ . At position  $x=1.5$  and  $y=5$ , there appears to be a small graben with antithetic faults complimenting the major east-west fault. At position  $x=3$  and  $y=10$  are smaller faults with approximately 30' of throw; downthrown to the south. The sense of throw on these faults at location  $x=3$  and  $y=10$  shows that the center of the LCB survey at position  $x=5$  and  $y=5$ ; resembles a horst structure. To the north of the east-west fault at position  $x=9$  and  $y=1.5$  on the LMM survey, the gentle dip of the Mississippian towards the fault ( $\sim 5^\circ$  south) places the formation at the same structural level as the horst block. Interpreting data using the time structures is only good for understanding the spatial distribution of features. Next, the Mississippian top time map was scaled to depth using geostatistics.

#### *4.2: Geostatistics*

In the study are spatial locations of approximately 350 wells that penetrated the top of the Mississippian limestone. The depth interpolation between the wells is shown using a simple kriging model. After this, the depth interpolation using cokrig with the Mississippian top time surface is shown as the secondary variable. Likewise, statistical creation of an isopach map is shown. The depth maps are not only necessary for integrating lateral wells but also isolating zones in the Mississippian play that are below the tuning thickness.

#### 4.2.1: Depth conversion

Prior to creating a variogram of the “Mississippian Top”, the major regional trends need to be extracted from the depth data. The first order local exponential polynomial interpolation with a scan radius of approximately 138,000’ reasonably approximates the background trend, which appears to be striking N-S. The histogram of the residuals show that they have a normal distribution indicating that the background trend was appropriately removed. The semivariogram model for the residual data was developed in a heuristic manner. The lags corresponding to the real location pairs were grouped into 12 bins spaced 3000ft apart implying that the model predictions were made up to 36,000 ft from any given well. The model attributes are as follow: the nugget is 0.19 variance units ( $\gamma$ ); the sill is 1.15 ( $\gamma$ ); and range is 33,266 feet (Figure 18a). The model is a stable function with an isotropic search neighborhood, no sectoring and no directional weighting.

The resultant depth map from kriging (Figure 19a) shows structural deepening at position  $x=2$  and  $y=4$ , however the transition appears gradual. Near position  $x=4$  and  $y=7$ , there is a structural “nose” extending from east to west. If shown to have closure, this feature could be a location for the accumulation of hydrocarbons. From the kriged map, the closure is not apparent. At position  $x=10$  and  $y=2$ , the structure is shallow and has similar strike components observed in features in seismic attributes (section 4.4). Model validation cross plots suggest that kriging was very successful in that the measured data are very well predicted (Figure 20a) and that the prediction errors are low (Figure 20c). However, the model seems to have a positive bias as the overall predicted data have a higher magnitude than the measured data. The most important structural element that is missing from the kriged map is the major east-west fault which was identified in the seismic data. This indicates that although accurate, information from kriging is not complete.

The use of Mississippian time structure as a secondary variable in cokriging for the Mississippian depth structure can be justified through a seismic-time and well-depth cross plot (Figure 21) which suggests a positive correlation ( $y=.0001x+.2049$ ) with 0.55  $r^2$  between the two variables. This coefficient

of determination, although not extremely high, is sufficient for cokriging. Prior to creating a co-semivariogram for the cokriging model, two preliminary variograms are built independently for the primary and the secondary variables. The variograms are then cross-correlated using their covariant relationship. The lags corresponding to the paired locations of both the primary and secondary variable were grouped into 12 bins spaced 2,000ft apart, implying that the model predictions were made up to 24,000ft from any given locations. The co-semivariogram model attributes are as follow: the cumulative nugget is .27 variance units; the sill is 1.27; and range is 16,248 feet (Figure 18b). A stable function is used in the covariance model as well with an isotropic search neighborhood. However the neighborhood was split into 4 sectors, with a maximum of 5 and a minimum of 2 required measure points required from each sector to make a prediction.

The cokriged map was more successful in imaging the major east-west fault bisecting the LCB survey (Figure 19b). In addition, at location  $x=4$  and  $y=7$ , the cokriged map shows a structural closure as opposed to the structural “nose” observed in the kriged map. The contribution of seismic data to the model process effectively de-risked the trapping mechanism for a possible hydrocarbon accumulation. With higher well density these features could be detected in the kriged map; however exploration in this way is not a cost effective way to image the subsurface, thus showing the added benefit of acquiring seismic data. Interestingly, cross plot between predicted and measured data show that cokriging has lower accuracy than kriging and many outliers (Figure 20b,d). Inspection of the residual error plots also shows outliers but the prediction is sufficiently accurate. Predictions from cokriging seems to have an overall negative bias with the predicted value less than the measured.

#### *4.2.2: Isopach*

Much like estimating the overburden velocities, the interval velocity of the Mississippian unit is also difficult to determine from seismic due to a lack of sufficient thickness that allows for discrimination in stacking velocities. However, the isopach model is critical for estimations of net pay, pinch-outs as well as lateral well integration. Much like for the Mississippian depth structure map, a statistically large



number of wells can be used for geostatistical isopach prediction. However, unlike the surface depth structure only wells that have both the Mississippian and the Woodford top interpreted in a vertical borehole are useful for isopach generation. This reduces the number of samples to 340, which is also adequate statistically. The semivariogram for kriging the isopach data is prepared using detrending the data using a first order polynomial determined within a scan radius of approximately 138,000'.

The regional trend has a thicker Mississippian section to the northwest of the seismic survey which indicates preservation of the section on the downthrown-side of the east-west trending fault. The histogram of the residuals show that they have a normal distribution indicating that the background trend was appropriately removed. The lags corresponding to the real location pairs were grouped into 12 bins spaced 2,000ft apart implying that the model predictions were made up to 24,000 ft from any given well. The model attributes are as follow: the nugget is 0.19 variance units ( $\gamma$ ); the sill is 1.19 ( $\gamma$ ); and range is 16,838 feet (Figure 22). Like with the depth surface, a stable function is most appropriate to fit the variance. For interpolation, an isotropic search neighborhood with no sectoring and no directional weighting was used.

The kriged isopach map shows an east-west trend in equal thickness that mimics the structural trend (Figure 23). The thicker section on the downthrown side was likely preserved from erosional processes that affected the upthrown side. At position  $x=3$  and  $y=7$ , the Mississippian section thins to approximately 90 feet. This dramatic thinning is situated atop the horst block that was subaerially exposed during the Late Mississippian/Early Pennsylvanian. As a result erosive processes reduced the formation thickness relative to section to the north. At position  $x=9$  and  $y=2$ , the thickness mimics the structural and seismic attribute (amplitude/frequency), enhancing the plausibility that the seismic attributes are reflecting reservoir characteristics (section 4.4). The measured versus predicted crossplot for validation of kriged isopach map shows significant scatter as compared to the structural model. The overall trend however remains increasing. Examination of the residual error suggest that the prediction is reasonably accurate with a slightly positive bias (Figure 24).

Next, as with the surface structure map, the data were cross correlated to determine if cokriging could yield a better result with higher resolution. The seismic equivalent to isopach is isochron, which is the time difference between two horizons picked on seismic in units of time. The isochron map was used as the secondary variable to create the cokriged isopach model. Ideally the isochron values should be calculated from the top of the Mississippian to the Woodford Shale, however the Woodford Shale is a difficult formation to pick because lateral inconsistencies in the seismic event. As an alternative, an isochron between the Mississippian limestone and Viola limestone was generated to test the correlation, of the Mississippian isopach to the isochron to determine the suitability of cokriging (Figure 25).

The  $r^2$  value for the Mississippian isopach vs the isochron is a .06, which is significantly low. The reason for a poor correlation could be that using the Mississippian limestone to Viola limestone isochron was an over simplified solution for not being able to interpret the Woodford top time surface. More subtle explanations and ones difficult to account for include: poorly picked Woodford and Mississippian tops, highly deviated boreholes, or not enough samples across the survey. Due to poor cross-correlation between the Mississippian isopach and an equivalent isochron, cokriging is not attempted. Although the kriged isopach map does not have the resolution which cokriging could potentially offer, it provides insight into first order thickness changes across the surveys.

#### *4.3: Wedge Modeling*

The isopach from geostatistical modeling shows that the thickness of the Mississippian across the surveys varies from 60 to 310 feet (Figure 23). Prior to attribute extraction and interpretation across the survey, it was necessary to determine the minimum thickness up to which the reflection amplitudes are reliable, i.e. changes that are reflective of the geology and not interference. To model the amplitude responses a wedge model was generated based on the Mississippian characteristics at the Ruark 1-29 SWD well.

Much like the well-to-seismic tie, the tuning analysis also requires a source wavelet. To make the

analysis realistic, a wavelet extracted from the seismic volume was used. However, unlike the well-to-seismic tie, extracting a wavelet from the LCBm survey is not reasonable because thickness does not vary significantly across the survey. The main thinning in the Mississippian occurs within the extents of the larger, LCB survey to the south on the upthrown side of the main fault. Thus, a wavelet extracted from the LCB survey will present the most likely tuning scenario and isolate most of zones in the survey where the amplitudes could be tuned.

The wavelet extracted from the LCB has a frequency spectrum from approximately 10-100Hz, with dominate frequency between 50 and 60Hz (Figure 26). Source and acquisition limitation are evident upon examination of the frequency. The dominate frequency may be the result of high fold data acquired by gun boat. From processing, water survey frequencies did not exceed 50Hz (personal correspondence, Werth, 2014). As a result, of high fold corresponding to 50Hz frequencies, the dominate frequency is 50Hz. Higher frequencies in the spectrum were acquired with dynamite as a source. Most low frequency data were field filtered (Section 2.2). Varying source types affect the frequency directly and thus impact the shape of the wavelet. The shape of the LCB wavelet has a sharp main lobe with side-lobes that are approximately 50% of the peak magnitude (Figure 26). Thinning will cause the side-lobes to constructively interfere creating an enhanced amplitude response 50% greater than it should at a  $\frac{1}{4}$  wavelength. A probable cause of the large side-lobes is the lack of low frequencies ( $<10$  Hz) content in the data.

Wedge model with an average Mississippian velocity was computed from the Ruark 1-29 SWD sonic log (Figure 27). In the model, the sections above and below the wedge have an average velocity of the Pennsylvanian and the Woodford respectively. After creating the depth model it was transformed into a reflectively series at 120 locations (Figure 28a), much like in the case of well-to-seismic tie. However, unlike the well-to-seismic tie reflectivity series which had several reflectivity coefficients, the individual series for the wedge model have two reflection coefficients only –corresponding to Pennsylvanian-Mississippian and Mississippian-Woodford interfaces.

The wedge reflectivity series was convolved then with the LCB wavelet and the amplitude representing the top of the Mississippian was extracted. The amplitude-thickness plot shows that even at the thickest section the reflection amplitude is affected by reflection of the Mississippian-Woodford interface, however this change is negligible. The maximum effect is at  $\frac{1}{4}$  of the dominant wavelength which corresponds to approximately 90 feet formation thickness (Figure 28b). Results imply that attribute interpreted from parts of the play that are thinner than 90ft may not be reliable. While wedge modeling helps in understanding the validity of amplitude variations, it can also provide a mathematically plausible opportunity for detuning them (Appendix C).

#### *4.4: Attributes*

Both complex and volume based attributes from the Mississippian top time surface were extracted. Physical attributes comprise instantaneous amplitude and frequency. Geometric attributes comprise incoherency and curvature.

##### *4.4.1: Instantaneous Amplitude*

The instantaneous amplitudes in each of the 3 surveys have a dynamic range of 1 to 16, i.e., the maximum amplitude is 16 times the minimum value (Figure 29). Although all surveys show reasonable amount of variability in amplitudes, it may not be necessarily related to lithology. A few of the key amplitude anomalies are discussed. A high amplitude anomaly at location  $x=4$  and  $y=7$  appears to be associated with the structural closure (Figure 19a). However, at this location the anomaly could be due to tuning (section 3.4; Appendix C) rather than fluids.

At location  $x=6$  and  $y=6$  amplitude decreases rapidly across the LCB fault from the south (upthrown) to the north (downthrown). Generally a decrease in amplitude occurs as porosity increases and/or lithology becomes “softer,” which would only be possible at this location in case fractures developed in the footwall in response to the main LCB fault or the Pennsylvanian uplift resulted in localized mass wasting. However, the low amplitude is fairly localized and located below the present day

Lake Carl Blackwell, increasing the possibility of it being a processing artifact. At location  $x=1$  and  $y=5.5$ , a low amplitude anomaly is observed north of the fault outside the present day lake; this may be related to lithology, fractures or detritus along the Pennsylvanian-Mississippian unconformity.

At position  $x=6$  and  $y=9.5$ , a circular feature with low amplitudes can be distinctly identified. A simple interpretation would be to consider it as a major karst feature in the Mississippian that filled with Pennsylvanian sediments, which would decrease the impedance contrast and explain the lowering of the amplitudes. This feature is also located on the downthrown-side of the fault indicating likely preservation of the Mississippian section. However, a concurrent display of the full-offset fold map (number of times a spatial location has been illuminated by reflections) shows that the same zone also suffers from low fold (Figure 8). The amplitude anomaly at this location is most likely a processing artifact.

At position  $x=10$  and  $y=2$  cyclic variations in amplitudes appearing like lineaments that strike NW can be seen; these lineaments appear to be changing their orientation to NNW at position  $x=7$  and  $y=1$ . The wedge model (Figure 28) does not indicate tuning at this location. Since these features are fairly localized and do not follow the source and receiver layout, which is NS and EW respectively, they may not be processing related. Thus, it is likely these amplitudes represent variation in reservoir quality. Geologically, they are reminiscent of a “beach ridge” morphology (Jackson, 2010).

#### *4.4.2: Instantaneous Frequency*

The instantaneous frequencies in each of the 3 surveys have a range from 10 to 60 Hz (the Nyquist frequency is 250 Hz) (Figure 30). In general, frequency variations are more difficult to interpret but in cases where attenuation is high, e.g., due to free gas or fault scattering, a sudden decrease in frequency can be expected (Taner, 2001). For example, at position  $x=6$  and  $y=6.5$  the low frequency anomaly is most likely due to the EW LCB fault. Another reason could be that the acquisition over the lake did not recover as high frequencies as their land counterpart. Similar processing-related anomaly is observed at position  $x=8$  and  $y=3$  associated with Lake McMurtry. High frequency anomalies are also

observed throughout the survey, for example at position  $x=6$  and  $y=8$  which may be due to a sharp velocity contrast at the Mississippian-Pennsylvanian interface. A potential limitation of the frequency attribute in this survey is the use of three different types of sources, which can contribute to spectral imbalance.

At position  $x=2$  and  $y=9$ , in the Lake McMurtry survey, the beach ridge type features that were imaged with instantaneous amplitude attribute also appear to be creating frequency anomalies; zones of high impedance show high frequencies indicating that they may comprise more competent lithology in a weak background. An alternate to the beach ridge interpretation is that these features may be reflecting the zones of differential erosion. The more competent material could be limestone-rich, whereas the less-competent material could be altered cherty zones. It is further possible the altered, incompetent zones were preferred paths for fluid flow, also making it plausible that the incompetent zone may also have higher fracture density.

#### *4.4.3: Curvature*

Both the negative and positive curvatures were extracted from the Mississippian Top time surface in each of the 3 surveys (Figure 31, Figure 32 and Figure 33). Extracted values for negative and positive curvature range from approximately .01 to -.07 and -.01 to .07 respectively. The east-west trending LCB fault is visible from high positive curvature values on the hanging-wall side and high negative curvature on the foot wall. This is probably the result of drag associated with the fault. Fault drags are created when bedding planes near a fault deform from the friction of the two blocks sliding past one another to form fold-like geometries. This results in concave folding on downthrown blocks and convex on upthrown blocks. This will be imaged in the seismic reflections and will cause lateral discontinuities, which will be detected by curvature. In this example, the fault created a convex structure on the edge of the hanging wall. As a consequence there is a high magnitude positive curvature

phenomenon. Conversely on the foot-wall there is a concave structure, which in turn will be detected by negative curvature. Lower instantaneous frequencies combined with high negative curvature suggests that the footwall has more fracturing relative to the hanging wall. On a related note, if intersecting fractures is intended in exploration, targeting the foot-wall will be beneficial and vice-versa.

At position  $x=5$  and  $y=3$ , on the LCBm survey, the primary orientation of curvature lineaments are generally N-W and east-west matching the direction of source and receiver layout (acquisition footprint). This implies that the curvature attribute in this survey is heavily contaminated by acquisition and processing. It is therefore not interpreted any further for geology. At position  $x=10$  and  $y=2$  in the LMM survey, there are many instances of high curvature with no apparent strike direction i.e. no east-west trends similar to the regional fault in LCB survey. A possible reason could be the rugged nature of the Mississippian top surface which has random orientation. Such changes may be due to intense fracturing or an erosional surface.

#### *4.4.4: Coherency*

The (in)coherency attribute was extracted along the Mississippian Top time surface in each of the 3 surveys (Figure 34). High values ( $>0.4$ ; darker shade) represents low trace-to-trace continuity, which is generally representative of faults. In addition to detecting vertical misalignment, incoherency also detects lateral changes in amplitude. This means that in addition to highlighting fault, in certain cases, it can also identify lateral changes as those arising from change in facies or diagenesis. For example, the EW LCB fault can be clearly identified. Further, at position  $x=4$  and  $y=7$  a sinuous, NS feature running oblique to the LCB fault can also be identified. This is thought to represent karsting that developed at the end of the Mississippian. In the LCMm survey, due to strong acquisition footprint in this attribute, geological interpretation is avoided. In the LMM survey, beach-ridge/erosional features that were interpreted in instantaneous amplitude and frequency maps do not appear in the same, linear manner. Instead, a chaotic mix of high and low incoherency exists which is fairly typical of an erosive surface.

#### *4.5: Clustering and classification*

While attributes are more indicative of transitions, e.g. from one facies to another or one fault block to another, geobodies can be occasionally isolated using clustering, i.e., grouping similar looking traces. Of the three surveys, the LCB survey has the maximum variation in thickness (from uplift, faulting and erosion) and opportunity to develop localized, distinct post-depositional geological facies with unique seismic character.

##### *4.5.1 Horizontal Classification*

The data was clustered based on the relation between negative curvature and instantaneous amplitude. The rationale for choosing these attributes is their quality and different origin; one is physically derived and the other is geometrically derived. The amplitude-curvature crossplot (Figure 35) indicates that generally lower amplitudes could be associated with higher negative curvature. The physically justification of this relationship is as follows: low amplitudes are created by low impedance which in turn can arise from fracturing. Curvature also identifies areas with increased flexure in the formation, which can also be caused from intense fracturing. Thus, clustering based on this crossplots can better define fractured zones. Mapping the survey area in this manner could be different than the incoherency or curvature mapping, which are more likely to pick the transitions.

In a heuristic manner, the number of cluster for the classification was determined to be 9 (Figure 36). The cross plot suggests that the purple (1), violet (2), dark blue (3), and green (7) classes that are associated with higher negative curvature will likely highlight faulted, fractured and/or diagenetically altered bodies (or their parts). On the other hand, the other powder blue (4), cyan (5), teal (6), brown (8), and orange (9) represent bodies (or their parts) with more gradual changes (Figure 36a). It is notable that the relatively flat parts (low curvature) of the data using this classification highlight model edges and faults. This is proposed because survey edges have slight manifestations of migration swings created by low fold and that fault edges show the maximum extent drag folding associated with negative curvature.



This information may help define the maximum extent of fractures related to faulting. It is also notable that mapping in this manner clearly highlights the sinuous feature oblique to the LCB fault, which was also apparent on the incoherency map.

#### *4.5.2: Vertical Classification*

The internal variability of the Mississippian play can be appreciated using a subvolume of the data spanning between Mississippian Top and Viola Tops (Figure 37). High internal variability may not allow appropriate geo-body isolation based on a surface-based classification approach. Instead a waveform-based classification, which vertically examines the shape of individual traces within a time window, could be more appropriate. The seismic waveform carries information about the phase, frequency and amplitude; any variation in these parameters is considered reflective of the lateral variations in lithology, porosity and fluid content. Using the waveform classification, traces are clustered into bins based on a similar amplitude and phase characteristic. The classes can then be displayed spatially to show cluster changes laterally across the survey.

The method of waveform classification can help define regions of differing seismic impedance and vertical trace character caused by facies changes, diagenetic, or interference created by wavelet limitations. Andersen (2004) illustrates the benefit for using waveform classification when analyzing the Slave Point carbonate play in Western Canada. From his trace analysis, he was able to differentiate between on-reef and off-reef settings that were not easily detected by analyzing instantaneous amplitude. Based on the rationale for the horizontal classification, the LCB survey clipped between a variable time window spanning from the top Mississippian to the top Viola was utilized for the vertical classification. Much like the horizontal classification, in a heuristic manner it was determined that clustering traces into 6 classes (A – F) provides optimal distinction between these classes (Figure 38).

The lower peak in the Mississippian section is the unique characteristic in the traces that drive the separation of the clusters. From class A to F the lower peak diminishes; resulting in a new class. The

fading of this event represents the thinning of the Mississippian section. In addition, slight variations in the phase and amplitude of the traces may reflect reservoir characteristics or acquisition/processing artifacts. Class A shows a region where the lower peak within the Mississippian has a distinct sharp amplitude at 35ms. This represents a thicker section on the downthrown-side of the east-west fault.

Class B differs from A by having a sharper Mississippian top peak at 0ms, higher amplitude trough at 20ms and a slightly diminished amplitude at the Woodford (55ms). Acquisition parameters indicate at position  $x=2$  and  $y=8$  fewer shots were taken due to surface permitting restraints. The fold at this location is approximately 25. This is where class A is dominant. At position  $x=2$  and  $y=4$  the subsurface was well sampled with a fold of 47 (Figure 8). This is where class B is dominant. The thicknesses of the Mississippian at these locations are similar, so tuning is not creating the difference. It is believed that the variations are a result of insignificant trace stacking (low fold) and/or lower frequency content. Without further data, such as well logs, this interpretation is inconclusive.

Traces in class C represent the change in thickness of the Mississippian that is still distinguishable in time. Similarly thinning is observed in class D, but differs by representing where the lower peak is near the zero crossing, ie near zero amplitude. This diminishing of the lower Mississippian peak is believed to be created by destructive wavelet interference in areas of thinning. Thus, dimming could be associated with acquisition and process issues as well.

In class E there is no lower Mississippian peak amplitude response. Spatially the distribution of class E exhibits a unique character. At position  $x=6$  and  $y=3$ , class E is discounted as acquisition limitations from the lake survey. However, at position  $x=3.5$  and  $y=4$  is a unique feature resembling a “spit”. This feature is south, and likely related to, the karst feature identified on the incoherency seismic attribute. The trace character for class F has low amplitude compared to the other classes. Spatial, class F is located around the edges of the survey, along the east-west fault, and where Lake Carl Blackwell is situated. These locations are most affected by acquisition and processing.

Waveform classification accounts for vertical variability in the seismic trace by binning traces with a similar semblance. Expectation of the classification process was to identify vertical changes in the trace features that represent lithological variations within the Mississippian. The method appeared to reveal unique characteristics, but the method was still over printed by fold and acquisition contamination. Similar to the horizontal classification, without log data penetrating features identified in seismic, interpretations are inconclusive.

The cluster analyses approach has two shortcomings. First, the interpretation is only qualitative, with clusters having no physical meaning without interpretation. Secondly, it only provides generic large-scale information. Intuitively, increasing the number of clusters may increase resolution. However, due to non-uniqueness issues cluster analysis should only be limited to a few classes.

#### *4.6: Fracture density prediction from Multivariate Non-Linear Regression*

Multivariate non-linear regression statistics can assist in high-resolution quantitative interpretation. Its effectiveness however, relies on correlation of the predictor and response variable as well as interrelationships of each predictor variable. Fracture density was used as the response variable and attributes as predictor variables. A multivariant model was developed for the Blair 1-24H well and tested on McMurtry 1-21H well; both wellbores are laterals and located in the LMM survey where attributes are reliable due to minimal acquisition and processing contamination (Figure 39).

The response variable, fracture density, is interpreted from the FMI log in the lateral section of the Blair 1-24H well (Figure 10). The predictors – amplitude, frequency, K1, K2 and coherency seismic attributes – are extracted along the Mississippian top time surface from the LMM survey along the vertical projection of the Blair 1-24H well. Much like well-to-seismic ties, log upscaling, so that the response and predicted variable have the same resolution scale, remains an open challenge. The FMI tool samples every 4 inches. In comparison, the distance between two seismic traces in the volumes is 110 feet. The FMI data were upscaled using a sequential Backus averaging approach, which preserves

gradational interfaces (Backus, 1962). In simplistic terms, the log data are averaged using a weighted method within a user-defined moving time window. The result of Backus averaging using two windows; shorter window (110 samples; 30 ft) maintains higher resolution but has fine-scale structure which may not be present in the seismic data (Figure 40). Longer window (1000 samples; 250 ft) results in smoothing which is more akin to the seismic data.

The fracture density from the Blair 1-24H FMI log was cross correlated to the attributes extracted along the well trajectory (Table 1). Fracture density does not have a high linear correlation with any individual seismic attribute. It also shows that none of the attributes being used in multivariate regression have mutual correlations. This implies that a) none of the attribute can be independently used to predict fracture density and b) all attributes are capturing different (and probably unique) aspects of lithostratigraphic variation. However, when the attributes are combined together using the multivariate non-linear regression (Figure 41), the fracture density in the Blair 1-24H well can be predicted to within 94% accuracy (Figure 42; Figure 43).

In the multivariate regression approach, it would be ideal to extract the attributes along the actual well-path where the fracture density was interpreted. However, with standard attribute mapping methods this is not possible as the well does not follow any particular horizon. Therefore, instead the fracture density is vertically project on the Mississippian top surface where the attribute have been mapped. The vertical projection can be conceptually challenged as most of the fractures encountered along the wellbore have dips less than 90°. To address this, a multivariate regression with a dip-corrected projection, was constructed to project fracture density onto the Mississippian top surface along the respective fracture dips (Figure 44). Dip-corrected projection assumes that a) fracture dips remain constant through the formation, i.e., no mechanical bending at internal sequences of the Mississippian play and (b) the maximum fracture dip is in the plane of projection. The dip information can also be obtained from the FMI logs.

Although conceptually more meaningful, the results were only marginally better than the vertical projection method (Figure 45). This is likely because a majority of the interpreted fractures had steep dips (between 75° and 85°) that led to only a minimal change from their vertically projected location on the Mississippian top surface. For example, a fracture intersecting the wellbore with a dip of 85° towards the heel of the well and a distance of 70' to the top of the Mississippian will reproject the fracture only 6'. This is an insignificant distance when compared to the 4,000' lateral. Using the multivariant model created using vertical-based projection, a fracture density map of the for the entire Mississippian top surface in the LMM survey area is created (Figure 46).

The fidelity of the fracture density map was tested using the McMurtry 1-21H well, which is located three miles to the east of the Blair 1-24H well. The comparison between model-predicted and observed fracture density was done using both approaches – vertical as well as dip-corrected projection (Figure 47; Figure 48). The attribute extracted along the projected wellbore path was combined using the same model which was developed from the Blair 1-24H well. Results are encouraging. Visually there appears to be a reasonable correlation in fracture density albeit minor offset. With vertical projecting, the magnitude of the predicted fracture density differs from the observed facture density by as much as 150%; with dip projection the difference is within 80% (Appendix D).

## CHAPTER V

### DISCUSSION

The evolution of the Mississippian play is a great example of how technology has reawakened a stagnant play. As academics and industry learn how to improve recovery for this play, knowledge gained will spur additional exploration to exploit similar reservoirs. Seismic data has been an important tool in exploring and exploiting hydrocarbon discoveries by identifying zones of better porosity and permeability in conventional siliciclastic reservoirs. In the Mississippian play, however, quantitative interpretation of seismic data has been severely challenging. As a result, operators have tended to use seismic in Mississippian only as a general structural guide. This research shows that seismic technique can be better utilized. The objective of this research demonstrates how statistical methods can greatly assist in quantitative interpretation. Although results have been presented for the Mississippian reservoir, the general work flow is applicable to any type of fractured reservoir.

#### *5.1: Fracture Density Prediction*

The culmination of this project was to predict fracture density. Only a few case studies exist in the literature that illustrate attribute-based fracture density prediction. The first to compare FMI interpretation and seismic attributes was discussed in Ericsson et al. (1998) who attributed fractures to the productivity of the Ilam Formation in the Arabian Gulf. As a consequence, predicting the location of the fractures was necessary for continual development of the play. This study found that fracture abundance interpreted from FMI logs in the Ilam reservoir increased in the proximity to faults and flexures inferred from seismic data. The study showed that 68% of wells drilled were successful when correlated to high

magnitude seismic curvature and FMI log interpretation.

Taking it a step further, Hunt (2010) investigated the accuracy of seismic attributes in predicting fracture density interpreted from FMI logs within the Nordegg Formation in west central Alberta, Canada. Using a multivariate linear regression approach, seismically derived attributes, amplitude versus azimuth (AVAZ) and positive curvature were combined to get a .74 correlation coefficient between the attributes and the borehole image logs.

Staples and Marfurt (2011) studied the Hunton Limestone in central Oklahoma where they found a relationship between curvature and fracture density. With this understanding they examined seismic data and horizontal-borehole-image and found weak correlations. They also examined other seismic attributes such as acoustic-impedance inversions, coherence, and isochron. They speculated that if these attributes were used in conjunction with curvature, subsurface-fracture identification would improve.

White and Marfurt (2013) studied the Mississippian Limestone in Osage County, Oklahoma where they correlated fracture density interpreted from a FMI logs to seismic curvature and petrophysical logs. Correlation between positive and negative curvature to fracture density was not conclusive. However they did observe a correlation between high fracture intensity with petrophysical logs that indicated brittleness: low gamma-ray, low neutron porosity, and high bulk density. They suggested that this correlation could indicate that fracture density was primarily controlled by mechanical layering within the Mississippian section where thinner beds were more highly fractured than thicker beds.

Work using seismic attributes done by Stables and White (2013) was a first step towards understanding how seismic attributes can be proxy for fractures. However their approach was limited by not viewing seismic attributes collectively, i.e. no multivariate analysis was done to improve correlations. Examination of each attribute independently may have revealed apparent correlations, but a quantitative approach is needed. This research, similar to Hunt, 2010, fracture density map was statistically generated from seismic attributes, but used non-linear regression rather than linear regression. Stable's (2013)

speculation about physical attributes providing more affective correlation to fracture density, was confirmed in the multivariate analysis.

Common problem encountered by Stables (2013), White (2013), and in this research were the projection of seismic onto the wellbore for comparison to FMI interpretation. Staples (2011), indicated that extracting seismic along the wellbore from a depth registered volume worked better than a vertical projected of the attribute from the surface of the formation. This was important because the wells given where not always parallel to the reflector surface. However using a depth-converted volume may introduce additional problems to the analysis. With depth conversion an accurate velocity model is needed to properly align the true phase of the trace to the wellbore. Given that an accurate velocity model is made; the three-dimensional approach may increase the correlation.

For this research a technique based on interrelationships of seismic attributes to fracture density interpreted along the lateral section of a horizontal well were used. From the model relationship derived at the wellbore fracture density could be propagated out along the surface of the Mississippian. Utilizing this method to correlate seismic attributes to FMI interpretation yielded very encouraging results.

In lieu of data limitations to make an accurate velocity model, this study used a simple dip reprojection method. This method involved the reprojection of the fracture onto the surface of the Mississippian formation based on their dips. Given the assumptions of the method (section 4.6), this allows for the fracture interpretation to be properly correlated to the surface expression of the Mississippian formation without the complexity of a velocity model. However, because of minor dips, fracture reprojection was minimal.

### *5.2: Multivariate Non-Linear Regression*

Multivariate statistics was used to draw a correlation of seismic attributes to fracture density interpreted along the lateral portion of a well. Part of determining the validity of a multivariate non-linear regression model is from analysis of the transforms of the variables. Variable relationships in the



model are linearized by using non-linear equations to best predict the response variable. A few of the tested transforms include positive and negative monotonically increasing, multi-order polynomial, and periodic functions. Positive and negative monotonic functions include logarithms,  $e^x$ , and  $x^2$ . Examples of data requiring these functions for linearization could be production decline curves or the permeability/porosity relationship. High order polynomial functions consist of equations with exponents greater than 3. High order polynomials should be used with caution. There is the risk of over training the data, which may create unrealistic results when data is extrapolated (Runge, 1901). The periodic function is mathematically described as repetitive oscillation. Although uncommon, sinusoidal functions are fit to variables with a finite range such as seismic phase or azimuthal attributes. The use of nonlinear regression requires an intuitive understanding of the selected transforms and what the resulting model physically represents (Motulsky, 1987).

Physical attributes that were used in the multi-variant model are instantaneous frequency and amplitude. The impetus is as follows. Higher frequencies correlated negatively to higher fracture density probably because high frequencies are likely to be removed due to attenuation from the fractured zones. Similarly, an increase in amplitude correlates negatively with fracture density. Lower amplitudes represent zones where the acoustic impedance is similar between two formations. In this research it is believed that fractures may also cause the reduction in impedance contrast between the Mississippian and Pennsylvanian formations.

Geometric attributes that were used in the multi-variant model include incoherency and positive and negative curvatures. All geometric attributes exhibit an inverse relationship from what was expected: as incoherence increased, fracture density decreases; as negative curvature decreased (gets more negative), fracture density decrease; and as positive curvature increased, fracture density decreased. The impetus for using geometric attributes is their potential relation to seismic flexure which is an indication of strain (Chopra, 2001). Possible explanation for the inverse relationship is that the flexure in the area is not significant enough to predict fracture distribution alone. As a result, the magnitude of the geometric

attribute may be too low to indicate structurally related fracturing.

### *5.3: Cluster analysis*

In addition to the multivariate analysis, two clustering techniques were used to check if lithology with high fractures can be isolated. Due to unavailability of vertical logs, the success of this method could not be fully assessed. The horizontal clustering shows structural and erosional features that could be related to faults and karst topography. The horizontal classification is limited in its scope because of its two-dimensional nature. Therefore a waveform classifications technique was employed that partitions data into class based on a defined window, amplitude and phase of the trace. This furthers the understanding of the Mississippian by showing how and where the internal waveform changed within the section. From this analysis, it was possible to detect where subhorizons within the Mississippian disappeared from the section; identifying spatially the nature and degree of erosion. Identification of these zones may lead to the discovery of altered zones with possible higher permeability and greater porosity.

An example where cluster analysis was an effective tool with seismic data was presented by Mukerji (1998), where a bivariate cluster analysis was performed using seismic acoustic impedance and elastic impedance. From the analysis, they were able to separate lithological and pore fluid content in a turbidite sequences, thus conceptually showing that it is possible to use seismic data to predict reservoir conditions. However, the inversion necessary to complete the research required near and far offset seismic impedance attributes. These attributes require trace gathers to create. Not all operators have the ability to process seismic gathers, due to software constraints, or the capital to hire a vendor to generate the attributes. Although these attributes are useful, the intent of this research was to understand characteristics of the Mississippian section using post stack seismic volumes and attributes, similar to what an operator may receive.

Expectation from clustering was to identify geomorphical features that may represent lithological

variations within the Mississippian. Due to in unavailability of log-based facies maps, interpretation of the groupings would be speculative and not confirmable. However from the analysis three observation where recognized. First, the attributes for the LCB survey are no reliable due to acquisition (tuning issues) and processing (fold issues). Second, without log data penetrating features identified in seismic, it is difficult to confirm interpretation. Third, however convenient, classification techniques will not provide unique solutions nor the resolution needed for play development. They can, however, be very useful in understanding the overall depositional or erosional context of the play.

#### *5.4: Seismic Attributes*

Seismic attributes contain valuable information about structures, lithology and pore fluids. However, linking a particular attribute with a specific aspect of geology is difficult and varies form one dataset to another. In this research a qualitative approach to examining various attributes independently was first performed. Instantaneous amplitude is the simplest attribute to extract, but may be non-intuitive for interpretation. The vector length of the helical trace is the reflection strength which represents the acoustic impedance contrast between lithological interfaces (Taner, 1979). Because impedance is a function of velocity and density, with an understanding of depositional environment, instantaneous amplitude can be used to indicate porosity or occurrences of hydrocarbon. Bachrach (2004) used heuristic forward modeling to show that in consolidated saturated sandstones, the amplitude response can be related to changes in porosity; increasing porosity decreases density and therefore a lateral lowering in amplitude. As a hydrocarbon indicator, high amplitudes called bright spots, can coincide with gas-filled sands, which proved very successful in the Gulf of Mexico (Avseth, 2005). Bright spots can also be caused by volcanic dikes, overpressure and wavelet tuning, thus inviting careful analysis (Avseth, 2005). In carbonate reservoirs, fracturing can lead to a decrease in density and velocity which will create a lower impedance response. This will decrease the amplitude of the interface when water filled or if charged with hydrocarbon will enhance the amplitude. Thus interpretation of instantaneous amplitude needs to be done with intense tuning and fluid replacement modeling to be reliable.

Barnes (1991) showed a relation between instantaneous frequency and seismic attenuation. This relationship can either be related to wave propagation effects or depositional characteristics. As such, frequency can be an effective discriminator of hydrocarbons, fractures zones, and bed thicknesses because these features attenuate the seismic signal (Taner, 2001). As the wave propagates through the reservoir, filled pores and fractures will scatter seismic waves, attenuating the signal. This attenuation will be reflected as an anomalously low instantaneous frequency response. Najmuddin (2003) compared the frequency spectrum above and below the South Texas Austin Chalk Formation and attributed the areas with high differential frequency to attenuation created by fractures. Frequency can also assist in identifying depositional characteristic, such as bed thickness. Higher frequencies indicate sharp, thin interfaces such as exhibited by laminated shales. In contrast, lower frequencies are indicative of more massive bedding geometries such as thick sand sequences (Taner, 2001)

K1 and K2 curvature are geometric seismic attributes that have been associated with structural strain because they represent flexure in the seismic trace. This, in turn, has been interpreted as flexure in the formation. High fracture density is assumed to correlate with structural curvature because intense curvature indicates intense strain that leads to intense fracturing in brittle rock (Nelson, 2001). Through clay modeling (Staples, 2011) and outcrop observations (Hennings, 2000; Pearce, 2011) a correlation between the degree of bed curvature and strain. Higher bed curvature correlated to high degrees of strain. This observation indicates that there should be a correlation between the magnitude of seismic curvature and fracturing. Thus seismic structural curvature may be used as proxy for fracture density estimation and orientation (Chopra, 2010). From the multivariate analysis this observation was not seen because structural flexure was minimal.

Seismic attributes are powerful because they contain unique information about the formation. However, this study shows that if the seismic data is not properly processed, attributes can be contaminated with false information. As part of the interpretation process it is important to understand the acquisition parameters for the survey. The study showed that instantaneous amplitude varied with the

change in processing fold on the LCB survey. Also, through wedge modeling areas of approximately 90 ft of Mississippian thickness had an enhanced amplitude response with a 50% increase. This means, in addition to a lack of fold balancing, amplitudes around 90 ft could not be trusted to reveal reservoir conditions. In addition, frequency information from the LCB was contaminated by using multiple source types and water survey limitations. The overprint in both these attributes was significant, rendering interpretation inconclusive on the LCB survey. All attributes generated in the LCBm survey were heavily contaminated with acquisition footprint, also rendering interpretation inconclusive. Examination of processing information for the LMM survey showed that attribute and fold trends cross-cut, meaning that some type of fold normalization was applied to the attributes. Of all three surveys, the LMM survey had the highest quality data, and thus made it the more appropriate candidate for multivariate analysis.

#### *5.5: Kriging and Cokriging*

Kriging's practical strength as an interpolation method lies in its ability to capture fine-scale variations in geology through a spatial variance model, thus yielding maps that look more geologically plausible as opposed to inverse distance or spline algorithms (Chambers, 2000). The capabilities of using statistical kriging method to generate a structure map of the Mississippian top surface were tested. The modeled surface was smooth and free of biases but lacked significant structures and resolution required to make well steering decisions in the subsurface. In response, a cokriged structure map was created using the Mississippian time horizon interpreted from seismic as a statistical guide. This map highlighted important information about faults and formation dip. Just as important as understand the structure is an understanding of the lateral changes in the thickness of the formation. Similar to the structure map, an attempt was made to show the comparison between kriging and cokriging techniques to create an isopach map. Unfortunately the relationship between isopach and isochron map was significantly low (.05). As a result, the kriged map was shown to be better.

It is evident that between kriging and cokriging that there is a trade-off of lower model prediction to having high data granularity. The benefit of cokriging is the higher data density from the incorporation of

the time structure grid. However as a result, there is higher model error compared to the kriging model. Scatter in the validation between both models are created by different limitations. In both models scatter is create by data locations that do not follow the mean variation of the dataset, thus they violate the stationarity requirement. There are many reasons why in the kriging model certain data points may deviate from the mean. These include well elevation inaccuracies, missed picked tops, or a geological anomaly that is not well sampled. Such locations should be investigated further; however, the lack of well information prevents this. Scatter in the cokriging model is a result of a more complicated process because it is a combination of the problems in the kriging model with the added complexity of errors introduced by the secondary variable. Errors introduced from the secondary variable include velocity processing variations, acquisition artifacts, or unaccounted geological features not imaged by the seismic. These errors are difficult to mitigate without reprocessing or reacquiring the data in some cases. Often, because of the expense, this is not possible, so being aware of the limitations helps to view the data subjectively.

The isopach model had significantly more scatter in the model validation than the structural kriging model. Reasons for the greater scatter are similar to the structural model, primarily that there are points that do not honor the mean variability of the dataset. Data quality issues that can cause this variability are incorrectly picked Woodford or Mississippian tops, extremely deviated wells, or low quality well logs. The more likely culprit for the deviation is geologic. In Payne County the top and base of the Mississippian section are marked by unconformities (Shelton, 1985) which can be difficult to model because of spatial variation of the erosion over a short distance.

Although kriging utilizes statistical algorithms to generate maps, if done correctly can render plausible interpretations. This can be useful for a quick, first-look at data regionally and at finer scales. A first-pass look at the data can be generated within one day and may be able to identify erroneous data quickly. This can save a significant amount of time before a geologist starts hand contouring data, which is time intensive.

### *5.6: Synthetic Seismogram*

An important step with seismic interpretation is tying the well data to seismic. This was accomplished by creating a synthetic trace at the Ruark 1-29 SWD well, which was manipulated until it was properly calibrated to the time section. Once aligned, the correlation coefficient between the synthetic trace and seismic data was a .74. This correlation is significant enough to identify key horizons in seismic. However, if inversion was included in this research, a more rigorous synthetic tie would be necessary, such as properly phase matching the well and seismic data (Sridhar, 2004). The tops at the well were then interpreted in depth and then translated to time to be picked across the seismic surveys.

### *5.7: Acquisition/Processing*

Seismic data has been proven to be a powerful tool when identifying subsurface features. But just as important as understanding the meaning of seismic attributes is the knowledge of the potential pitfalls. The datasets provided showed signs of data contamination created by acquisition, processing, and bandwidth limitations.

In land datasets, low-frequency ground roll can have an overwhelming effect on reflective events, especially at the near offset source (Sheriff, 1982). However, removing lower frequencies can also affect the data quality in an adverse manner. Lower frequencies map the large scale velocity structure of the subsurface. As a result, data that lack lower end of frequency spectrum often have larger side-lobes associate with the main reflection pulse. The data examined in this research had a low-cut field filter; removing all frequencies below 10 hz. This adverse effect of the field filtering was observed during wedge modeling, when constructive interference created 50% larger amplitude response. In addition, removal of low frequency data affects inversion methods that use amplitudes for estimating fluid saturation and porosity (Bertram, 2011; Bagaini, 2010). Goloshubin (2006) illustrate this by showing that anomalies in lower frequency spectrum have better correlations with hydrocarbon saturation than their higher-frequency counterparts.

An observation from the water portion of the surveys is that the data had significantly lower data quality than that acquire on land. This was unexpected because water borne surveys generally have high frequencies. Upon further investigation, frequency content received from the airgun boat did not exceed 50 hz (personal communication, Kevin Werth, 2014). Higher frequencies are speculated to be lost for three possible reasons: cylindrical spreading, muddy bottom conditions or geophone coupling. In shallow water, cylindrical divergent energy effectively channels and diminishes on surface of seabed boundaries in the horizontal direction (O'Brien, 2002). Lake Carl Blackwell averages about 18 ft deep (Johnson, 1998), which may cause cylindrical divergences, thus being a possible culprit to the decreased frequencies on the LCB survey. Another possibility is the condition of the lake bottom, whether it is lithified or muddy. McCauley (2000) explains that frequency content output from sediment types with a deep mud layer interface show little high frequency energy recorded. Given the nature of the artificial lake, the bottom is likely muddy. Lastly, geophones were strung across the bottom of the lake. Doing this creates doubt on whether the geophones were properly coupled to the bottom of the lake. This may also result in lower frequencies being recorded.

To be a successful seismic interpreter, an understanding of acquisition and processing is important to mitigate data inaccuracies. If not well understood, decisions based on seismic interpretation with erroneous data could lead to expensive mishaps. As such, five suggestions are proposed to interpreters before they begin interpreting 3D seismic data, especially when evaluating seismic attributes. One, understand the source and receiver layouts, as part, examine areal imagery of the area. Two, know what sources are being used in the shoot, ie vibroseis, dynamite, and/or gunboat. Three, examine wavelet and frequency spectrum. Four, determine the processing fold for each bin on the survey. Five, make a wedge model when the formation being evaluated changes in thickness. These simple suggestions will help decrease improper interpretation and will help with communication with acquisition crews and processors.



### 5.7: Play types

Seismic data helps with lateral resolution; increasing knowledge between wellbores. As such, it is the best tool for identify drilling opportunities. From the analysis of the seismic data, three potential prospect types were identified – fracture, diagenetic, and structural closures.

A spatial knowledge of fracture density is a powerful tool for exploiting zones of higher permeability within the Mississippian formation. Within the LMM survey zones of higher fracture density were successfully delineated. Based on the analysis, the area with the highest probability of connecting with multiple fractures is at position  $x=3.75$  and  $y=3.75$  (Figure 46), with the borehole oriented to the NNE. As such, this workflow increased spatial granularity improving our understanding of hydrocarbon recovery in a spatially complex play.

Dolomitization has great potential for increased storage capacity. The Nemaha ridge and its associated faults provide opportunities for vertical fluid migration from deeper in the Anadarko basin. This can result in the alteration of limestone to dolomite potentially increasing the porosity of the formation which may be detectable with seismic data. At position  $a=1.5$  and  $y=5$  there appears to be a structural sag, similar to those observed in the Albion-Scipio trend, Michigan, and Lady Fern trend Canada (Ells, 1962; Grammer, 2010; Boreen, 2004) (Figure 50). The sags in these trends are associated with fluid migration and subsequent dolomitization within the strike-slip fault zone. The process of changing from limestone to dolomite can reduce the volume of the formation by 11% (Weyl, 1960). In this area on the downthrown-side of the fault the Mississippian limestone has an approximate thickness of 250 ft determined from the statistically generated isopach map. If dolomitizing fluids are migrating up fracture networks associated with the east-west fault, this may cause shrinkage within the Mississippian section. An 11% reduction in the volume of the formation would change that thickness to 222.5 ft. Dolomitization volume reduction coupled with brecciation within the fault zone is the mechanism to explain the structural sag. Because of the similar seismic characteristics and regional structural framework to analogs, this location is a potential prospect.

Structural closures inhibit the lateral migration of fluids. At position  $x=5$  and  $y=5$ , a four-way closure was identified from the cokriging model (Figure 19). At this location seismic attributes show unique characteristics: high amplitude, high frequency and a unique karst feature. This response may correlate to a charged zone within an altered section of the Mississippian. Rogers (2001) describes the development of tripolitic chert in the Mississippian section as the weathering or erosion of limestone that was deposited as debris flows. The chert was created by the replacement of silica in the carbonate at the molecular level. Due to uplift associated with the Nemaha Ridge, meteoric waters dissolve the remaining calcite resulting in abundant secondary vuggy and moldic porosity. Chert is widespread; however, it is not continuous throughout the Mississippian section and not always porous (Rogers, 2001). Zones with limestone and non-porous chert can be highly fractured creating ideal horizontal drilling targets when drilled perpendicular to the fracture sets. These zones can be identified with seismic data (Roy, 2012) however, the Mississippian is approximately 90 ft thick, which coincides with a tuned response, therefore amplitude and frequency that may represent these intervals must be discounted. Structural closure, thinning and the unique karst feature necessitated further investigation using well log data. Of the 350 wells known to this study, two wells have penetrated the structure through the Mississippian section.

## CHAPTER VI

### CONCLUSION

The lateral variability in the seismic character of the Mississippian limestone suggests that it may be a heterogeneous and complex reservoir. Advanced data analysis methods such as variography, clustering, and multivariate regression can identify depositional architecture and delineate potential play types. The overarching conclusion from this research is that selected seismic attributes can be statistically combined to predict fracture density. The model used for fracture prediction is developed using a statistical multivariate non-linear regression algorithm. It was created locally for the Blair 1-24 well to relate the amplitude, frequency, positive/negative curvature and incoherency attributes to the upscaled FMI fracture density log; upscaling was done using Backus averaging with a moving window of 250ft. The model was then applied to the entire LMM 3D survey. Good correlations were observed at the McMurtry 1-21H.

Instead of interpreting the attribute maps independently for geology, grouping wavelets with similar properties through cluster analysis resulted in a better geobody visualization. Data clustering in cross plot of instantaneous amplitude and negative curvature clearly delineated faults and karst patterns that were not easily identifiable in the attribute maps alone. Data clustering based on phase and amplitude characteristics of the whole trace within the Mississippian section may help infer erosional and stratigraphic facies.

The Mississippian top time surface can be statistically mapped to depth using variography. The benefit of this approach is that depth conversion can be performed even in absence of knowledge of

interval velocities. Two variographic methods were used: kriging and cokriging. Kriging resulted in a smooth interpolated surface with low prediction error, however some of the known geologic features such as a prominent east-west fault could not be realized. The cokriged surface on the other hand had more structures and higher prediction errors, but was geologically more representative. In the study cokriging was the best method for the Mississippian top depth surface and kriging for the Mississippian isopach. The choice of kriging or cokriging depended on the correlation between the primary and secondary variable. The primary variable was the well-markers. The secondary variable was the time surface and the isochron respectively.

Fidelity of seismic attribute maps can be severely affected by acquisition and processing artifacts such as non-uniform fold distribution and use of multiple sources in the same survey. Both LCB and LCBm surveys had severely non-uniform fold distribution that manifested in the form of geological looking features in the attribute maps. The LMM survey was generally free of processing artifacts, making it suitable for multivariate analysis. Variation in formation thickness can also introduce features that can be misinterpreted for porosity or fluid induced changes. Thickness effects on amplitude can be realized through wedge modeling. For this study the peak tuning thickness occurs at 90 ft of Mississippian section. Interpreting any attribute maps where Mississippian was below 100 ft thick will not reflect reservoir properties.

The seismic datasets used in this thesis have increased our appreciation for the play types that could potential exist in the Mississippian. Three potential play concepts were identified within the scope of this study: diagenetic, fracture-controlled and structural. The most significant exploration finding was a structural sag feature associated with the EW fault in the LCB survey which could be analogous to the Lady Fern trend in Canada, or the Albion-Scipio trend in the Michigan Basin. Also identified was a potential fracture-controlled play in the LMM survey and a structural closure approximately 4 square miles, south of the east-west fault on the LCB survey. Play concepts discovered in this thesis can be

better defined using wider bandwidth, better quality seismic data which can potentially lead to the discovery of more plays.

### *6.1: Recommendations*

In the past, the primary role of seismic was to identify structural prospects and mitigate geohazard risk. Today, there are fewer large-scale new structural plays left because of the success of seismic. However, seismic data has not become any less relevant. Seismic data contains unique information about the formation that can be enhanced by seismic attributes analysis. But in order to properly analyze them requires high data fidelity. As such, the LCB, LCBm and LMM are excellent surveys for avoiding hazards and geosteering, they are not, however, the best for seismic attribute analysis.

There are two options that can improve data quality. One, is reprocessing and subsequent merging of the data. The high dimensionality of seismic data has led to the realization that in order to properly interpolate and normalize it requires a high dimensional methodology. With the advent of the 5D interpolation seismic processing method, data semblance is calculated by using inline, crossline, azimuth, offset and time. The method attempts to discover the direction of maximum semblance from the surrounding data paying particular attention to offset and azimuth (Wojslaw, 2012; Ferdinand, 2012; Chopra, 2013). This reprocessing method is ideal because it can help with normalizing fold, remove acquisition footprint and boost lower frequencies. Unfortunately this cannot be guaranteed because of the field filtering of lower frequencies. Two, would be more expensive, but will get the lower frequencies to stabilize the wavelet; reshooting the data. The design would need altering to utilize geophones that can record lower frequencies and the sources to sweep starting at lower frequencies (section 2.2.1).

## REFERENCES

- Abad, A. F., 2013, 3D Seismic Attribute expression of the Ellenburger Group karst-collapse features and their effects on the production of the Barnett Shale, Forth Worth Basin, Texas [Master: University of Oklahoma, p. 102.
- Abrahamsen, P., 1996, Geostatistics for Seismic Depth Conversion: Statistics Analysis of Natural Resource Data, SAND, v. 6, p. 1-9.
- Andersen, E., and Boyd, J., 2004, Seismic Waveform Classification: Techniques and Benefits: CSEG Recorder, March 2004, p. 26-29.
- Avseth, P., Mukerji, T., and Mavko, G., 2005, Quantitative Seismic Interpretation: Common techniques for quantitative seismic interpretation, Cambridge University Press, p. 168-211.
- Bachrach, R., and Mukerji, T., 2004, The effect of texture and porosity on seismic reflection amplitude in granular sediments: Theory and examples from a high-resolution shallow seismic experiment: Geophysics, v. 69, no. 6, p. 1513-1520.
- Backus, G. E., 1962, Long-Wave Elastic Anisotropy Produced by Horizontal Layering: Geophysical Research, v. 67, no. 11, p. 4427-4440.
- Bagaini, C., Bunting, T., El-Emam, A., Laake, A., and Strobbia, C., 2010, Land Seismic Techniques for High-Quality Data: Oilfield Review, v. 22, no. 2.
- Bahorich, M., and Farmer, S., 1995, 3D seismic discontinuity for faults and stratigraphic features: The coherence cube: The Leading Edge, v. 14, no. 10, p. 1053-1058.
- Ball, M. B., Henry, M. E., and Frezon, S. E., 1991, Petroleum geology of the Anadarko Basin Region, Province (115), Kansas, Oklahoma, and Texas: Open-File Report, v. 88-450W, p. 1-36.
- Barnes, A. E., 1991, Instantaneous frequency and amplitude at the envelope peak of a constant-phase wavelet: Geophysics, v. 56, p. 1058-1060.
- Bertram, M. B., and Margrave, G. F., 2011, Recovery of Low Frequency Data from 10Hz Geophones, Recovery- CSPG CSEG CWLS Convention, p. 1-4.
- Boreen, T., and Davies, G., 2004, Hydrothermal dolomite and leached limestones in a TCF gas play: the Ladyfern Slave Point reservoir, CSPG Seminar and Core Conference: Calgary Alberta, p. 17.

- Burchett, R. R., Luza, K. V., Eck, O. J. V., and Wilson, F. W., 1985, Seismicity and Tectonic Relationships of the Nemaha Uplift and Midcontinent Geophysical Anomaly, Oklahoma Geological Survey, Special Publication 85-2, p. 1-33.
- Cardott, B.J., 2012, Thermal maturity of Woodford Shale gas and oil plays, Oklahoma, USA: International Journal of Coal Geology, v. 103, p. 109-119.
- Chambers, R. L., Yarus, J. M., and Hird, K. B., 2000, Petroleum Geostatistics for the Nongeostatistician- Part 1: The Leading Edge, v. 19, no. 5, p. 474.
- Chopra, S., and Marfurt, K. J., 2010, Integration of coherence and volumetric curvature images: The Leading Edge, v. 29, p. 1092-1107.
- , 2013, Preconditioning seismic data with 5D interpolation for computing geometric attributes, SEG Houston 2013 Annual Meeting, p. 1368-1373.
- Chopra, S., and Pickford, S., 2001, Integrating Coherence Cube Imaging and Seismic Attributes: CSEG Recorder, December 2001, p. 21-22.
- Claprod, M., Gloaguen, E., and Malo, M., Using Kriging with External Trend for Time to Depth Conversion of Seismic Horizons to Characterize Deep Saline Reservoirs for CO2 Storage in Becancour, Quebec, *in* Proceedings Recovery- CSPG CSEG CWLS2011.
- Clarke, P. H., 1963, Petroleum Geology of Pawnee County, Oklahoma, *in* USGS, ed.
- Cooper, J. K., and Lawton, D. C., 2007, The Wedge Model Revisited, Let it flow-2007 CSPG CSEG Convention, p. 369-372.
- Crowell, J. C., 1974, Sedimentation along the San Andreas Fault, California: Modern and Ancient Geosynclinal Sedimentation Society of Economic Paleontologists and Mineralogists Special Publication, v. 19, p. 292-303.
- Dams, J., 2009, Low-frequency with passive, Mikroniek, Volume 3, p. 24-28.
- Dick, J. P., 2011, Osage Exploration & Development- Executive Summary: Pinnacle Energy Services, L.L.C.
- Dolton, G. L., and Finn, T. M., 1989, Petroleum Geology of the Nemaha Uplift, Central Mid-Continent, USGS, Report 88-450D, p. 1-39.
- Durham, L. S., 2013, Mississippi Lime- A 'Thoughtful' Challenge, AAPG Explorer.
- Ekstrom, M. P., Dahan, C., Chen, M.-Y., Lloyd, P., and Rossi, D. J., 1987, Formation imaging with microelectrical scanning arrays: Log Analyst, v. 28, p. 294-306.
- Elebiju, O. O., Matson, S., Keller, G. R., and Marfurt, K. J., 2011, Integrated geophysical studies of the basement structures, the Mississippi chert, and the Arbuckle Group of Osage County region, Oklahoma: AAPG Bulletin, v. 95, no. 3, p. 371-393.
- Ells, G. D., 1962, Structures associated with the Albion-Scipio oil field trend, Geological Survey Division Michigan p. 1-33.

- Ericsson, J. B., McKean, H. C., and Hooper, R. J., 1998, Facies and curvature controlled 3D fracture models in a Cretaceous carbonate reservoir, Arabian Gulf: Geological Society (London) Special Publication, v. 147, p. 299-312.
- Fatti, J. L., Smith, G. C., Vail, P. J., Strauss, P. J., and Levitt, P. R., 1994, Detection of gas sandstone reservoirs using AVO analysis: A 3D seismic case history using the Geostack technique: Geophysics, v. 59, no. 9, p. 1362-1376.
- Ferdinand, K., Stein, J. A., and Wojslaw, R., 2012, Multidimensional Interpolation on a Very Sparse 3D, an Example from East Texas, SEG 82<sup>nd</sup> Annual Meeting, v. 5, p. 3329-3333.
- Gaillot, P., Brewer, T., Pezard, P., and Yeh, E.-C., 2007, Borehole Imaging Tools-Principles and Applications: Scientific Drilling, v. 5.
- Garven, G., 1995, Continental-scale Groundwater Flow and Geologic Processes: Annual Review of Earth and Planetary Sciences, v. 23, p. 89-117.
- Gay, S. P., 2003, The Nemaha trend-A system of compressional thrust-fold, strike-slip structural features in Kansas and Oklahoma: Shale Shaker, v. 54, no. 2, p. 9-49.
- Goloshubin, G., VanSchuyver, C., Korneev, V., Silin, D., and Vingalov, V., 2006, Reservoir imaging using low frequencies of seismic reflection: The Leading Edge, v. 25, p. 527-531.
- Grammer, G. M., Schulz, J., Barnes, D., Gillespie, R., Harrison, W. B., and Thornton, J. E., 2010, Stratigraphic Control on the Lateral Distribution of Hydrothermal Dolomites away from Major Fault Zones: Search and Discovery Article, v. #50277.
- Gregg, J. M., and Shelton, K. L., 2012, Mississippi Valley-type Mineralization and Ore Deposits in the Cambrian-Ordovician Great American Carbonate Bank: AAPG Memoir, v. 98, p. 163-186.
- Hans-Hermann, B., 2008, Origins and extensions of *k*-means algorithm in cluster analysis: Electronic Journal for History of Probability and Statistics, v. 4, no. 2, p. 1-18.
- Hardage, B., 2010, Instantaneous Seismic Attributes Calculated by the Hilbert Transform: Search and Discovery Article, v. #40563.
- Harilal, Biswal, S. K., Sood, A., and Rangachari, V., 2006, Identification of Reservoir Facies within Carbonate and Mixed Carbonate-Siliciclastic Sequences: Application of Seismic Stratigraphy, Seismic Attributes and 3D Visualization, 6th International Conference & Exposition of Petroleum Geophysics: Kolkata 2006, p. 937-944.
- Hennings, P. H., Olsen, J. E., and Thompson, L. E., 2000, Combining outcrop data and 3D structural models to characterize fractured reservoirs with outcrop fracture and fault data for reservoir characterization: AAPG Bulletin, v. 84, p. 830-849.
- Hunt, L., Reynolds, S., Brown, T., Hadley, S., Downton, J., and Chopra, S., 2010, Quantitative estimate of fracture density variations in the Nordegg with azimuthal AVO and curvature: A case study: The Leading Edge, v. 29, p. 1122-1137.



- Jackson, C. A. L., Grunhagen, H., Howell, J. A., Larsen, A. L., Andersson, A., Boen, F., and Groth, A., 2010, 3D Seismic imaging of lower delta-plain beach ridges: lower Brent Group, northern North Sea: *Journal of the Geological Society*, v. 167, p. 1225-1236.
- Johnson, K. S., and Suneson, N. H., 1995, Rockhounding and Earth-Science Activities in Oklahoma, 1995 Workshop, *in* USGS, ed., Volume 96.
- Johnson, K. S., 1998, Mountains, streams, and lakes of Oklahoma, Oklahoma Geological Survey, Information series, no. 1.
- Journel, A. G., 1986, Geostatistics: Models and Tools for Earth Science: *Mathematical Geology*, v. 18, no. 119.
- , 1989, Fundamentals of Geostatistics in Five Lessons, Short Course in Geology, AGU, Volume 8: Washington DC.
- Kirkland, D. W., Denison, R. E., Summers, D. M., and Gormly, J. R., 1992, Geology and organic geochemistry of the Woodford Shale in the Criner Hills and western Arbuckle Mountains, Oklahoma: Source rocks in the southern mid-continent: 1990 Symposium Oklahoma Geological Survey Circular, v. 9, p. 38-69.
- Mai, H. T., and Marfurt, K. J., 2009, Coherence and volumetric curvatures and their spatial relationship to faults and folds, an example from the Chicontepec basin, Mexico, 79th Annual International Meeting of the SEG, Volume Expanded Abstracts, p. 1063-1067.
- Martin, N., and Stewart, R. R., 1994, The effect of low frequencies on seismic analysis: CREWES Research Report, v. 6.
- Matson, S. E., 2013, Mississippi Lime Play: From Outcrop to Subsurface - The Evolution of a Play: Search and Discovery Article, v. #110170.
- Mazzullo, S. J., Wilhite, B. W., and Woolsey, W., 2009, Rhythmic Carbonate Versus Speculite Deposition in Mississippian Hydrocarbon Reservoirs in the Midcontinent USA: Causative Factors and Resulting Reservoir Petrophysical Attributes: Search and Discovery Article, v. #10209.
- McBee, W., 2003, Nemaha Strike-Slip Fault Zone: Search and Discovery Article, v. #10055.
- McCauley, R. D., Fewtrell, J., Duncan, A. J., Jenner, C., Jenner, M.-N., Penrose, J. D., Prince, R. I. T., Adhitya, A., Murdoch, J., and McCabe, K., 2000, Marine seismic surveys: Analysis and propagation of air-gun signals; and effects of air-gun exposure on humpback whales, sea turtles, fishes and squid, Australian Petroleum Production Exploration Association, Report R99-15, p. 1-198.
- Mitchell, G. C., and Berge, T. B., 2009, Structural Attribute Analysis used in Barnett Resource Development: Search and Discovery Article, v. #110095.
- Mitchell, T. M., and Faulkner, D. R., 2012, Towards quantifying the matrix permeability of fault damage zones in low porosity rocks: *Earth and Planetary Science Letters*, v. 339-340, p. 24-31.
- Mitchum, R. J., 1977, Glossary of seismic stratigraphy: AAPG Memoir, v. 26, p. 205-212.

- Motulsky, H. J., and Ransnas, L. A., 1987, Fitting curves to data using nonlinear regression: a practical and nonmathematical review: Federation of American Societies for Experimental Biology, v. 1, p. 365-374.
- Mukerji, T., Jorstad, A., Mavko, G., and Granli, J. R., 1998, Applying statistical rock physics and seismic inversions to map lithofacies and pore fluid probabilities in a North Sea reservoir, SEG.
- Najmuddin, I. J., 2003, Austin Chalk Fracture Mapping using Frequency data derived from Seismic data, Texas A&M University, p. 1-59
- Nelson, R., 2001, Geological Analysis of Naturally Fractured Reservoirs, Gulf Professional Publishing, 2<sup>nd</sup> ed. p. 1-352.
- O'Brien, P. E., 2002, Impacts of Marine Acoustic Technology on the Antarctic Environment, SCAR, p. 1-62
- Ogiesoba, O. C., 2010, Porosity prediction from seismic attributes of the Ordovician Trenton-Black River groups, Rochester field, southern Ontario: AAPG Bulletin, v. 94, no. 11, p. 1673-1693.
- Ogiesoba, O. C., 2014, Seismic Multiattribute Analysis for Shale Gas/Oil within the Austin Chalk and Eagle Ford Shale in a Submarine Volcanic Terrain, Maverick Basin, South Texas: Search and Discovery Article, v. #10601.
- Olabode, O. P., and Enikanselu, P. A., 2008, Analysis of Seismic Time-Depth Conversion using Geostatistically-Derived average velocities over "Labod" Field, Niger Delta, Nigeria: Ozean Journal of Applied Sciences, v. 1, no. 1.
- Pearce, M. A., Jones, R. R., Smith, S. A. F., and McCaffrey, K. J. W., 2011, Quantification of fold curvature and fracturing using terrestrial laser scanning: AAPG Bulletin, v. 95, p. 771-794.
- Pennington, W. D., 2002, Calibration of Seismic Attributes for Reservoir Characterization, Michigan Technological University, DE-AC26-98BC15135, p. 1-185.
- Pickett, A., 2012, New Technology Allows Mid-Continent's Operators to Capture New Reserves, The American Oil & Gas Reporter, Volume October 2012.
- Quijada, M. F., and Stewart, R. R., 2007, Density estimations using density-velocity relations and seismic inversion: CREWES Research Report, v. 19.
- Redden, J., 2013, Mississippi Lime: Independents cashing in on low-cost play, World Oil, March 2013, p. 1-8.
- Remero, A. M., and Philp, R. R., 2012, Organic geochemistry of the Woodford Shale, southeastern Oklahoma: How variable can shales be?: AAPG Bulletin, v. 96, no. 3, p. 493-517.
- Roberts, A., 2001, Curvature Attributes and their Application to 3D Interpreted Horizons: First Break, v. 19, p. 1092-1107.
- Rogers, S. M., 2001, Deposition and diagenesis of Mississippian chat reservoirs north-central Oklahoma: AAPG Bulletin, v. 85, p. 115-129.

- Rotimi, O. J., Ako, B. D., and Zhenli, W., 2014, Application of Rock and Seismic properties for prediction of Hydrocarbon potential: *Petroleum & Coal*, v. 56, no. 1, p. 41-53.
- Roy, A., Dowell, B.L., Marfurt, K. J., 2012, Characterizing a Mississippian Tripolitic Chert reservoir using 3D unsupervised seismic facies analysis and well logs: an example from Osage County, Oklahoma, SEG Las Vegas 2012 Annual Meeting, p. 1-5
- Runge, Carl 1901, Über empirische Funktionen und die Interpolation zwischen äquidistanten Ordinaten, *Zeitschrift für Mathematik und Physik* 46: 224–243.
- Sharma, R. K., and Chopra, S., 2013, Poisson impedance inversion for characterization of sandstone reservoirs, SEG Houston 2013 Annual Meeting, p. 2549-2553.
- Shelton, J. W., Ross, J. S., Garden, A. J., and Franks, J. L., 1985, Geology and Mineral Resources of Payne County, Oklahoma, *in* USGS, ed., Volume Bulletin: 137.
- Sheriff, R. E., and Geldart, L. P., 1982, *Exploration Seismology*, Cambridge University Press.
- Skirius, C., Nissen, S., Haskell, N., Marfurt, K. J., Hadley, S., Ternes, D., Michel, K., Reglar, I., D'Amico, D., Delencourt, F., Romero, T., D'Angelo, R., and Brown, B., 1999, 3D seismic attributes applied to carbonates: *The Leading Edge*, v. 18, p. 384-393.
- Soubotcheva, N. L., and Stewart, R. R., 2005, Delineating a sandstone reservoir at Pikes Peak, Saskatchewan using 3C seismic data and well logs: CREWES Research Report, v. 17.
- Sridhar, K., Sundaram, A. A. K., Tilak, V. B. G., and Mohan, S., 2004, Seismic Inversion on 3D Data of Bassein Field, India, 5th Conference & Exposition on Petroleum Geophysics: Hyderabad, India, p. 526-532.
- Staples, E. R., 2011, *Subsurface and Experimental Analysis of Fractures and Curvature*: University of Oklahoma, p. 1-88.
- Taner, M. T., 2001, *Seismic Attributes: CSEG Recorder*.
- Taner, M. T., Koehler, F., and Sheriff, R. E., 1979, Complex seismic trace analysis: *Geophysics*, v. 44, no. 6, p. 1041-1063.
- Urgeles, R., Camerlenghi, A., Garcia-Castellanos, D., Mol, B. D., Garces, M., Verges, J., Haslam, I., and Hardman, M., 2011, New constraints on the Messinian sealevel drawdown from 3D seismic data of the Ebro Margin, western Mediterranean: *Basin Research*, v. 23, p. 123-145.
- Wang, J., and Dopkin, D., 2008, Visualization, Analysis, and Interpretation of Seismic Attributes for Characterizing a Carbonate Reservoir, 7th International Conference & Exposition on Petroleum Geophysics.
- Weyl, P. K., 1960, Porosity through dolomitization: conservation-of-mass requirements: *Journal of Sedimentary Petrology*, v. 30, no. 1, p. 85-90.
- WhiteIII, H. G., 2013, *Fracturing of Mississippi Lime, Oklahoma: Experimental, seismic attributes and image logs analyses* [Master: University of Oklahoma.
- Widess, M. B., 1973, How thin is a thin bed?: *Geophysics*, v. 38, no. 6, p. 1176-1180.

Wojslaw, R., Stein, J. A., and Langston, T., 2012, 5D semblance-based interpolator in exploration-theory and practice, 74th EAGE Conference and Exhibition, Extended Abstracts, Volume B024.

Woodward, M. J., 2008, A decade of tomography: Geophysics, v. 73, no. 5, p. VE5-VE11.

Yilmaz, O., 1987, Seismic Data Processing, SEG: Tulsa, Oklahoma.

Zheng, D., Zhang, L., and Shen, F., 2011, Characterization and Modeling Study of Karst Networks in the Ordovician Carbonate Reservoirs, Tarim Basin: Search and Discovery Article, v. #40795.

## LIST OF TABLES

	Fracture Density	Amplitude	Frequency	Phase	Incoherence	Negative Curvature	Positive Curvature
Fracture Density	● 1.0	● 0.132	● 0.065	● -0.335	● -0.476	● 0.269	● -0.183
Amplitude	● 0.132	● 1.0	● 0.722	● -0.039	● -0.271	● 0.458	● 0.193
Frequency	● 0.065	● 0.722	● 1.0	● -0.357	● -0.377	● 0.203	● 0.031
Phase	● -0.335	● -0.039	● -0.357	● 1.0	● 0.651	● 0.146	● 0.310
Incoherence	● -0.476	● -0.271	● -0.377	● 0.651	● 1.0	● 0.293	● 0.594
Negative Curvature	● 0.269	● 0.458	● 0.203	● 0.146	● 0.293	● 1.0	● 0.750
Positive Curvature	● -0.183	● 0.193	● 0.031	● 0.310	● 0.594	● 0.750	● 1.0

Table 1: Attribute cross correlation Table. Fracture interpreted in FMI are in the subsurface along a wellbore. They are first projected vertically up to the Mississippian Top so that they are consistent with attributes, which that are mapped along a surface. Table showing linearity of a single attribute with the rest including fracture density. Higher magnitude indicates better correlation between two attributes. The multivariate model uses attributes in (Figures Figure 29Figure 30Figure 31Figure 32,Figure 34) as input and outputs fracture density.

## LIST OF FIGURES



Figure 1: Mississippian Play. The green outline represents the extents of the Mississippian Limestone play covering parts of Kansas and Oklahoma. In the south-western portion, labelled in red, is where the dataset for this research is located.

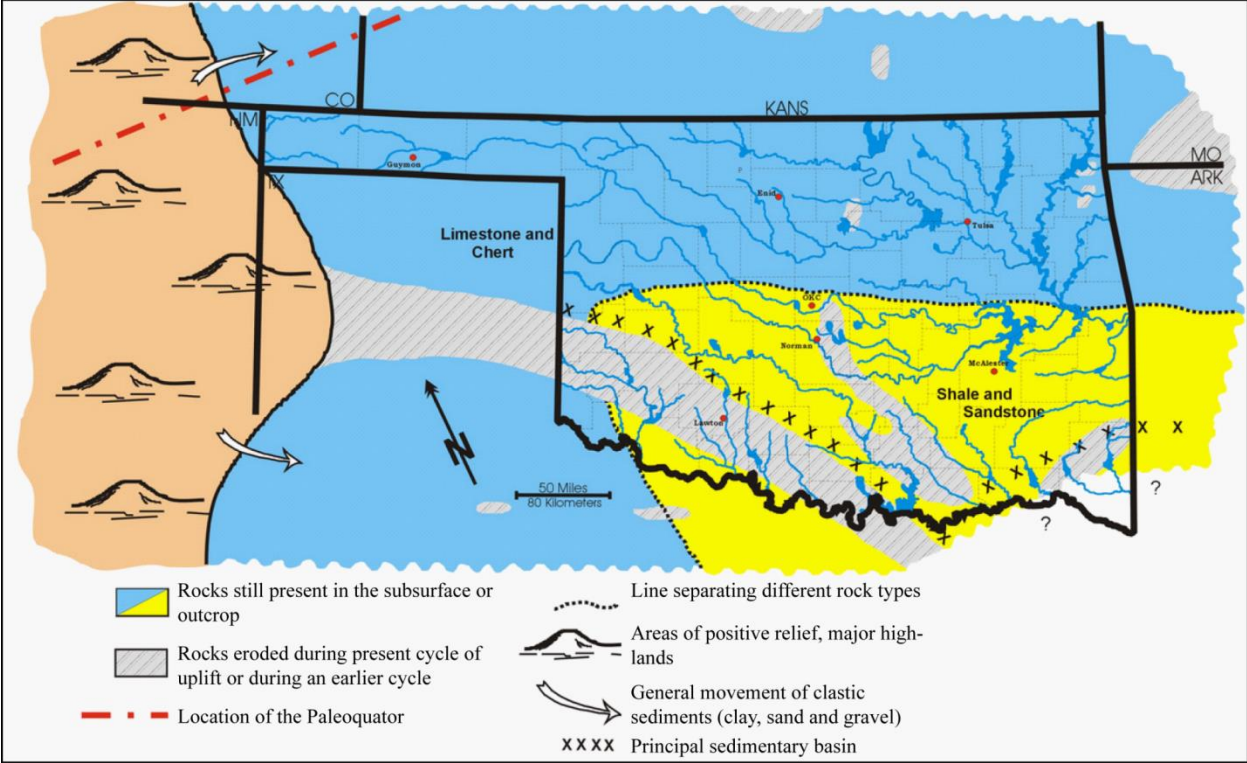


Figure 2: Paleogeography during the Mississippian. The Oklahoma-Kansas border was near the paleo-equator, creating conditions for carbonate generation (Johnson, 1995).

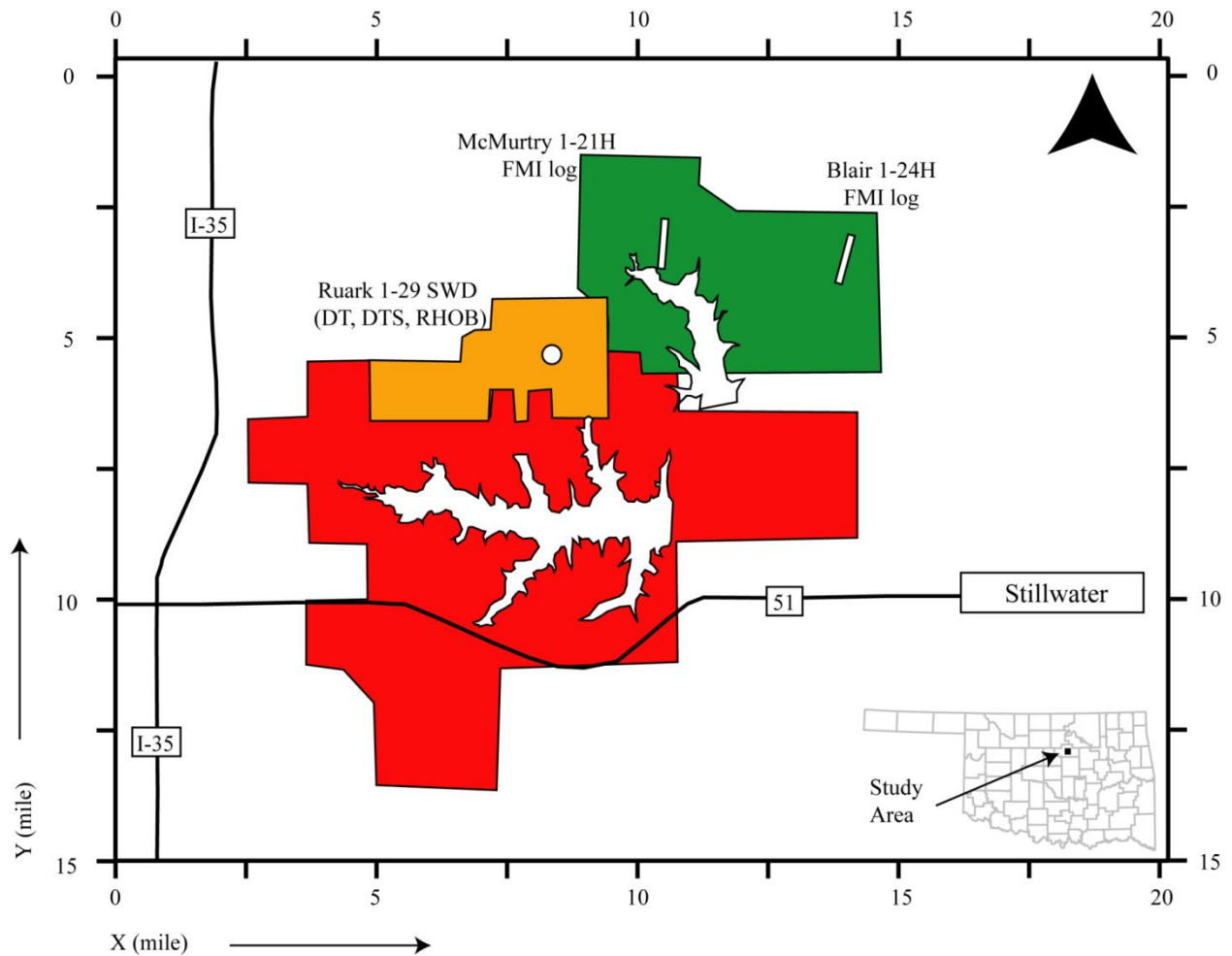


Figure 3: Base map showing the location of seismic and well data used in this study from the northwest portion of Payne County, Oklahoma. The surveys are outlines in red, orange, and green and hereafter referred to as Lake Carl Blackwell, Lake Carl Blackwell mini, and the McMurtry survey. Wells used in this thesis are indicated with solid dots and labeled. Logs available in the Ruark 1-29 SWD are DT: Sonic, DTS: Shear-sonic; Rhob: Density and FMI's were logged along the horizontal section of the Blair 1-24H and McMurtry 1-21H wells. Lakes Carl Backwell and McMurtry are outlined.




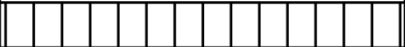

<b>System</b>	<b>Subsurface Nomenclature (Subsystem/Group/Formation)</b>
<b>Carboniferous</b>	<b>Pennsylvanian</b>
	 <b>Mississippian "Limestone"</b>
<b>Devonian</b>	<b>Woodford Shale</b>
	
<b>Silurian</b>	<b>Hunton Group</b>
<b>Ordovician</b>	<b>Sylvan Shale Viola Group Simpson Group</b>
	<b>Arbuckle Group</b>
<b>Cambrian</b>	 <b>Reagan Sandstone</b>
<b>Proterozoic</b>	<b>Basement Crystalline Rocks</b>

Figure 4: Stratigraphic column. Generalized stratigraphic column for Payne County, Oklahoma.

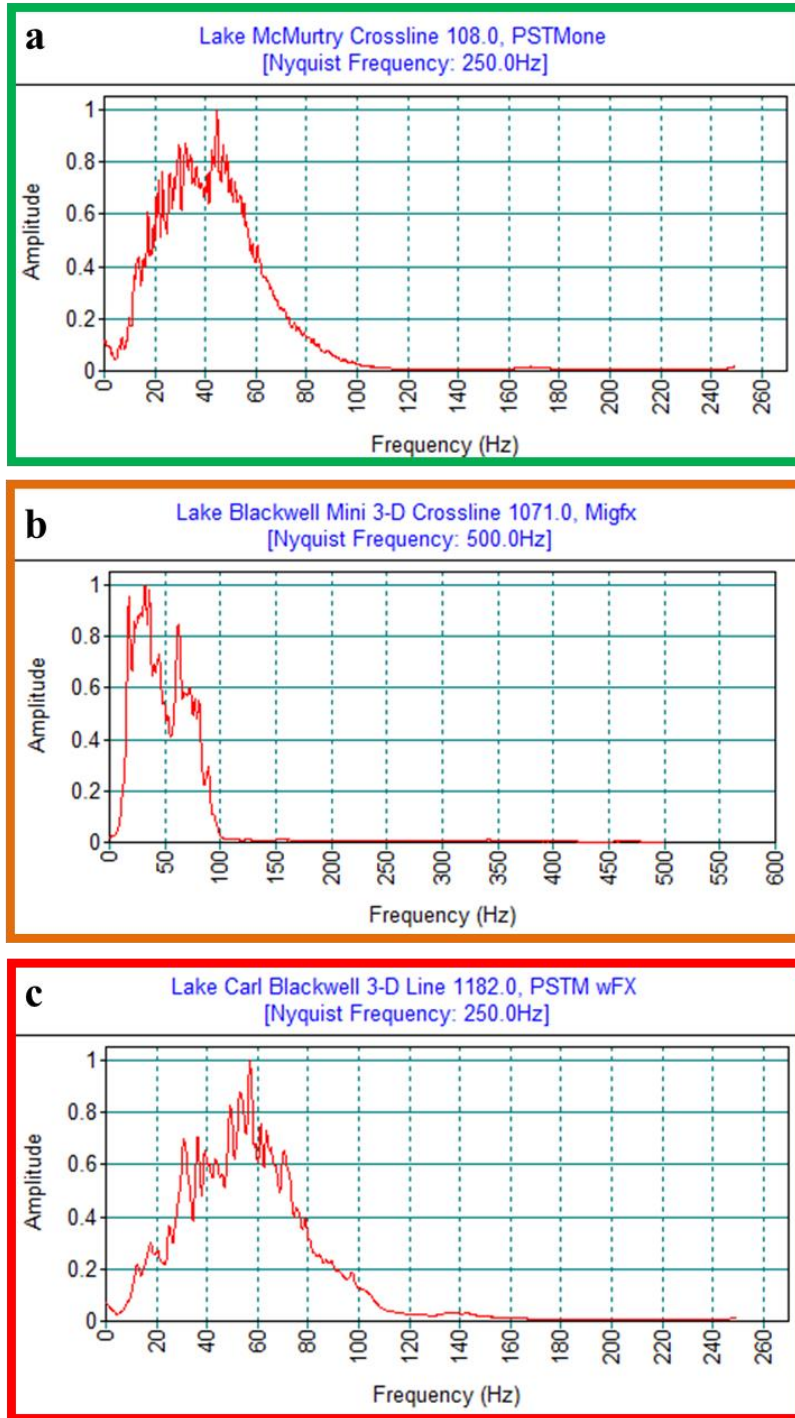


Figure 5: Frequency spectrum for the LMM (a), LCBm (b) and LCB (c) surveys. The frequency content and spectrum shape will determine the character of the survey's wavelet. This is important when evaluating tuning thicknesses.

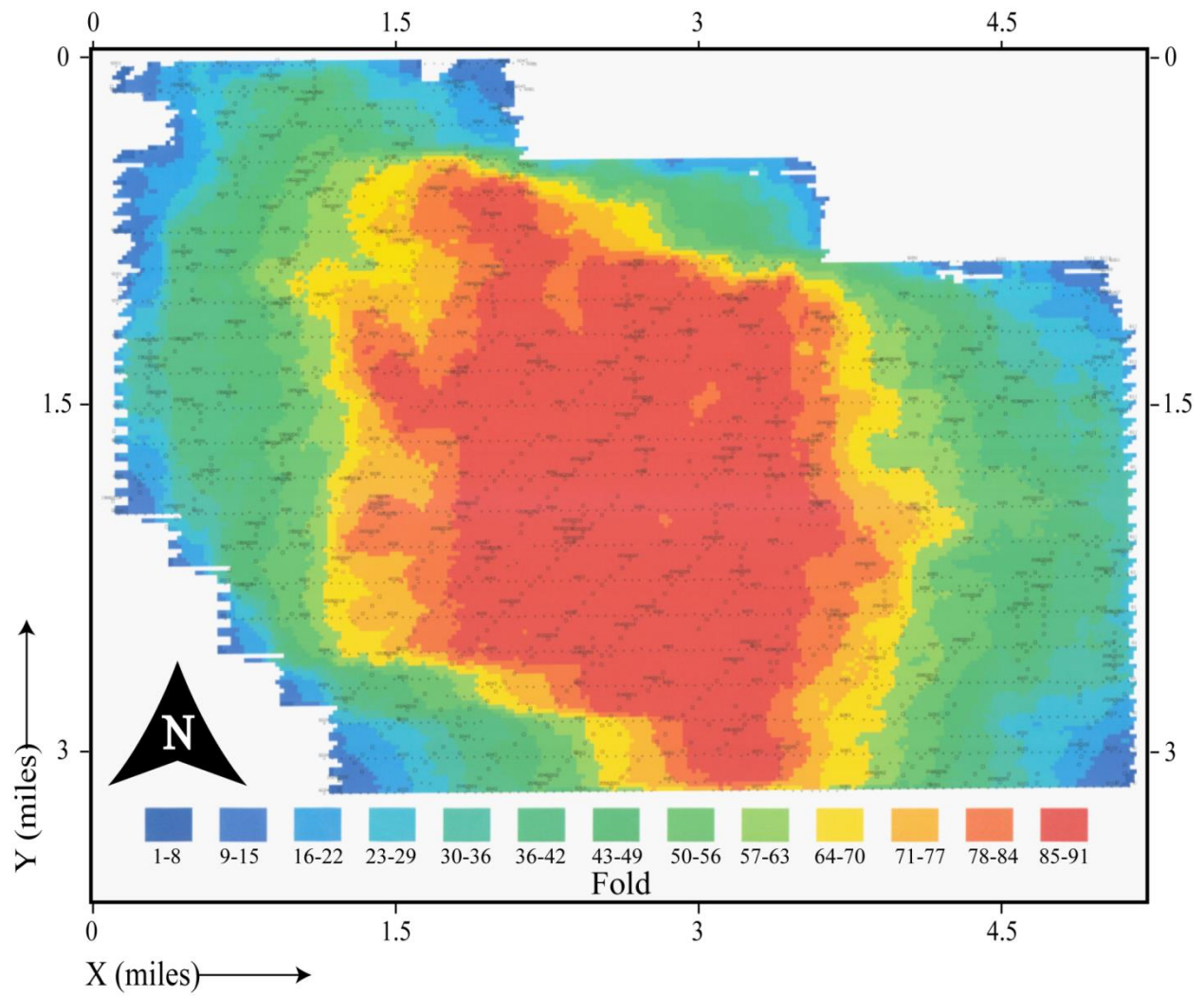


Figure 6: The LMM survey fold map has a maximum fold of 91. Fold map shows trends that cross-cut attribute trends. This means that there was likely some type of fold normalization. Out of all the surveys the LMM is the best candidate for better seismic attribute analysis.

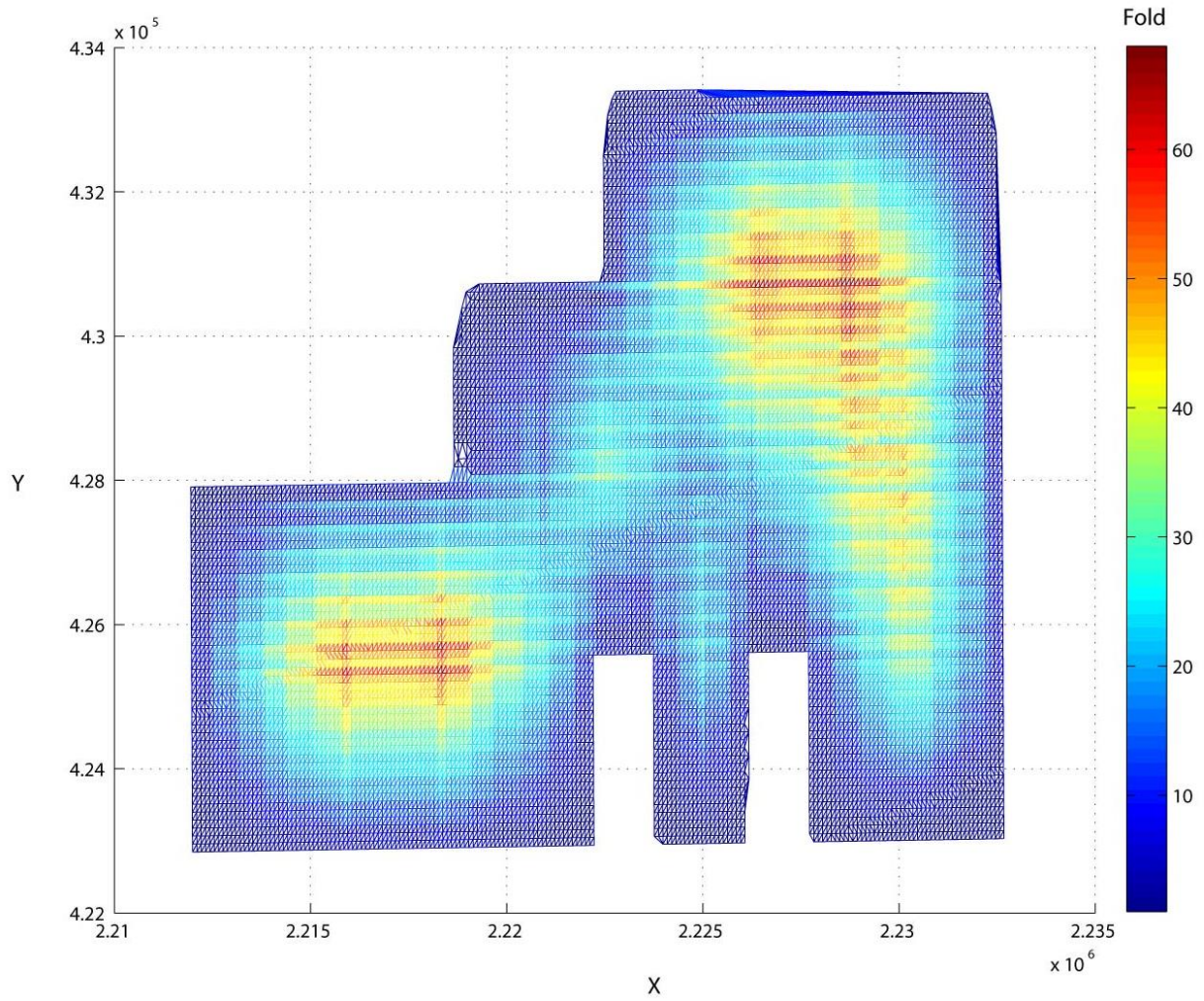


Figure 7: The LCBm survey fold map has a maximum fold of 70. It too has a high visual correlation to fold. However, in addition, it also has apparent foot-print that is evident in the fold map and amplitudes.

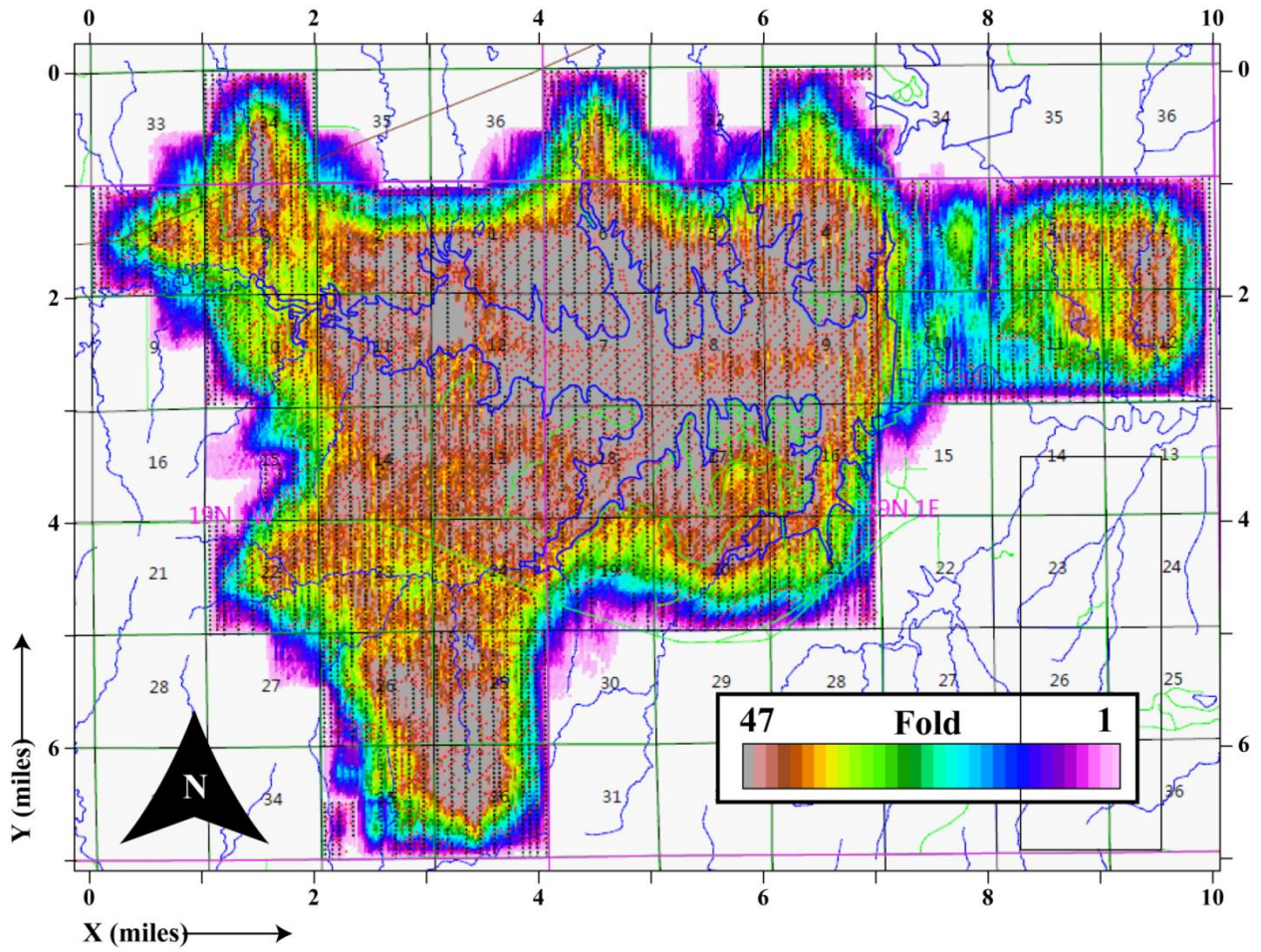


Figure 8: The LCB survey fold map has a maximum fold of 47. Fold indicates the number of traces that were stacked to a single bin location. This map represents the traces that were stacked out to 7000 ft away used to process the data set. Visually there is a high correlation between fold and amplitude along the top of the Mississippian.

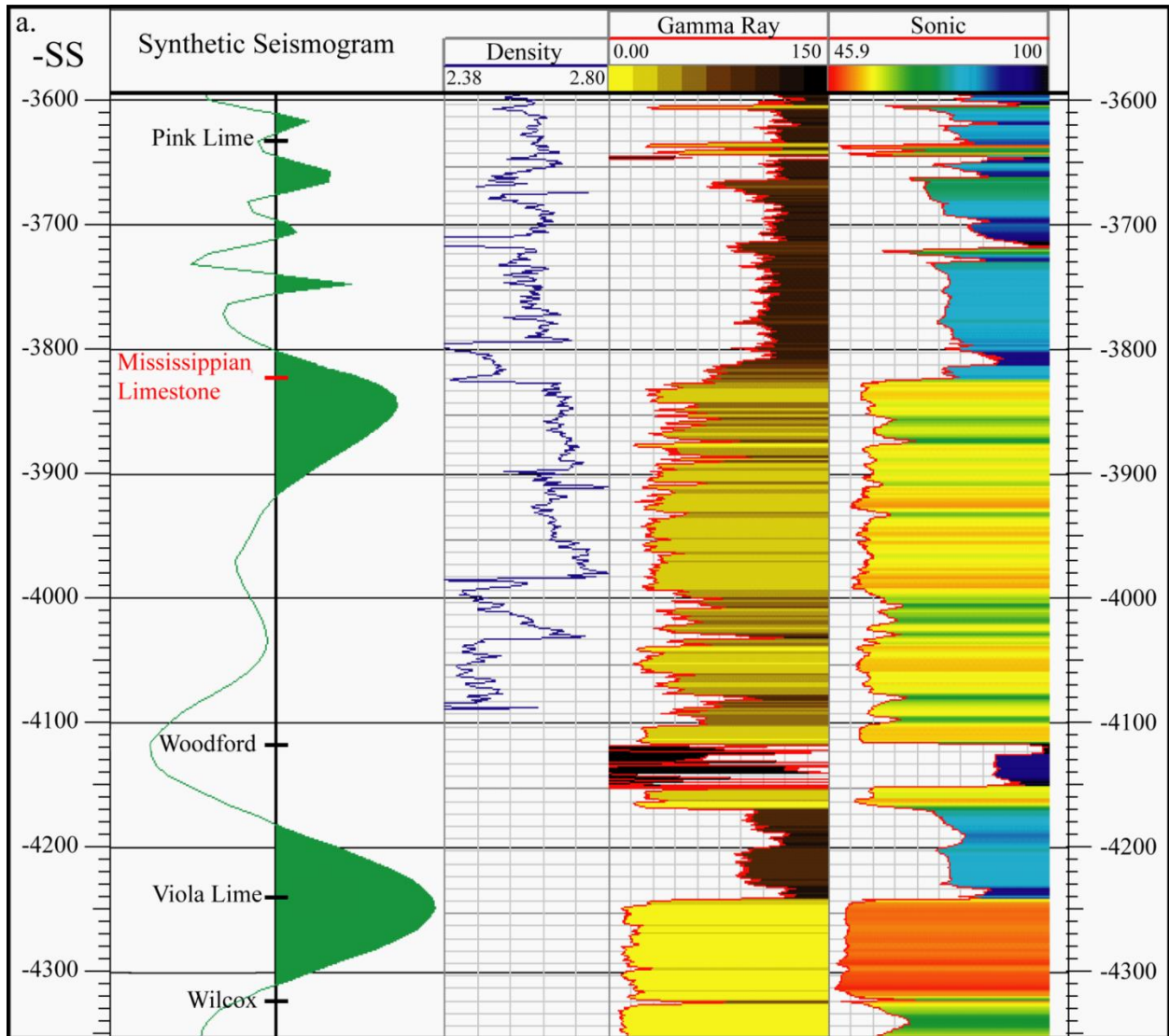


Figure 9: Interpretation of formations that have reflectivity in seismic data on Ruark 1-29 SWD log suite: density, gamma-ray, and sonic log. Figure also shows synthetic seismogram. The Mississippian and the Viola top are the two strongest reflections and therefore most readily identifiable in the seismic volume.

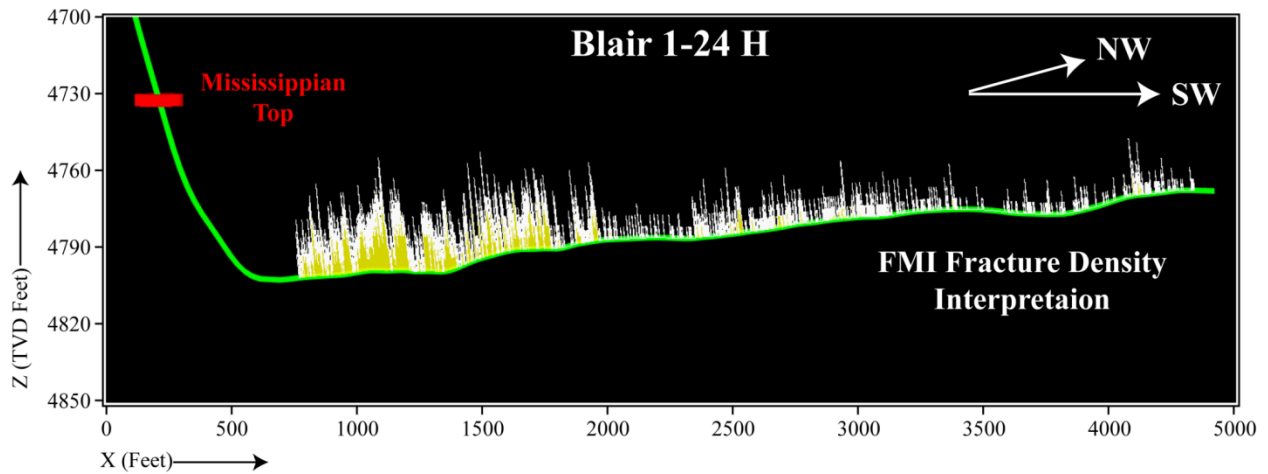


Figure 10: Fracture density interpreted from the FMI log is superimposed on the Blair 1-24H 1-24H wellbore trajectory.

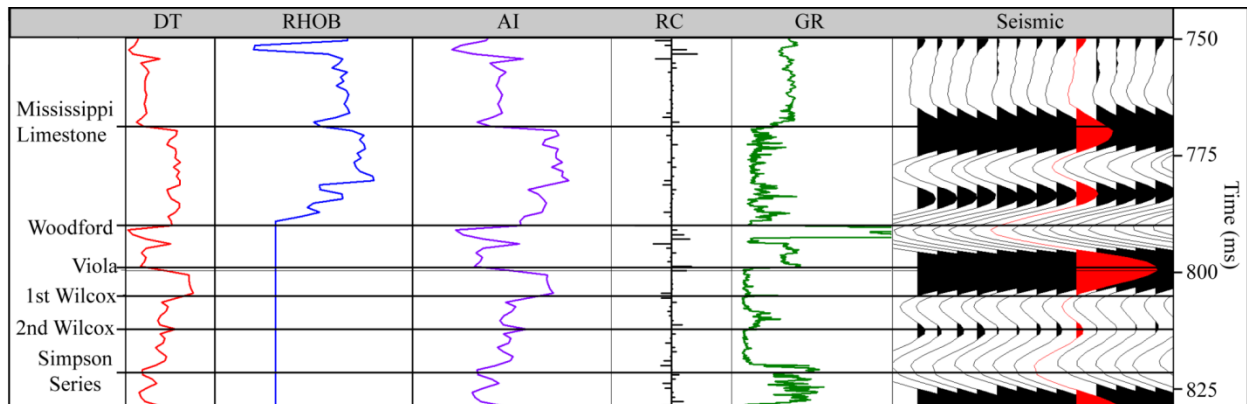


Figure 11: Generation of the Ruark 1-29 SWD well synthetic seismogram. Log-symbols have the following meaning. DT: sonic, RHOB: density, AI: acoustic impedance, RC: reflectivity series, GR: gamma-ray, and Seismic data extracted from around the wellbore. The formations are labeled. Note that the density log was not recorded below the Woodford.

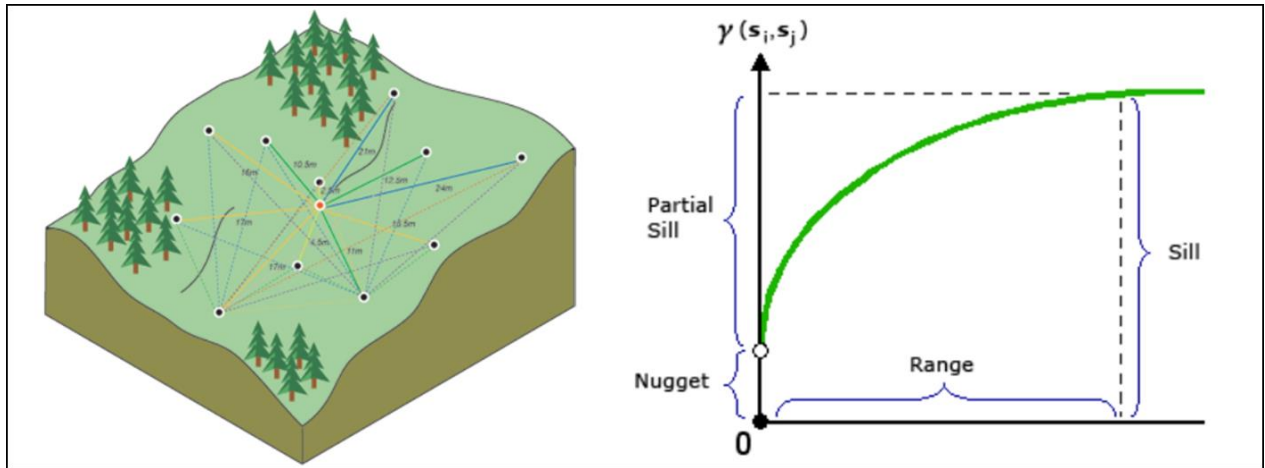


Figure 12: Geostatistical mapping cartoon illustrating how variance is determined. For a given set of spatial data, a model, known as a variogram, captures the variation in data between sets of two points with respect to the increasing separation between data pairs. The guiding principle is that variability in data from a location pair is irrespective of the spatial location of the pair. Consequently, although the variability increases with distance between the location-pairs, the increase is predictable. Range represents distance between the location-pairs past which data variability does not increase significantly. Sill is the value of variability at the range. Nugget represents variability at data from location-pairs with infinitely small separation.



## Kriging



## Cokriging



Figure 13: Kriging and cokriging flow chart. In kriging data is interpolated between sampled locations only based on data variability between sample pairs. In cokriging the primary variable is interpolated using the secondary variable as a guide. Fidelity of cokriging depends on how well the primary and secondary variables are related.

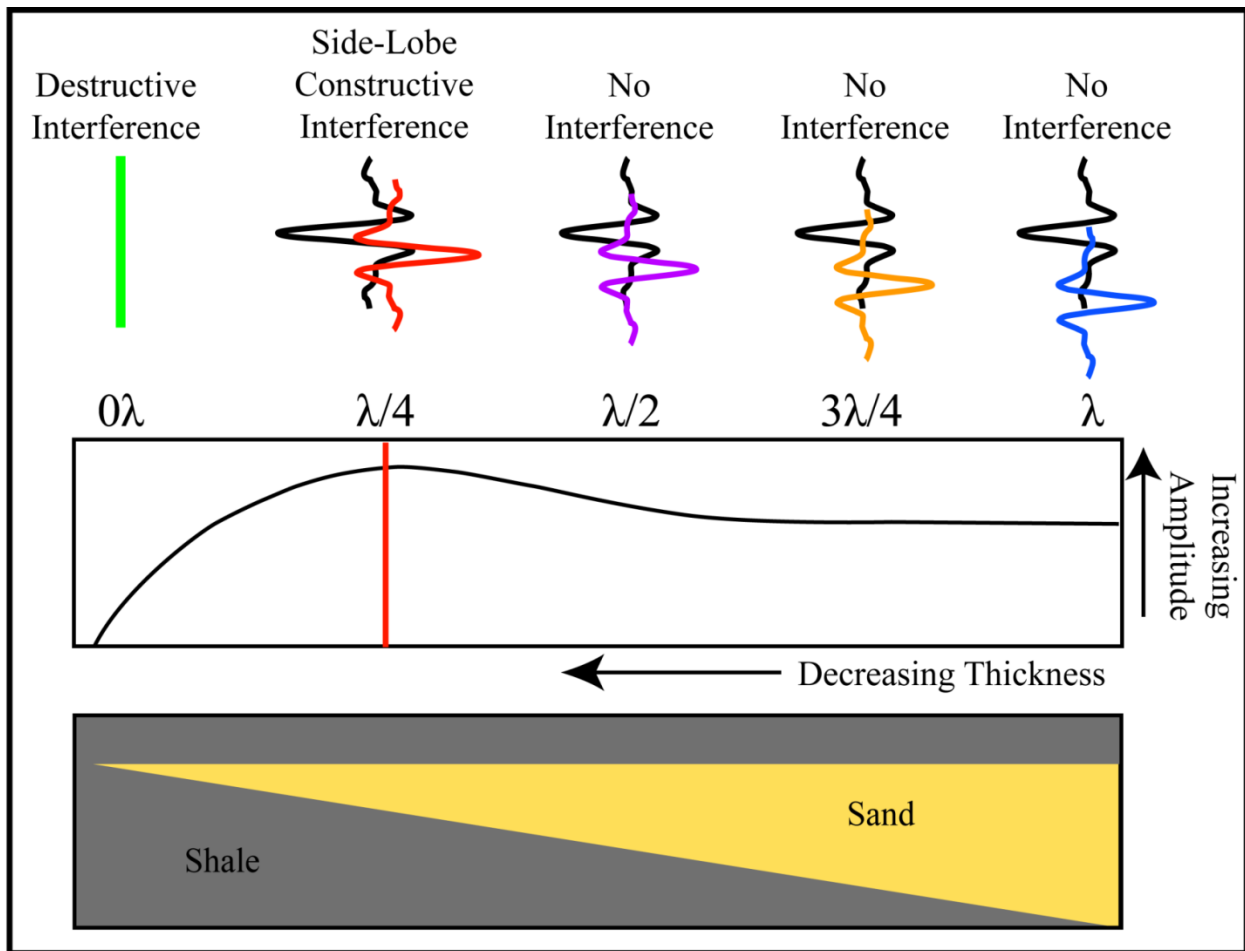


Figure 14: An example of a wedge model seismic amplitude response. A wedge shaped sand feature is encased in shale. Wavelets reflected from top and base of the wedge starts interfering at tuning thickness. The wavelet constructively interferes at a tuning thickness of  $\frac{1}{2}$  wavelength, reaching a maximum at  $\frac{1}{4}$  wavelength after which the interference becomes destructive.

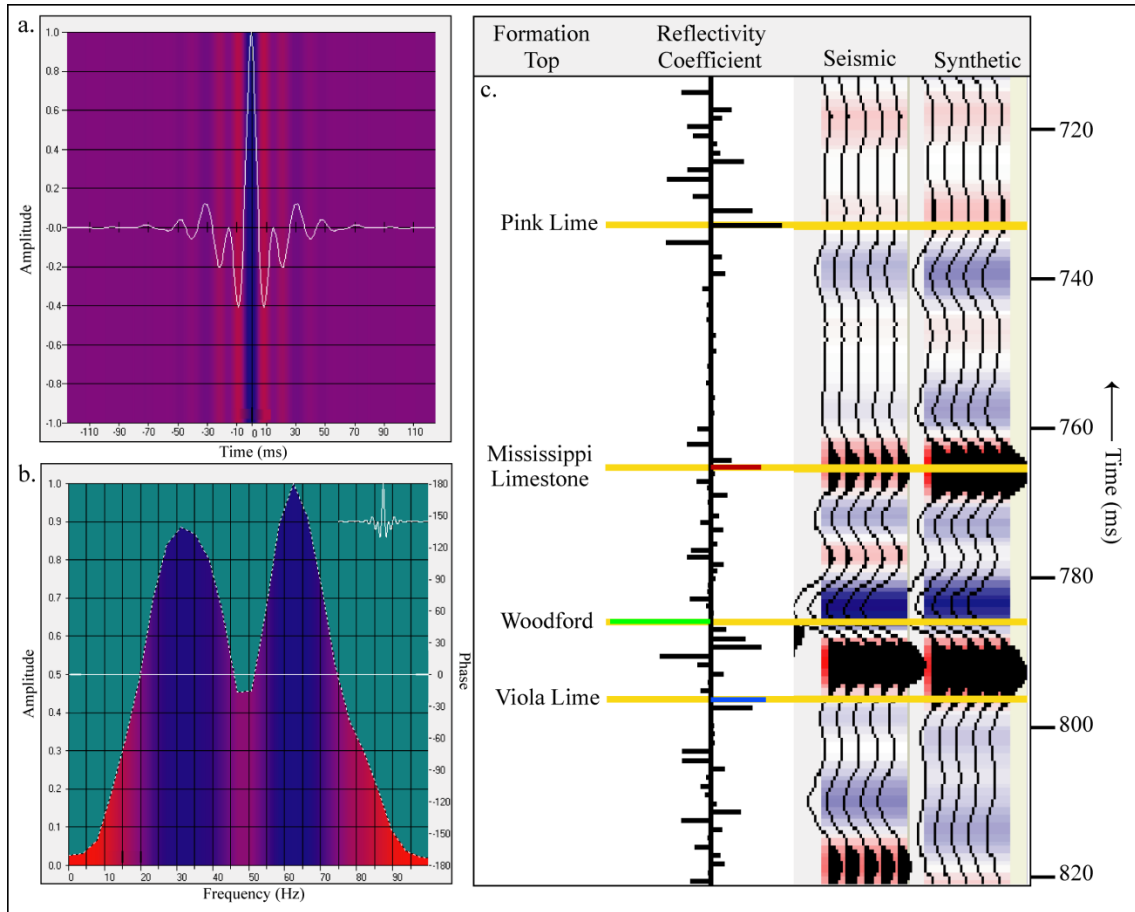


Figure 15: Well to seismic tie at Ruark location. (a) Wavelet extracted from the seismic volume. (b) Frequency spectrum. Note the bimodal nature of the frequency content which could be a consequence of imperfect merger of land and lake survey. (c) Synthetic tie. The correlation coefficient between synthetic and real data has a reasonably high value of 0.79. Phase of the synthetic data compares better to real data than amplitudes. Key formations are labeled.

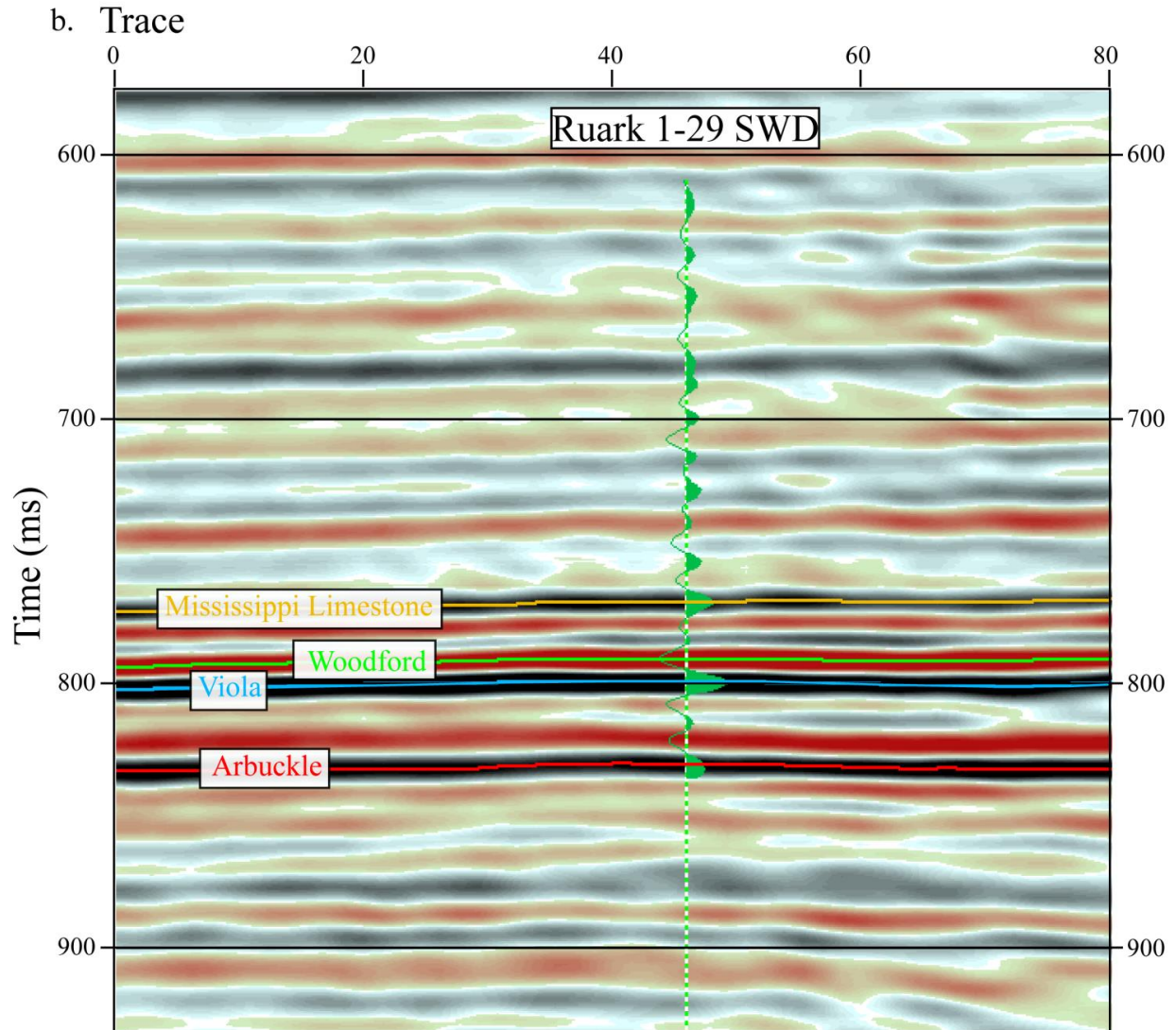


Figure 16: An image of the representative seismic section illustrating the tie between the synthetic trace and key reflectors in the vicinity of the Ruark 1-29 SWD. Horizons are identified using the well-to-seismic tie and then are extended across the surveys. The Pennsylvanian-Mississippian interface has a significant acoustic contrast and is identified as a strong peak. Likewise, the impedance between the Mississippian carbonate section and Woodford Shale is also dramatic, and thus creates a strong trough. The importance of identifying these two interfaces is that the boundary of the Mississippian section is constrained.

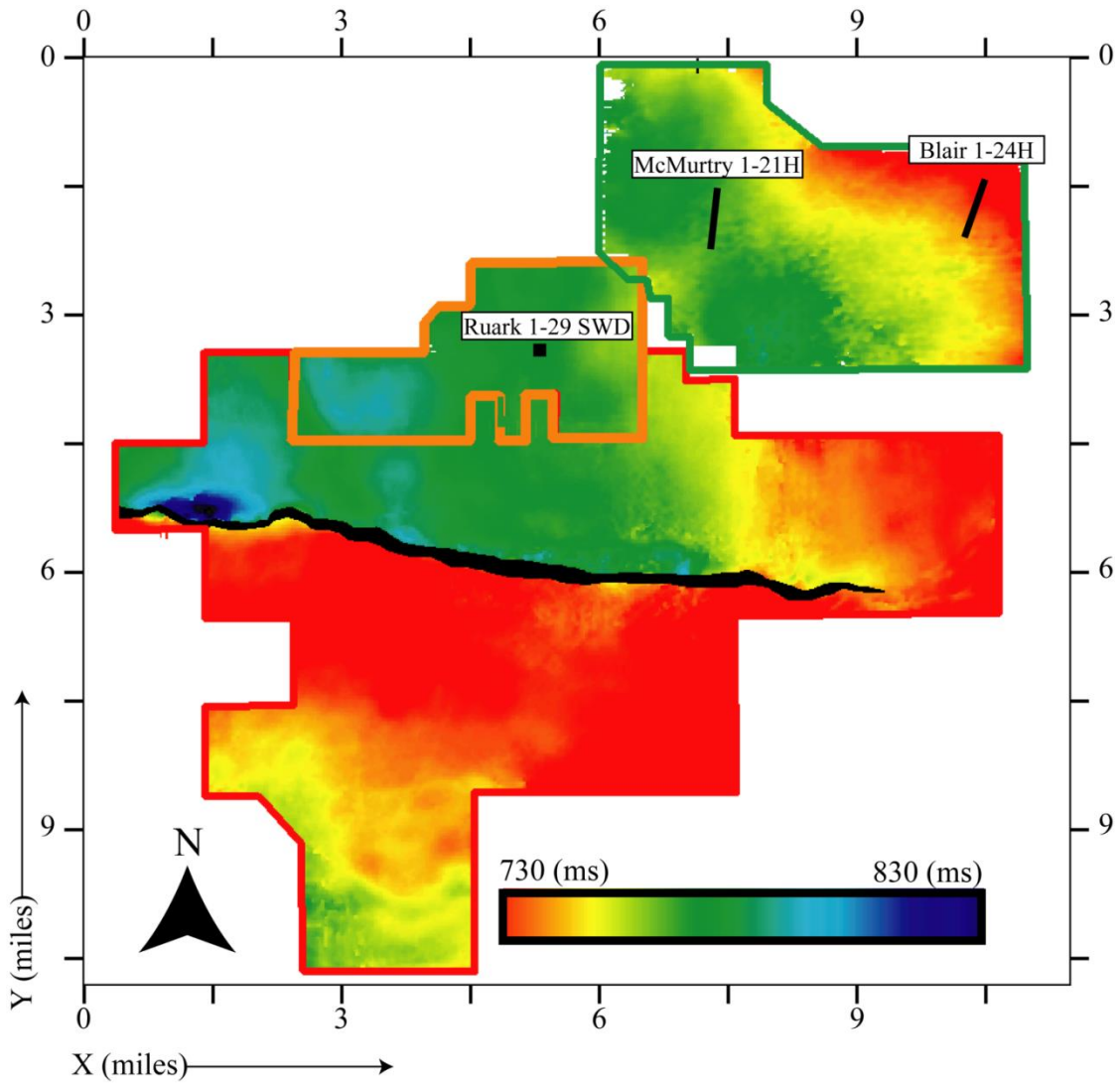


Figure 17: The Mississippian time surface structure map interpreted on all seismic surveys. Time structure after merging the three seismic surveys. The prominent east-west fault with downthrown side to the north corresponds to the location of Lake Carl Blackwell. For exploration and production, the time structure map needs to be converted into a depth structure map. In this thesis, the depth map is obtained through a geostatistical cokriging method.

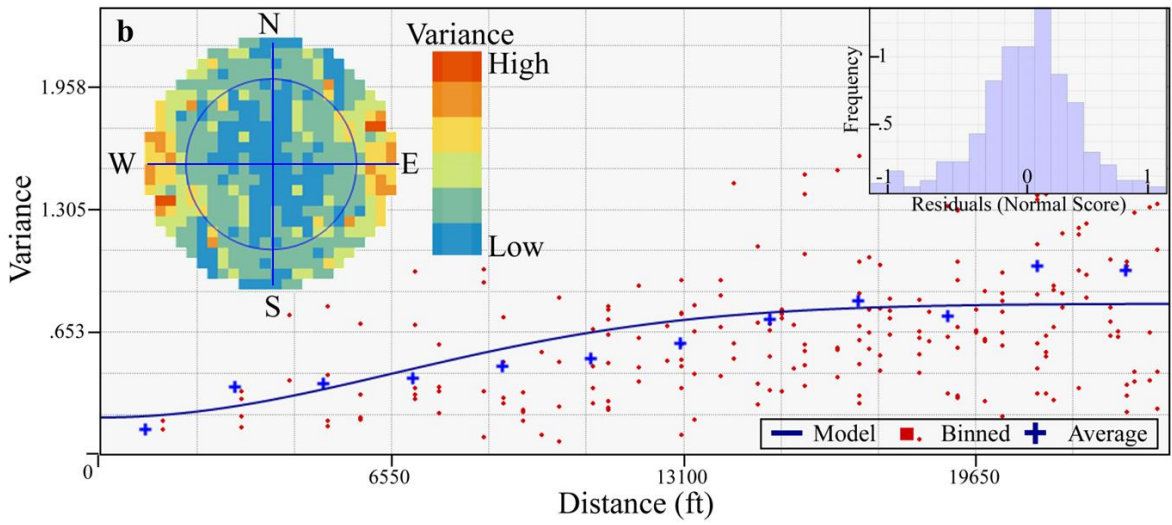
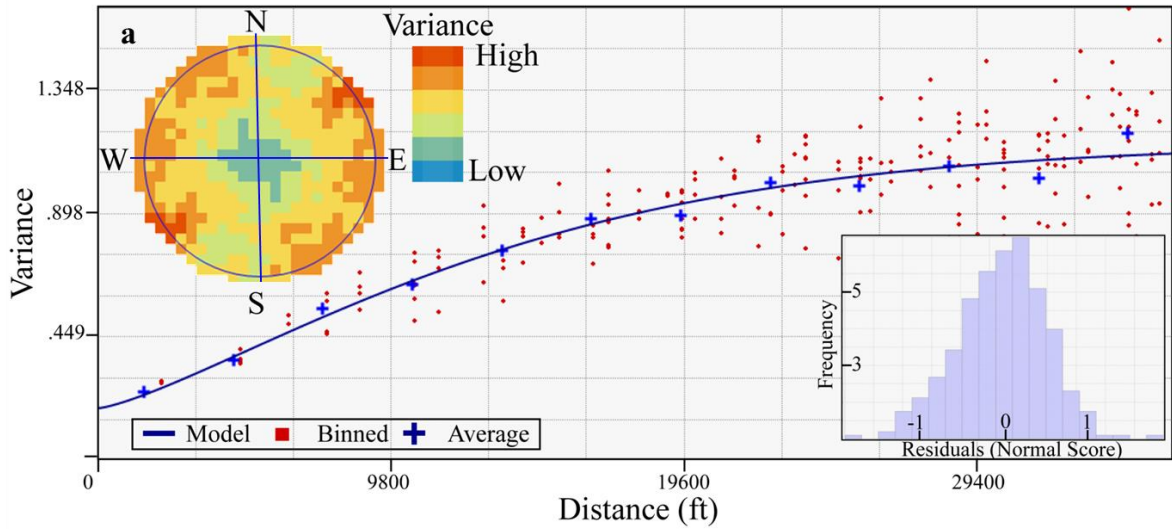


Figure 18: Geostatistical models comparing data variance between a (a) kriging semivariogram and (b) cokriging semivariogram. In (a) and (b) red dots represent data variance between location pairs, blue crosses represent average variance for 320ft wide bins and the solid blue line represents the model predictions; the variance cloud inset shows the azimuthal behaviour of the model, the blue and red colors in the cloud represent lower and higher variance respectively and the circle represents the range. In (a) and (b) histogram of data variance after detrend is shown in inset. As expected, variance increases with lag.

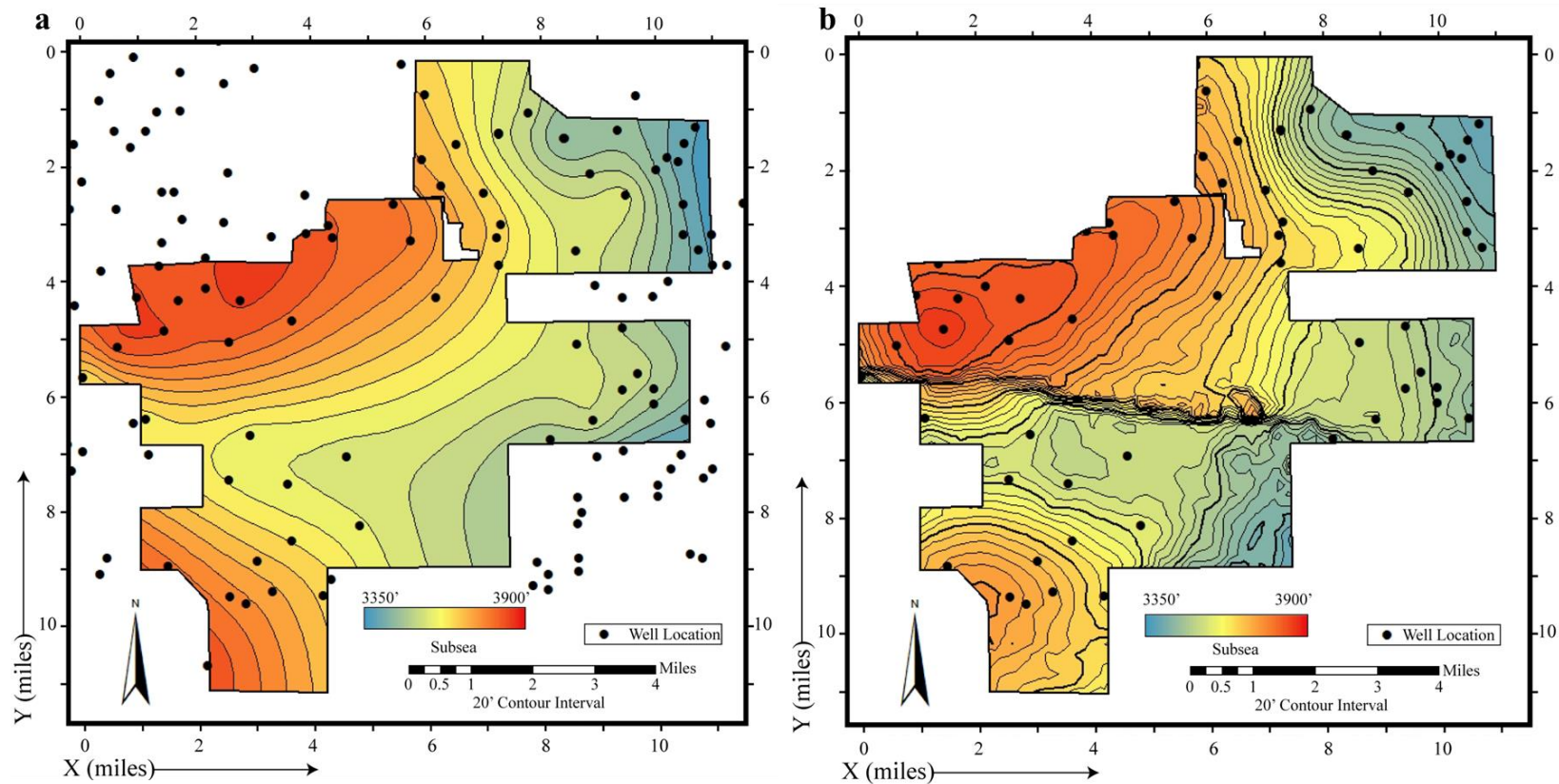


Figure 19: Subsea depth structure maps created from (a) kriging and (b) cokriging techniques. In (a) the model uses 350 wells. Note that the expected east-west fault trend (underlying Lake Cark Blackwell; Figure 3) does not appear in (a) as this trend is not sampled by wells. In (b) the model only utilized 65 well depths as primary variable and the time-structure (Figure 17) as secondary variable. Note the clearly imaged east-west fault trend strongly illustrating the utility of seismic data in geostatistical modeling.

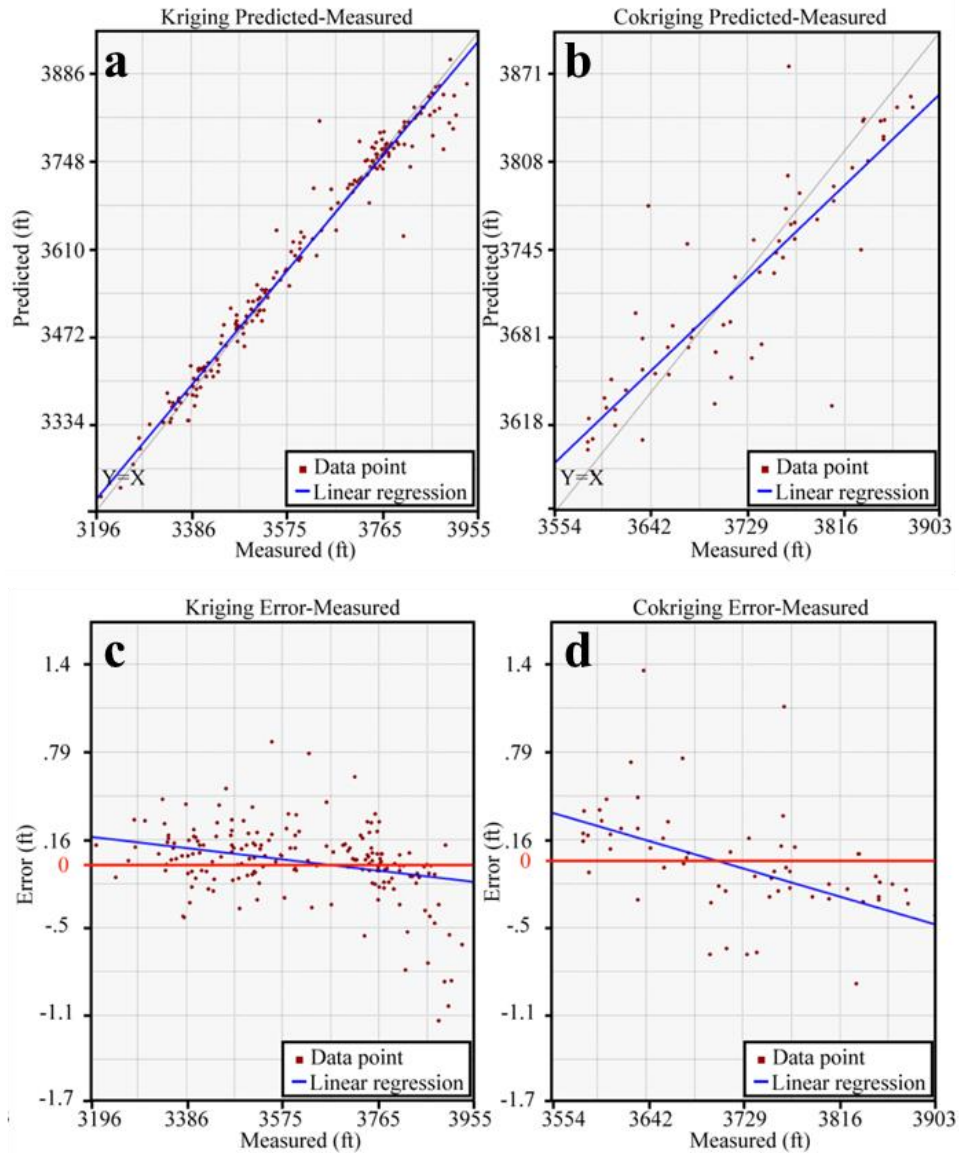


Figure 20: Validation of geostatistical structure maps. Predicted versus measured Mississippi top depth from (a) Kriging and (b) Co-kriging. In (a) and (b), prediction from a hypothetical ideal model is indicated in grey line. Prediction error versus Mississippi top depth from (c) Kriging and (d) Co-kriging. Although model prediction is better from Kriging, geological features that are not sampled by wells can only be predicted by Co-kriging (Figure 19b). In (c) and (d) the zero error line is in red. In Kriging prediction error is minimum at shallow depths while no such correlation exists in the Co-kriging model.



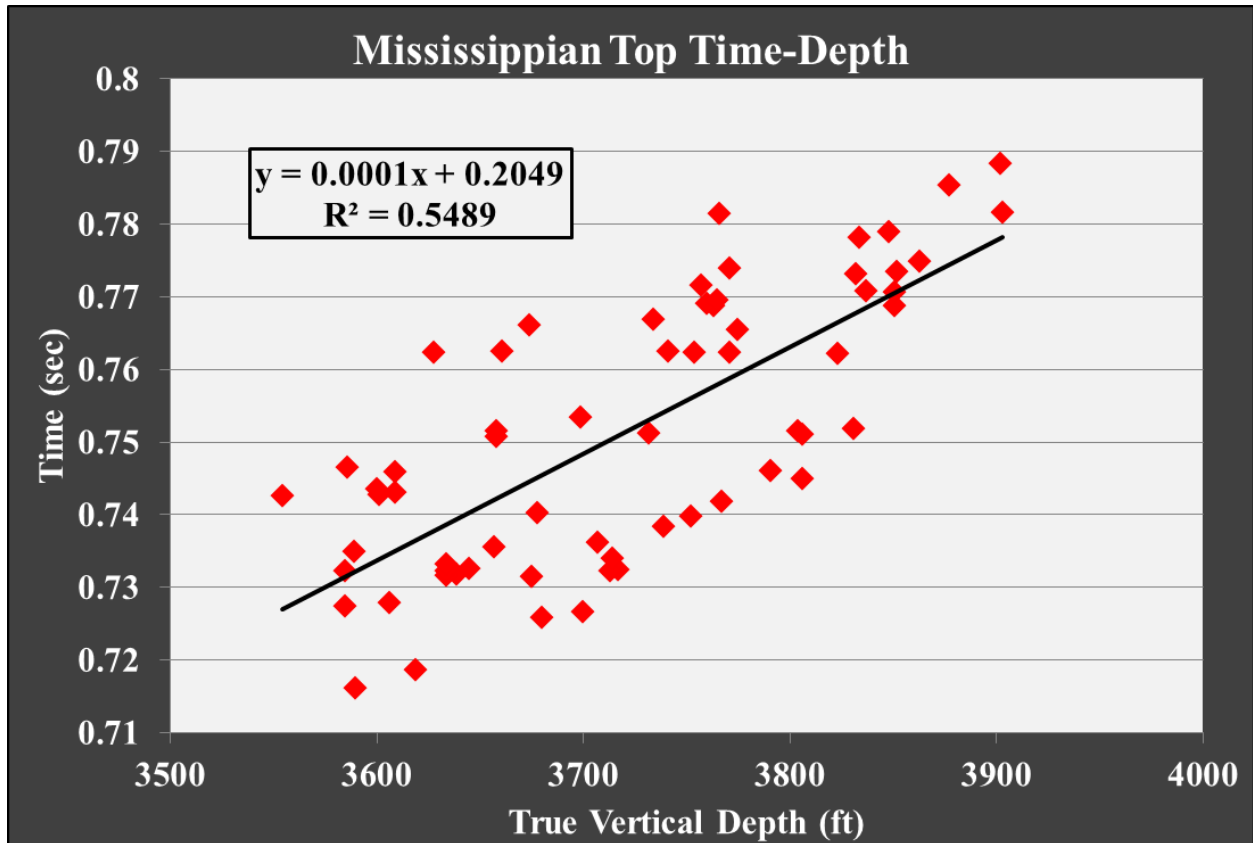


Figure 21: Plot of Mississippian true vertical depth (feet) against seismic time in seconds. The  $r^2$  correlation between the depth and time at the all the wells in the survey is 0.55. A correlation of unity would imply a uniformly varying overburden velocity field which has been adequately captured in processing. The plot therefore suggests that there is a reasonable variation in overburden velocity. The correlation value is however adequate for cokriging the primary variable (depth) with the secondary variable (time).

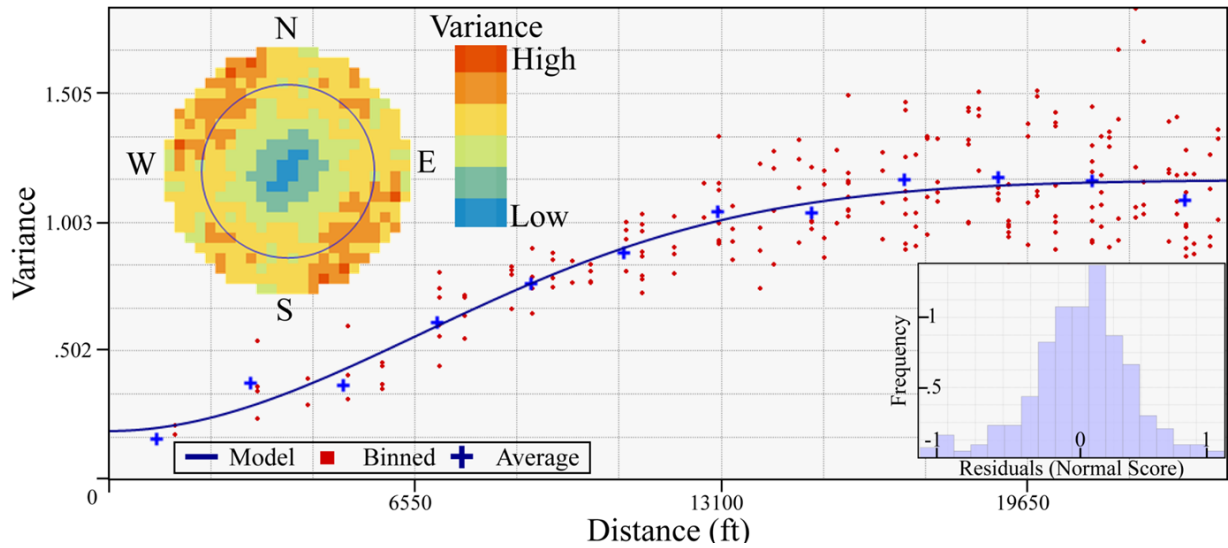


Figure 22: Semivariogram model for kriging isopach. Red dots represent data variance between location pairs, blue crosses represent average variance for 2100ft wide bins and solid blue line represents the model predictions; the variance cloud inset shows the azimuthal behaviour of the model, the blue and red colors in the cloud represent lower and higher variance respectively and the circle indicates the range. The histogram of data variance after detrending is shown in inset. The variance increases significantly with distance.

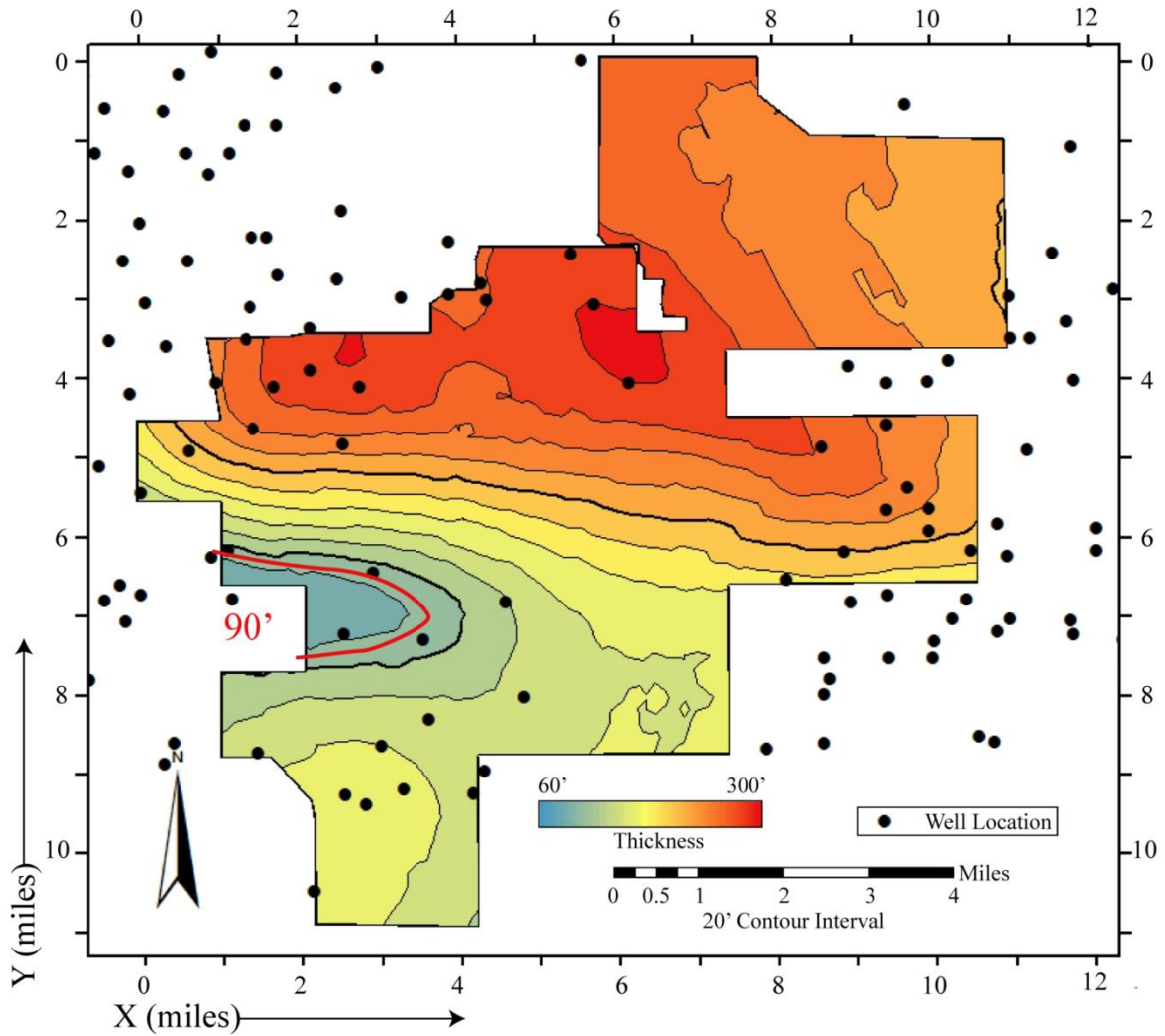


Figure 23: Geostatistically generated Mississippian isopach map created from well data. Formation thickness significantly changes across the east-west trending fault (Figure 19b); the downthrown side (north) has a thicker section. The thinning on the upthrown (south) is likely due to erosion. Formation thickness affects amplitudes through tuning (Figure 14). The contour representing the limit of amplitude reliability (90 ft in this case; Figure 28) is marked in red.

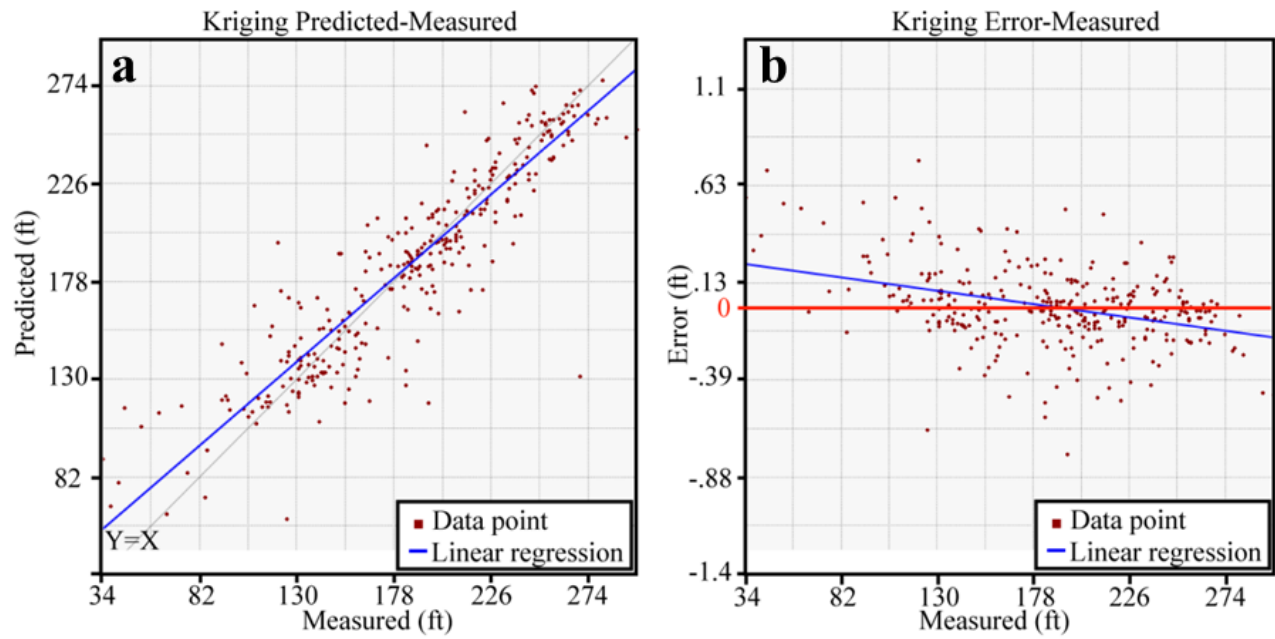


Figure 24: Validation of geostatistically generated isopach map. Predicted thicknesses from the statistical model versus measured Mississippian isopach from (a) kriging. In (a), prediction from a hypothetical ideal model is indicated in grey line. Prediction error versus Mississippian isopach from (b) Kriging. In (b) the zero error line is in red. The best prediction is for intermediate thicknesses, which is not intuitive.

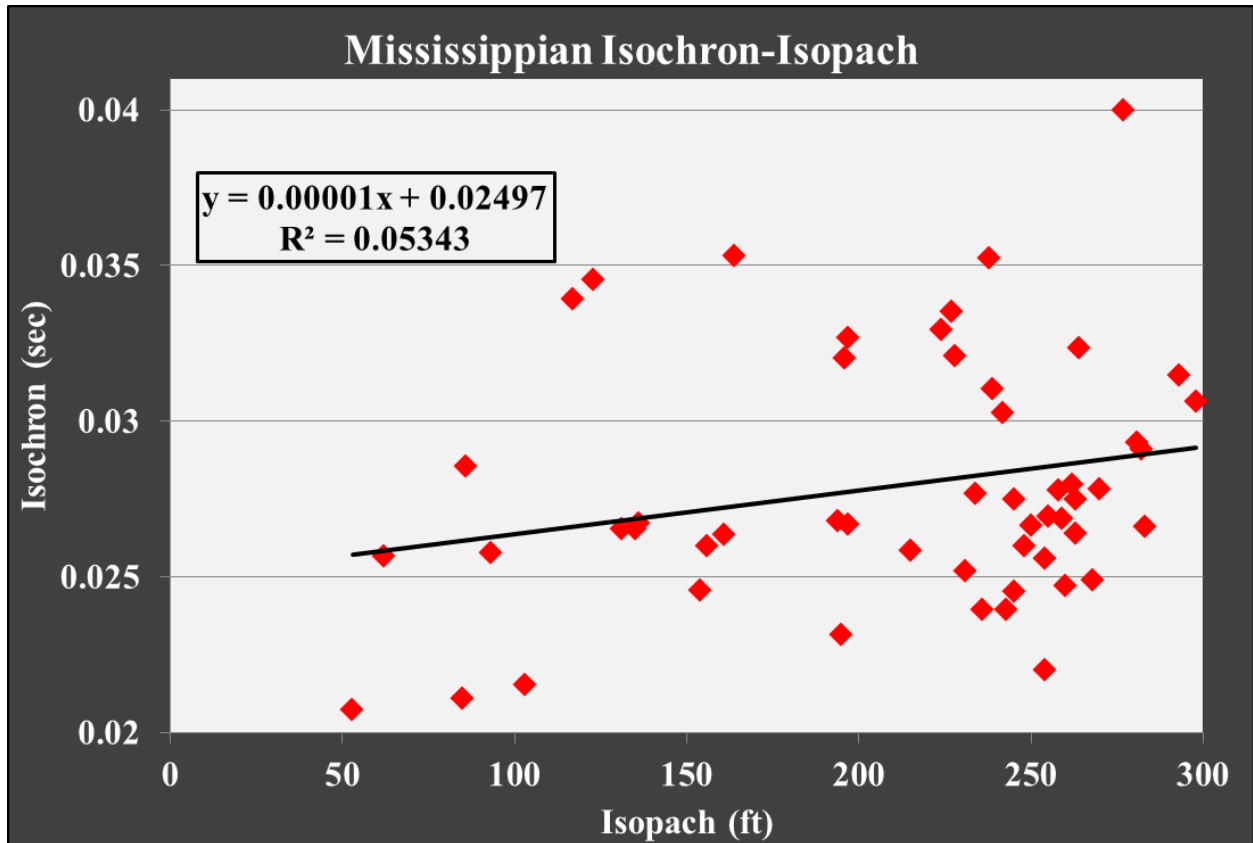


Figure 25: Plot of Mississippian isopach value (feet) against isochron value in seconds. Although the isopach is only for the Mississippian, the isochron starts at the Mississippian top and ends at the Viola top as the Woodford top could not be confidently picked in the seismic. Poor correlation ( $r^2 = 0.06$ ) discourages use of cokriging in this case.

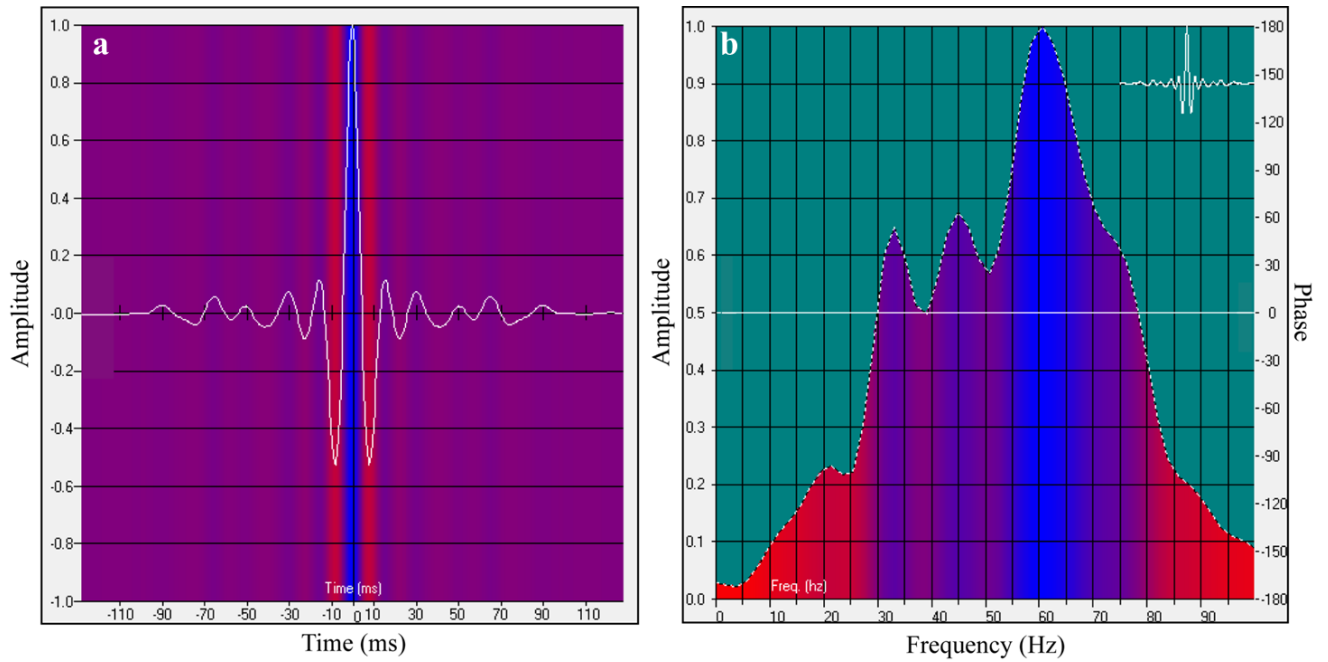


Figure 26: LCB frequency and wavelet used in the wedge model. (a) Wavelet extracted from the LCB survey. (b) Frequency spectrum of the LCB wavelet. This wavelet is convolved with the wedge model because the isopach map shows that there is significant thinning across the survey which may cause tuned amplitudes.

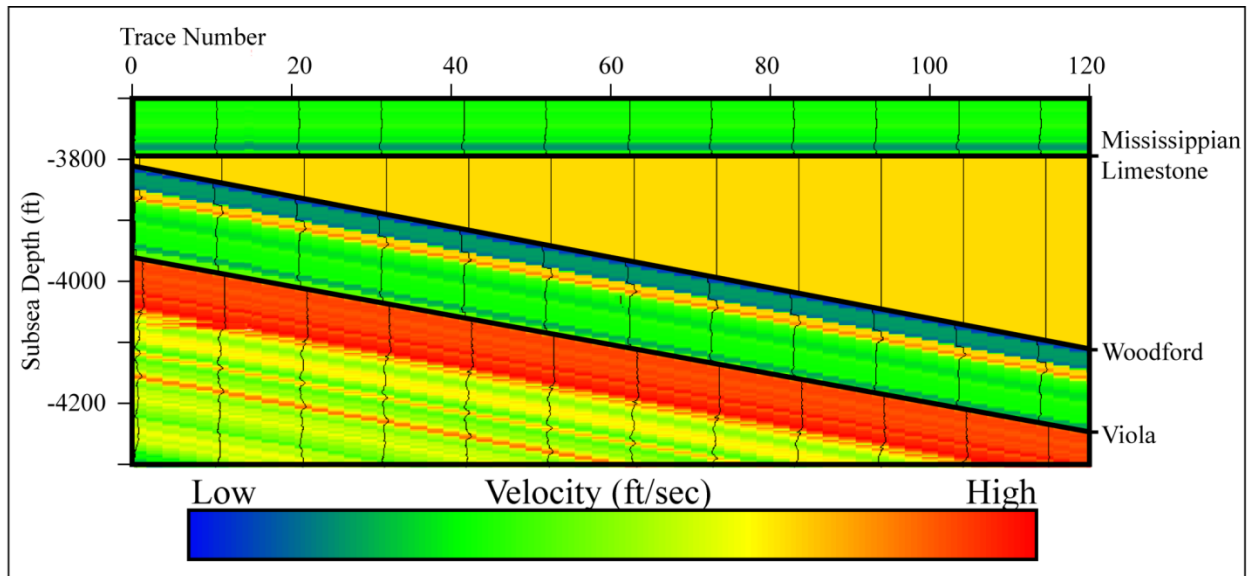


Figure 27: Mississippian wedge model in depth. The model is developed using the sonic and density logs from the Ruark 1-29 SWD. The model is conceived with a constant velocity so that amplitude changes can be related directly to thickness changes. The Mississippian carbonate has a higher velocity than the overlying Pennsylvanian and underlying Woodford shale.

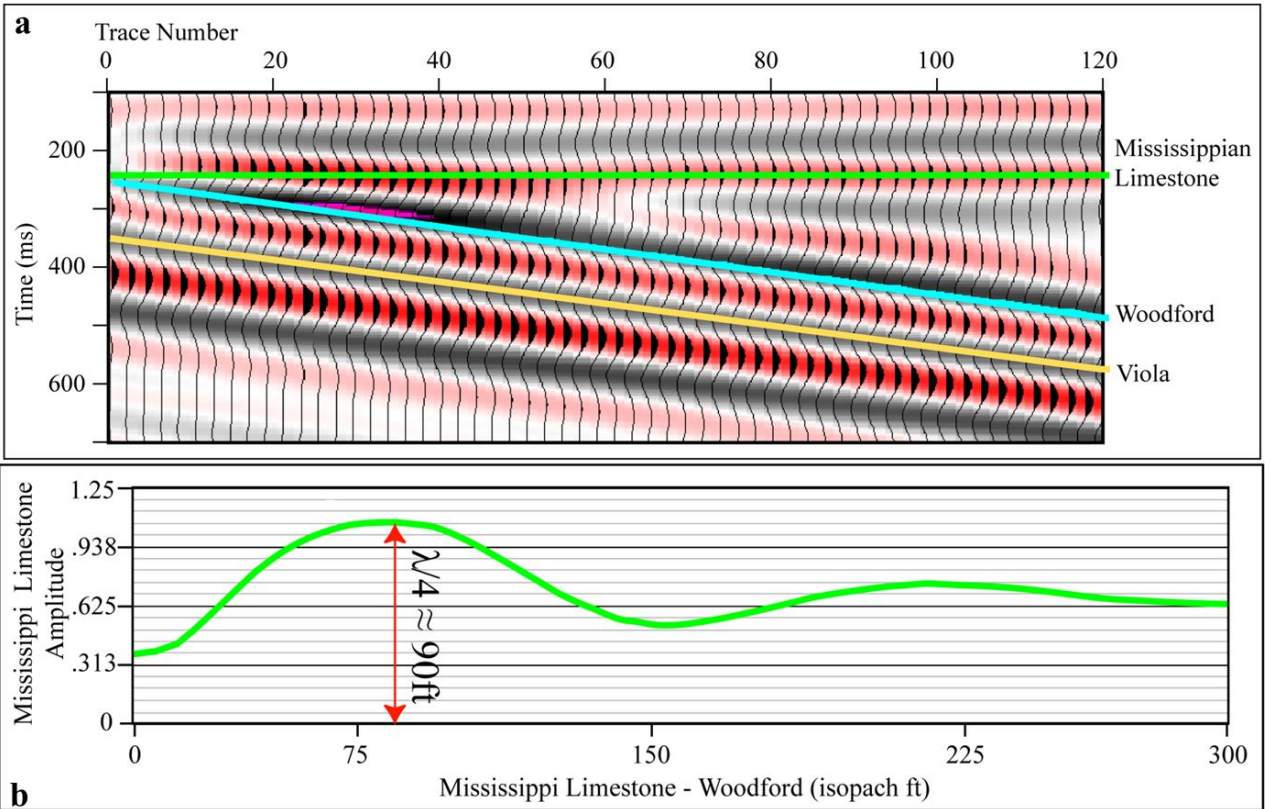


Figure 28: Mississippi wedge model in time. Model in (a) is from convolution of the LCB wavelet (Figure 26) with the depth model (Figure 27). Amplitude extracted along Mississippian top (green line) is plotted against the formation thickness in (b). In (b) red line indicates the nominal amplitude of the reflected wavelet. Perturbation in the reflected amplitude occurs due to tuning. Maximum tuning occurs at  $\lambda/4$  wedge thickness or at an isopach of  $\sim 90\text{ft}$ .



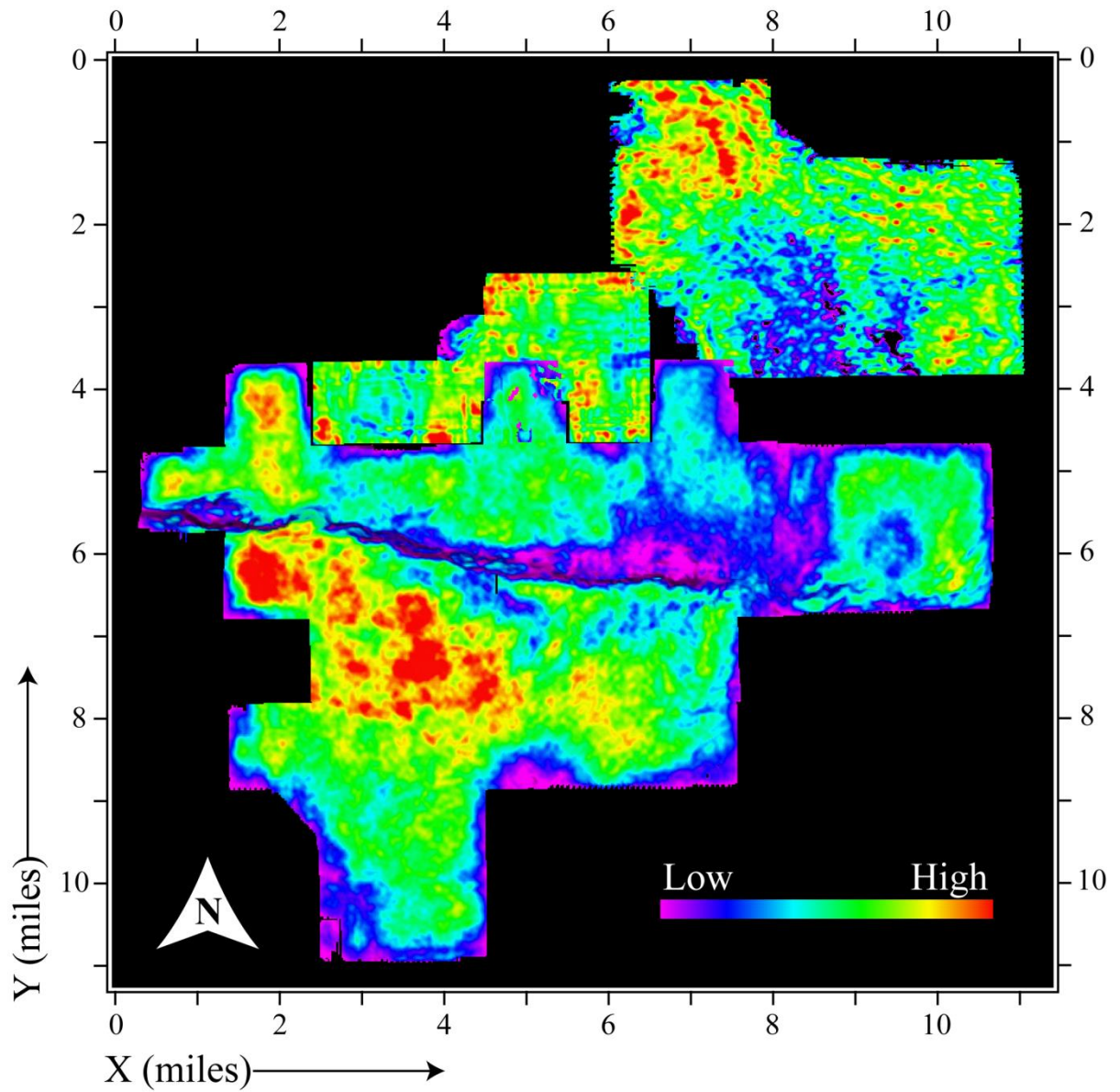


Figure 29: Instantaneous amplitude attribute map generated by the reflection from the Pennsylvanian-Mississippian interface. The three surveys were spliced together to form a single map. In individual survey, red and blue respectively represent higher and lower amplitudes. High reflection amplitude implies a large part of seismic energy returning from the reflector as opposed to being transmitted through or scattered by it.

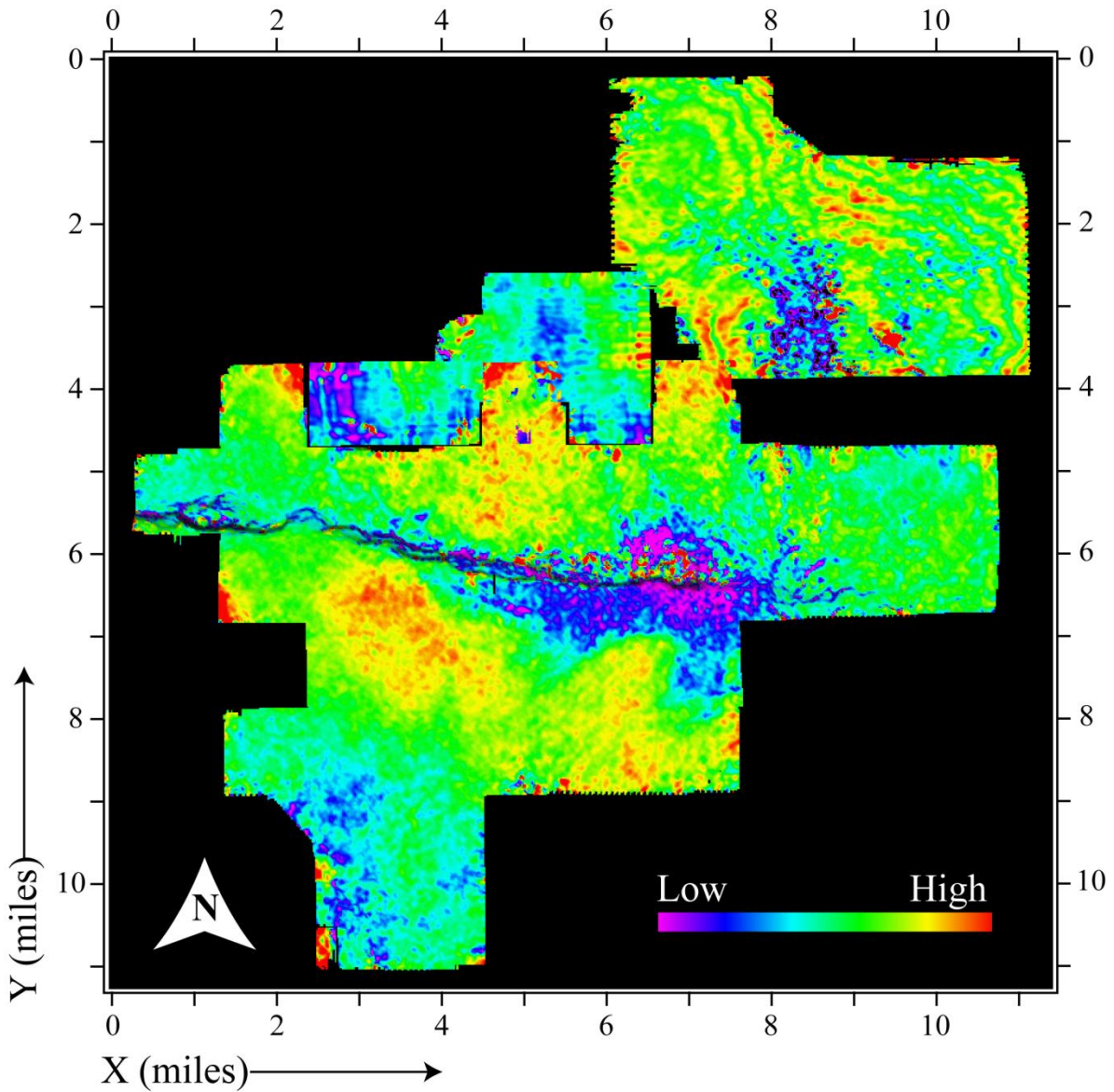


Figure 30: Instantaneous frequency attribute map extract at the Pennsylvanian-Mississippian interface. The three surveys were spliced together to form a single map. In individual survey, red and blue respectively represent higher and lower amplitudes. Low frequency indicates that a large portion of the impinging seismic energy is being absorbed by the target formation.

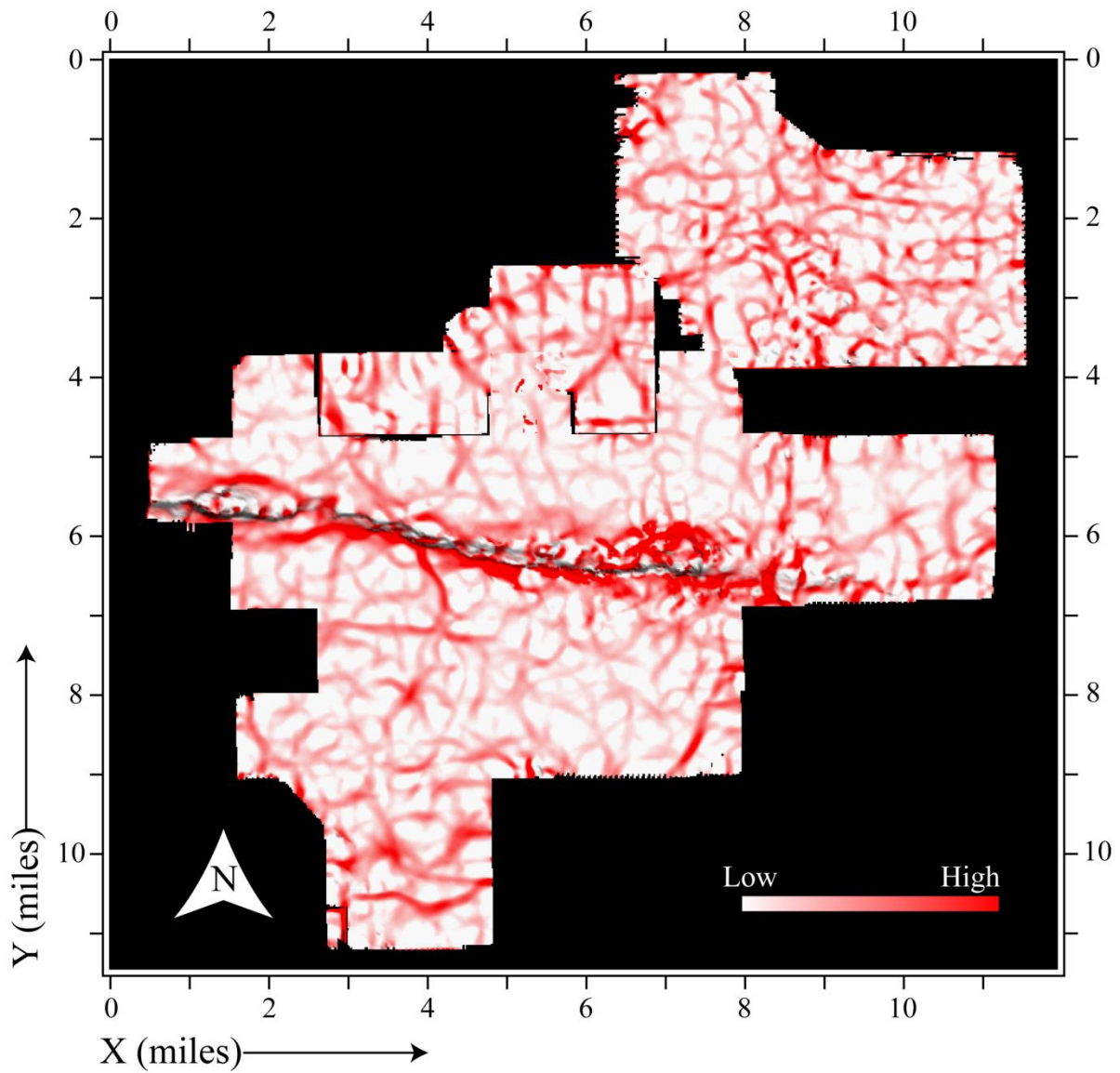


Figure 31: Positive curvature attribute map. The three surveys were spliced together to form a single map. Higher intensity of red indicates higher lateral discontinuity in the vertical alignment of the traces along the Pennsylvanian-Mississippian interface.

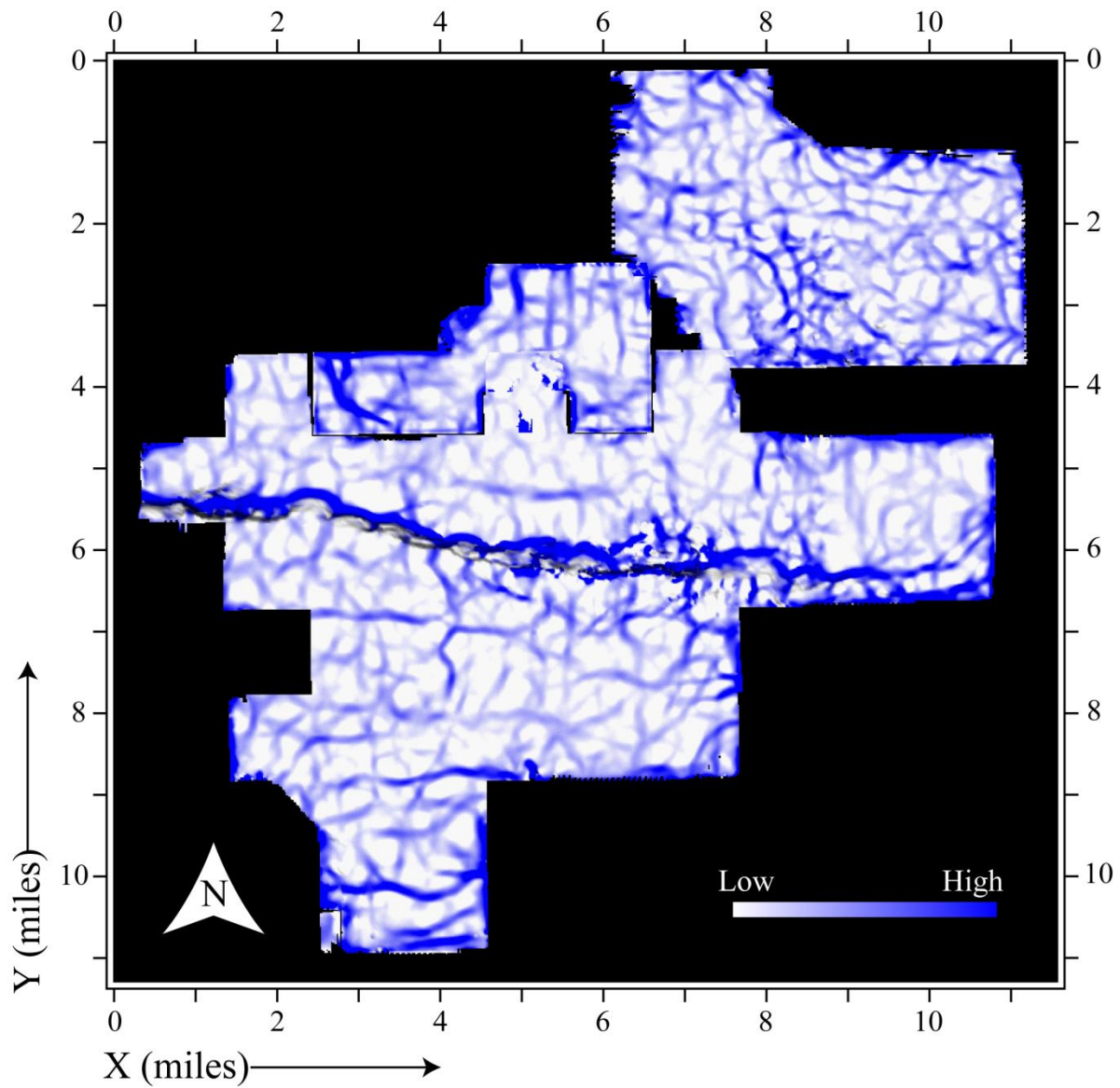


Figure 32: Negative curvature attribute map. The three surveys were spliced together to form a single map. Higher intensity of blue indicates higher lateral discontinuity in the vertical alignment of the traces along the Pennsylvanian-Mississippian interface.

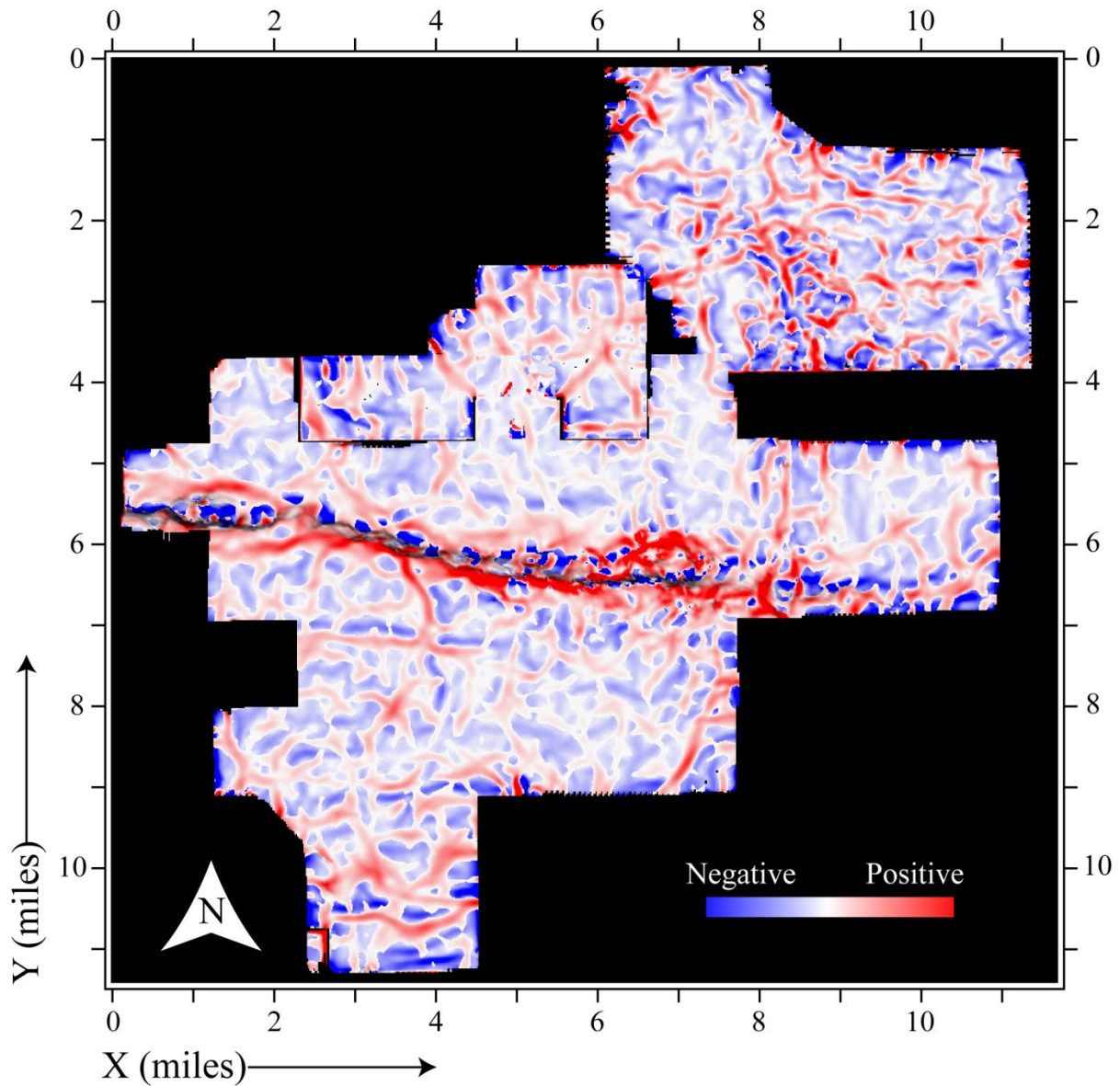


Figure 33: Combined positive and negative curvature attribute map. Positive and negative curvature combined (Figure 31; Figure 32) from all three seismic surveys suggesting that the top of Mississippian has broader valleys and sharper ridges.

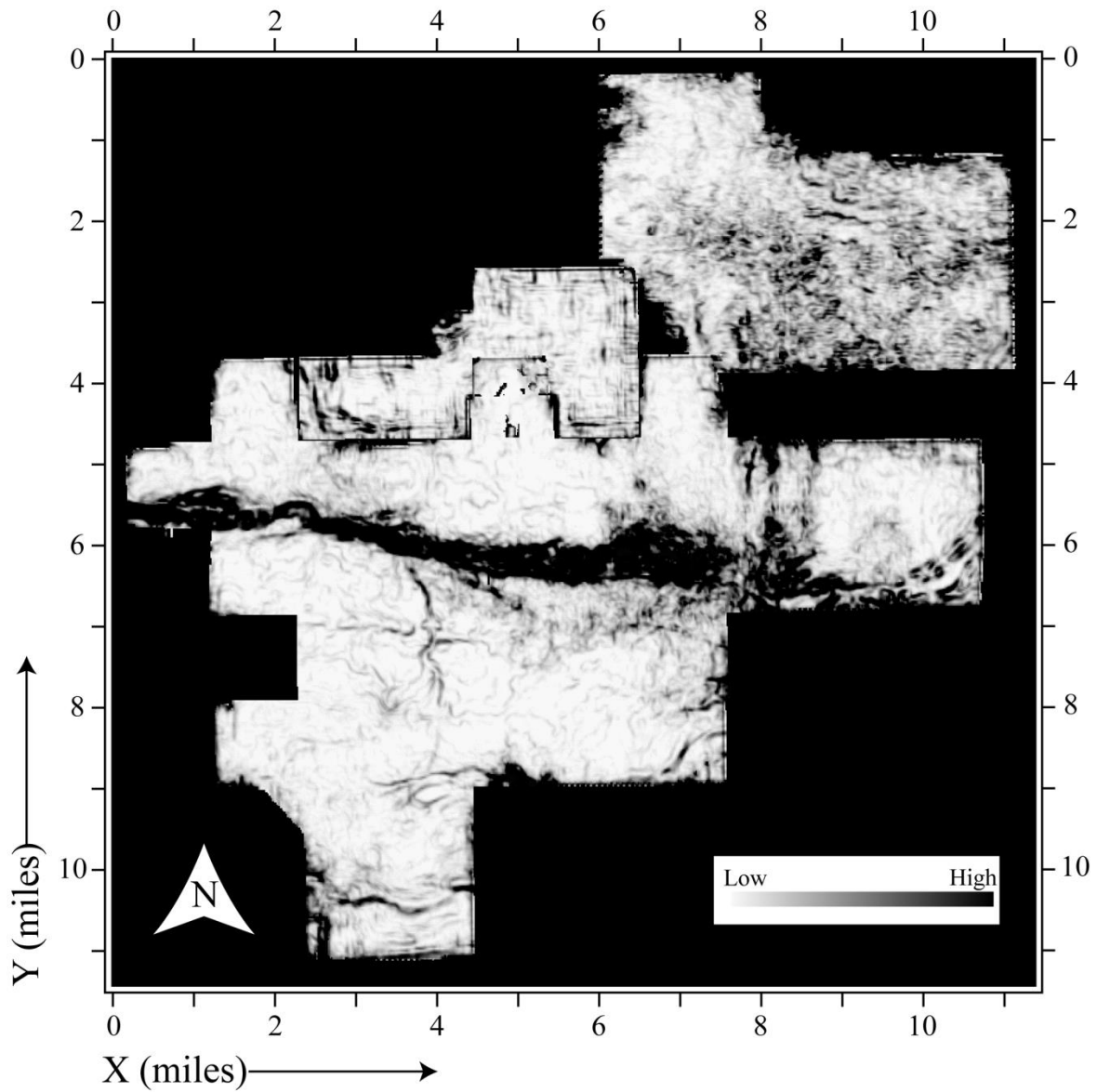


Figure 34: Coherency attribute map. The extraction is along the Pennsylvanian-Mississippian interface. The three surveys were spliced together to form a single map. Darker zone indicate trace-to-trace discontinuity in seismic amplitudes that can be interpreted as faults, erosional features, or lateral facies changes.

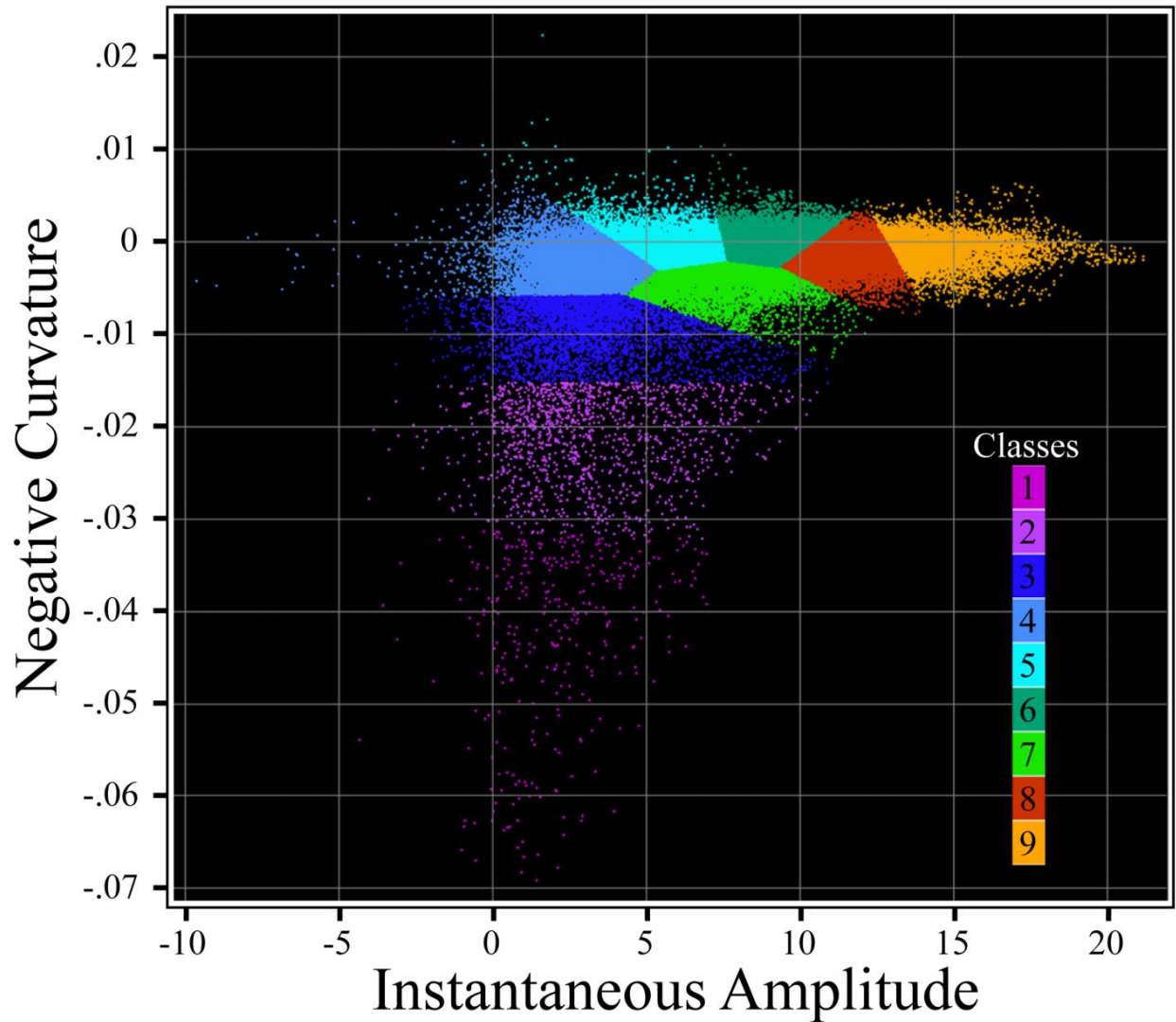


Figure 35: Cross plot of seismic amplitude against negative curvature. The plot shows that high negative curvature is only associated with lower amplitudes implying that the subtle ridge-shaped features either scatter seismic energy or their compositional make up favors energy transmission (higher porosity?). The data can be generically classified into 9 groups where the centers are as distant and radii are as small as possible.

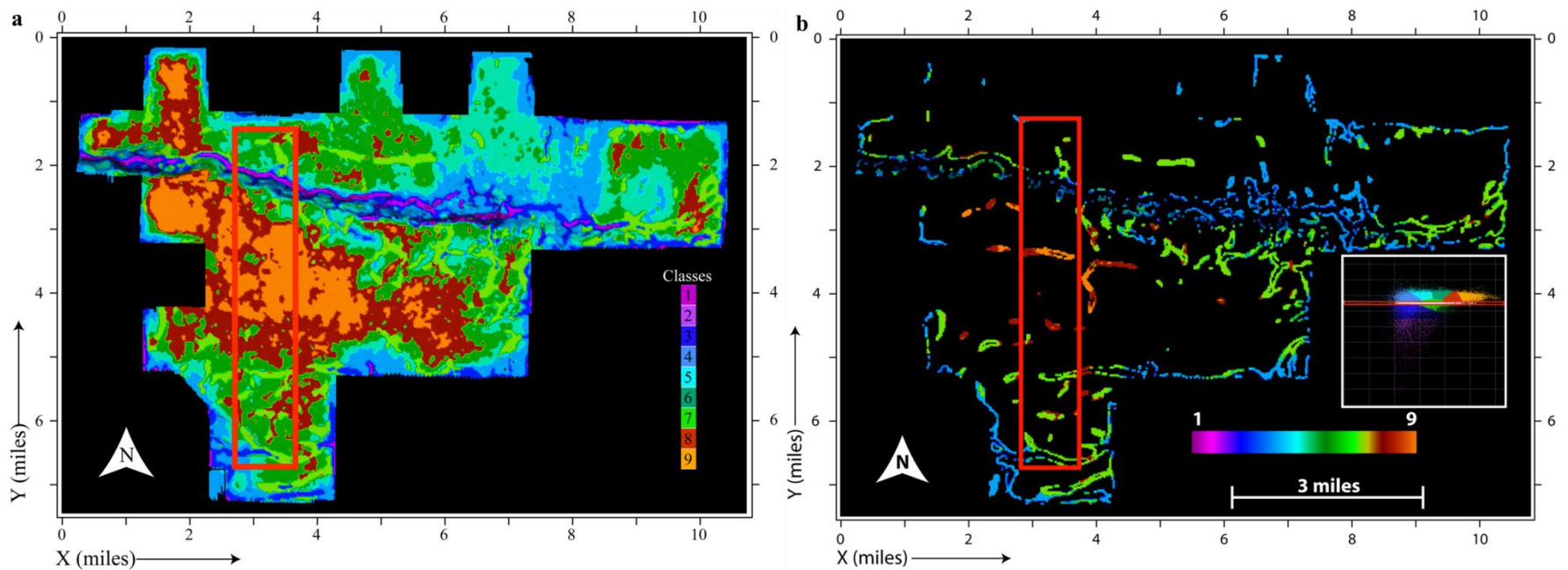


Figure 36: Map showing the result of horizontal classification. Classification is based on two attributes extracted along the Pennsylvanian-Mississippian interface. (a) Zones 1 – 9 for the entire range of negative curvature and amplitude and (b) Zones 1 – 9 for low negative curvature only irrespective of amplitudes. In (a) extremely high negative curvature zone (Zone 1) appears to be associated with the east-west trending fault. The appearance of this “valley” like feature could be due processing rather than geology. The zone with least curvature (flat topography) appears to be associated with erosion and thinning of the Mississippian. In (b) survey boundaries and faulted zones getting highlighted indicates that curvature cannot be directly interpreted in terms of geology; processing artifacts may persist. In (a) and (b), the red box marks a data volume prism (Figure 37).



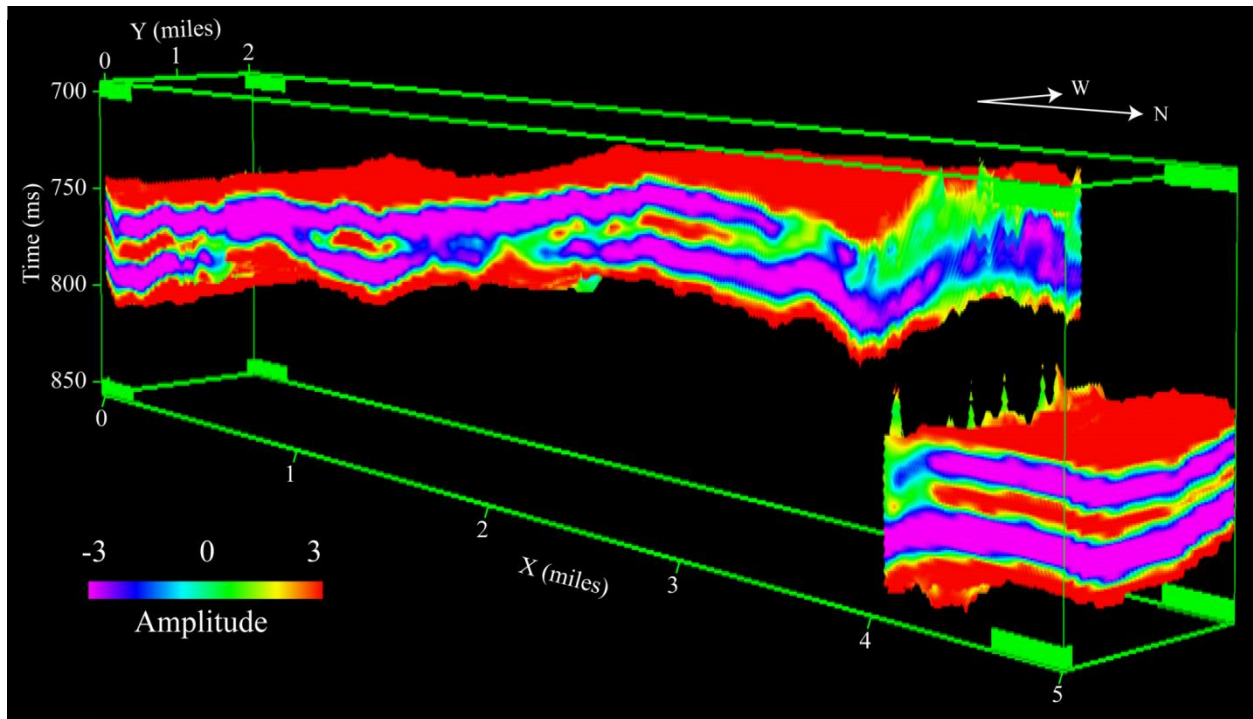


Figure 37: Volume prism showing the vertical seismic character of the Mississippian section. Data volume between the Mississippian and the Viola Top. High variability in amplitude is indicative of geological heterogeneities which cannot be easily evaluated with attributes extracted along a horizon. Classification based on shapes of traces within a volume could be more effective.

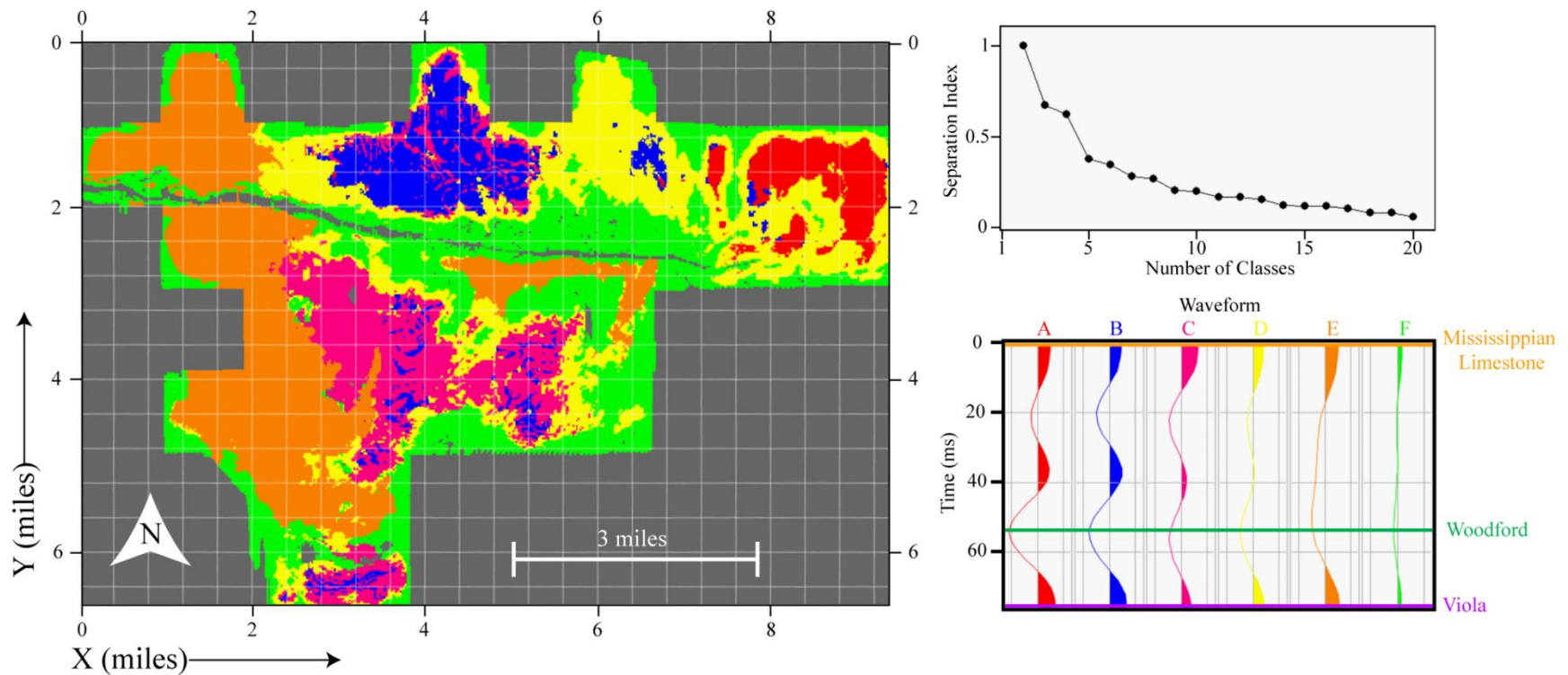


Figure 38: Vertical classification of Mississippian section. Map shows six classes based on trace types within a time window spanning between Mississippian and Viola tops. Representative traces from each class is shown in inset. Unlike horizontal classification (Figure 36), the model edges and region around the east-west fault fall under a single category (Class F). The remaining classes could be related to geology (facies changes) as much as aspects of processing.

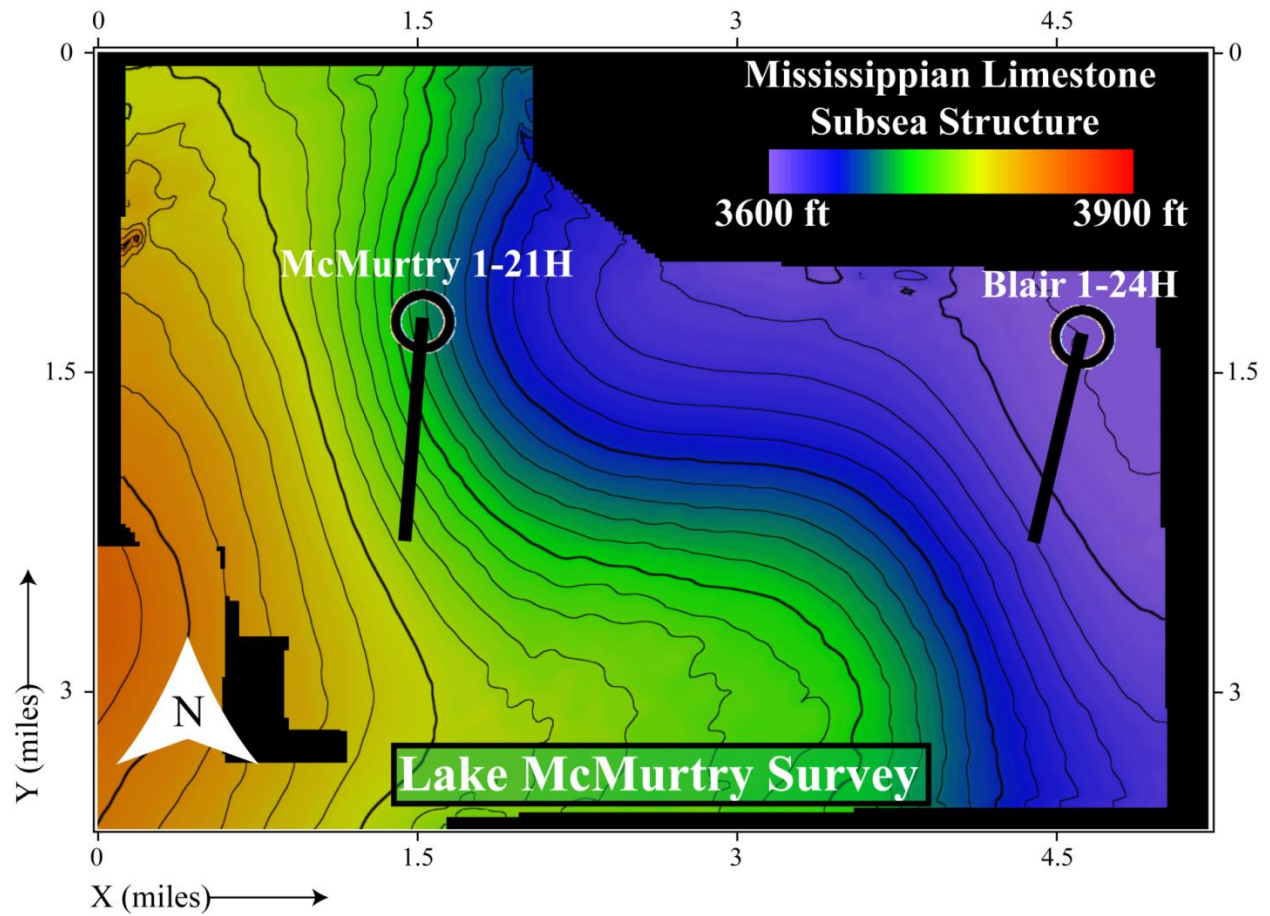


Figure 39: Mississippian depth structure map on the LMM survey. The map is generated using cokriging. Location of the lateral wells 1-21H and 1-24H are shown. Both wells have fracture micro-imaging (FMI) logs that were used to create and validate the fracture density model.

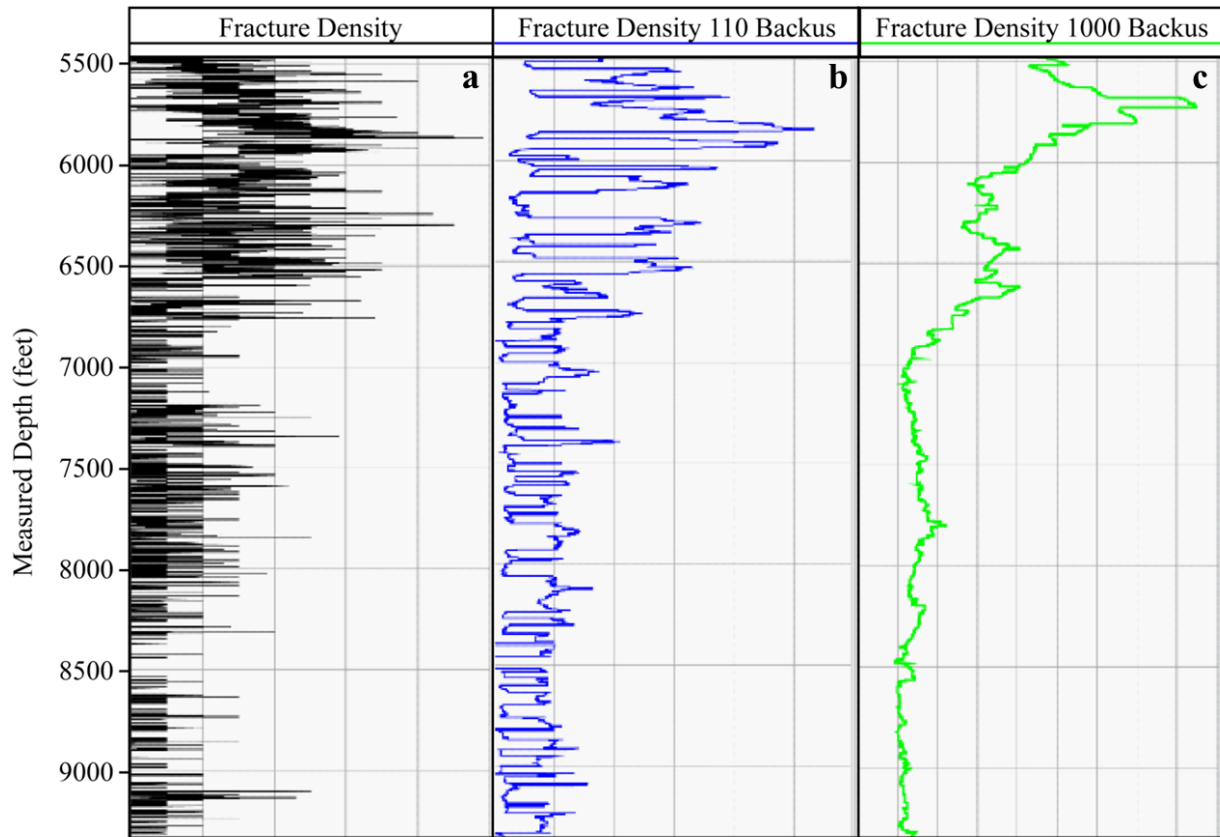


Figure 40: FMI upscaling techniques. (a) Fracture density interpreted every 4 inches along the lateral portion of the 1-24H well. Comparing fractures interpret at this scale cannot be equated with features interpreted from seismic. (b) Interpretation in (a) upscaled using Backus averaging at 110 samples. (c) Interpretation in (a) upscaled using Backus average of 1000 samples; this is the resolution of the fracture model which is created using a combination of attributes (Figure 29Figure 30Figure 31Figure 32,Figure 34).

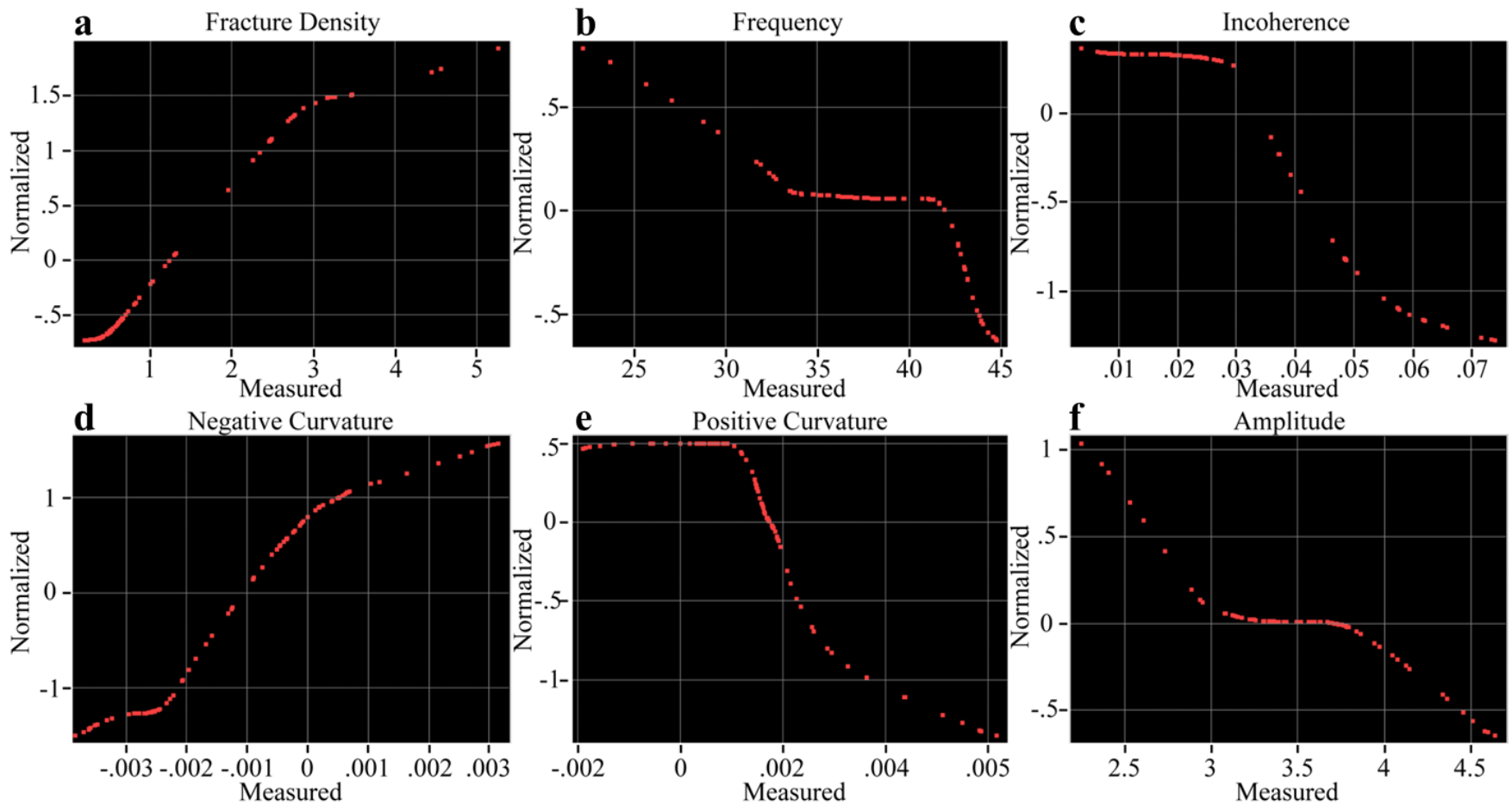


Figure 41: Blair 1-24H multivariate model inputs. Fracture density is modeled as a non-linear function of attributes. Individual attributes transforms in a) fracture density, (b) frequency, (c) incoherence, (d) negative curvature, (e) positive curvature and (f) amplitude were used as model inputs.

# Fracture Density

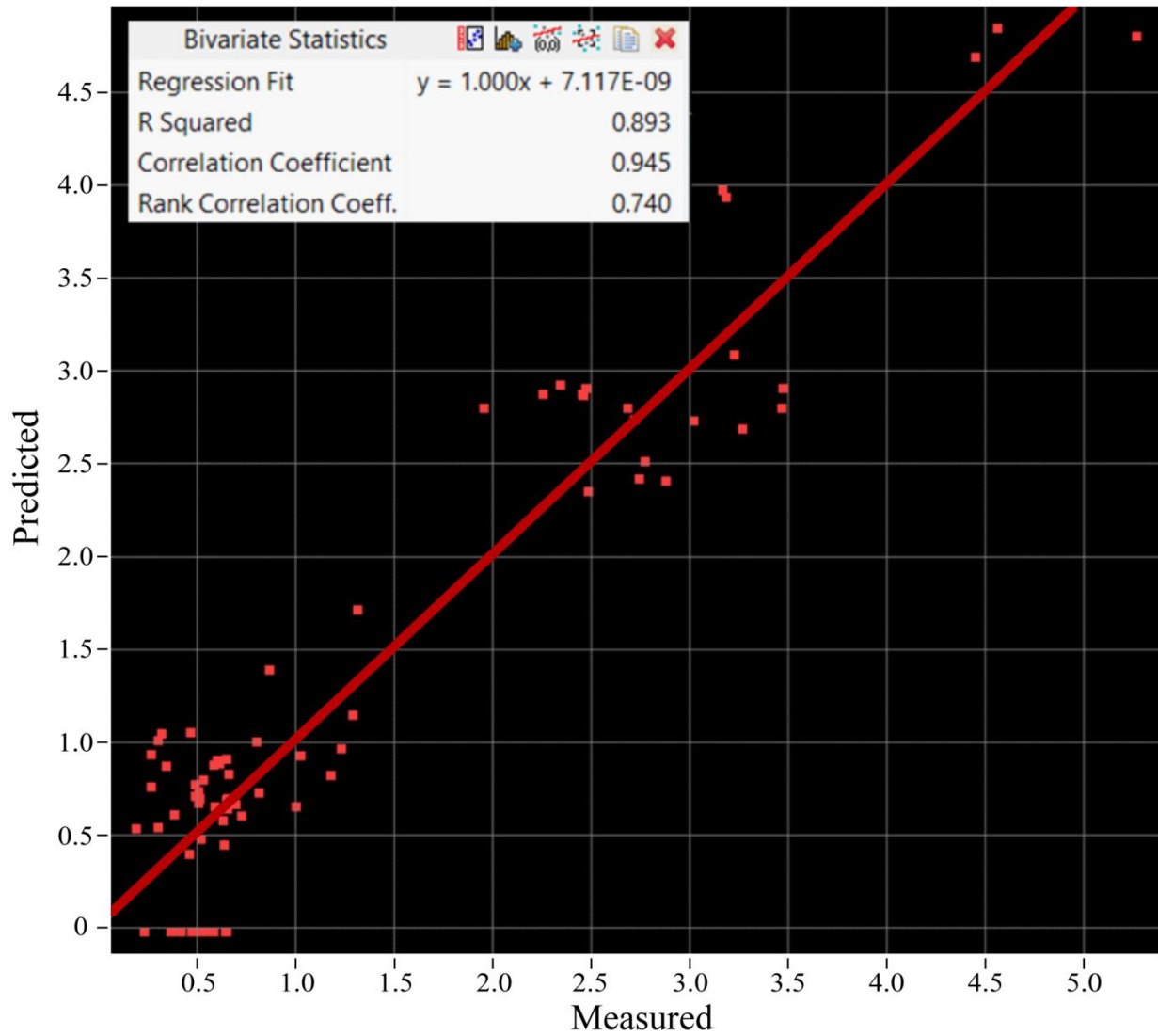


Figure 42: Blair 1-24H multivariate model output. Measured fracture density is plotted along x-axis. Fracture density predicted using the multivariate non-linear regression is plotted along y-axis. Observed and predicted data have a correlation coefficient of 0.945 and  $r^2$  of 0.893.

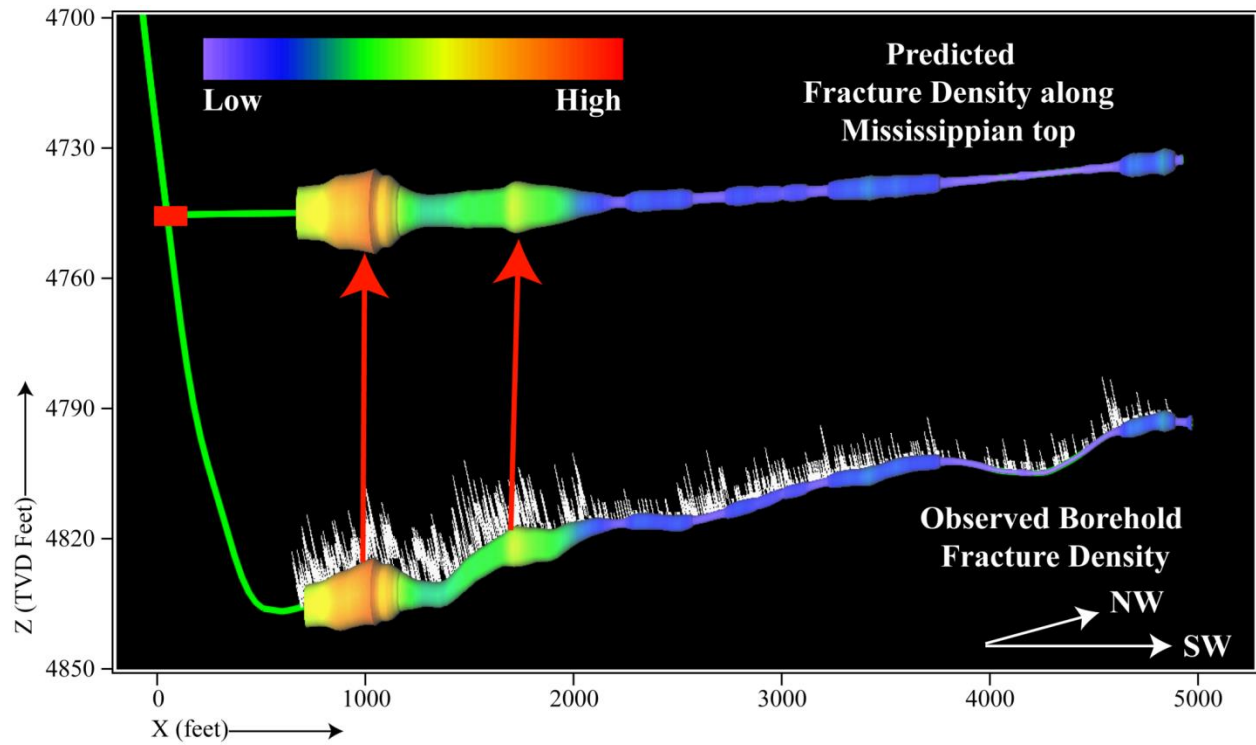


Figure 43: Blair 1-24H fracture density comparison: along-trajectory view. Observed fracture density posted along the wellbore. Predicted fracture density along the Mississippian Top surface. Colors represent fracture density with red and blue respectively implying higher and lower. Mississippian top geometry is from cokriging (Figure 19b). Projection direction of fractures from well-path to Mississippian top is vertical.

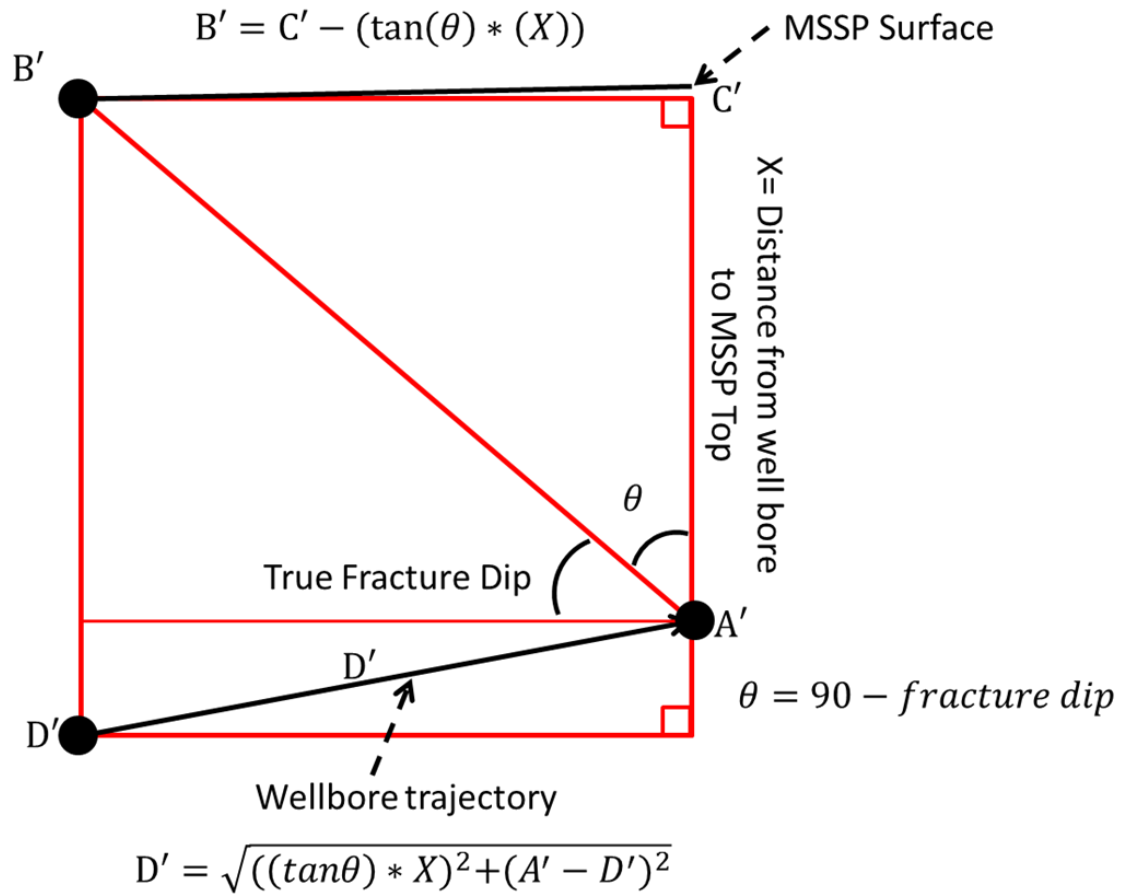


Figure 44: The dip projection method repositions fractures to the Mississippian top along using the dip of the fractures. A'D' is the well trajectory. A'B' is the fracture dip. Method assumes that a) fracture dip remains consistent within the Mississippian formation, b) the overall wellbore trajectory comprises multiple flat intervals and c) maximum fracture dip is in the plane of projection.



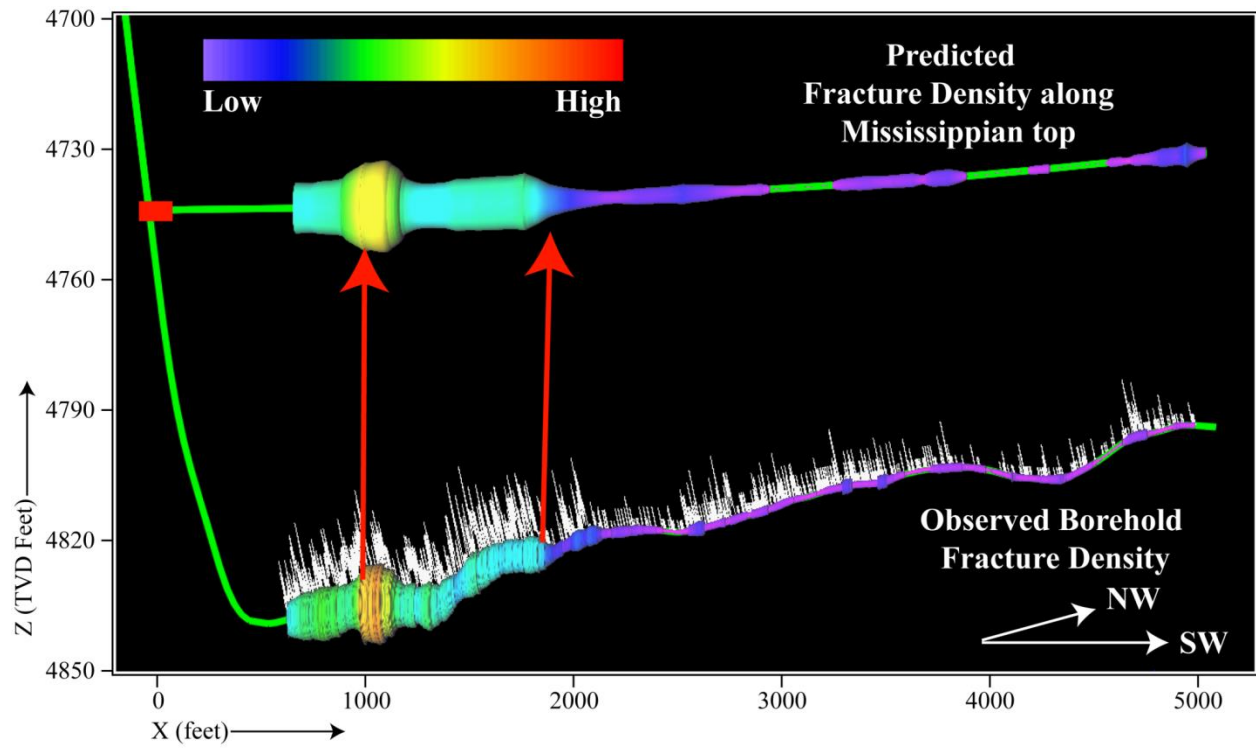


Figure 45: Blair 1-24H fracture density re-comparison: along-trajectory view. Same as Figure 43 with projection direction of fractures from well-path to Mississippian top being along-dip.

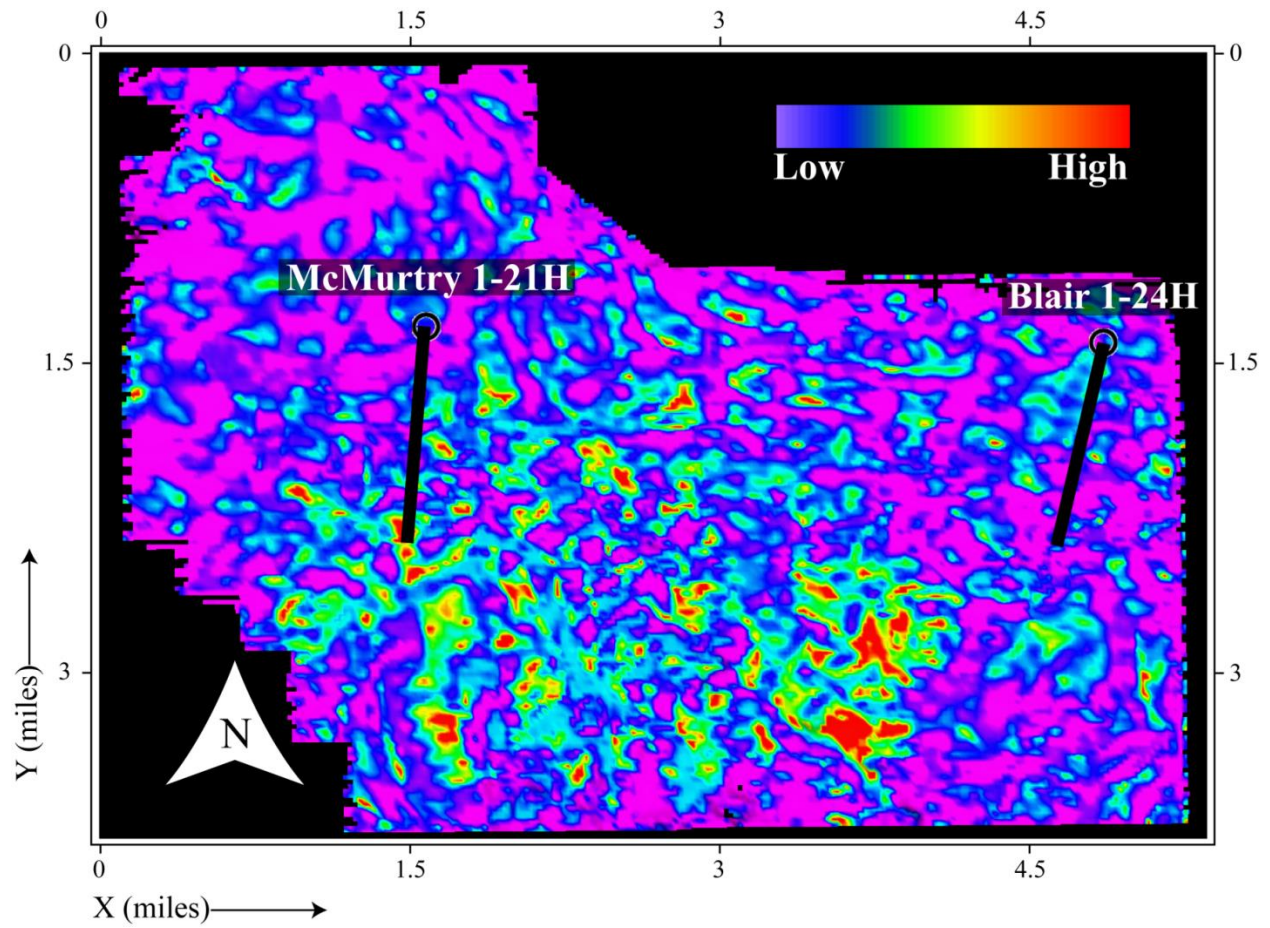


Figure 46: Predicted fracture density map at the Mississippian Top. Red and blue colors respectively represent higher and lower fracture density. Trajectory of McMurry 1-21H and Blair 1-24H wells, shown in black, are projected onto Mississippian surface.

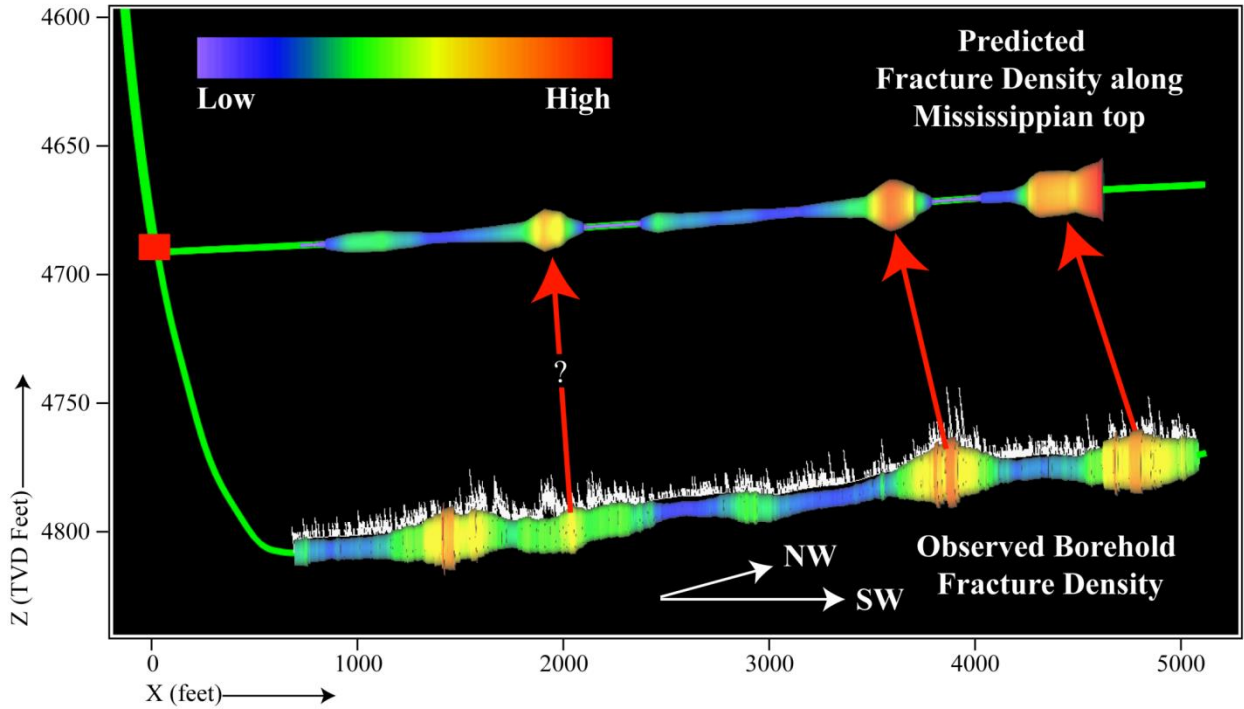


Figure 47: McMurry 1-21H fracture density comparison: along-trajectory. Observed fracture density is posted along the wellbore. Predicted fracture density is posted along the Mississippian Top surface. Colors represent fracture density with red and blue respectively implying higher and lower. Mississippian top geometry is from cokriging (Figure 19b). Projection direction of fractures from well-path to Mississippian top is vertical.

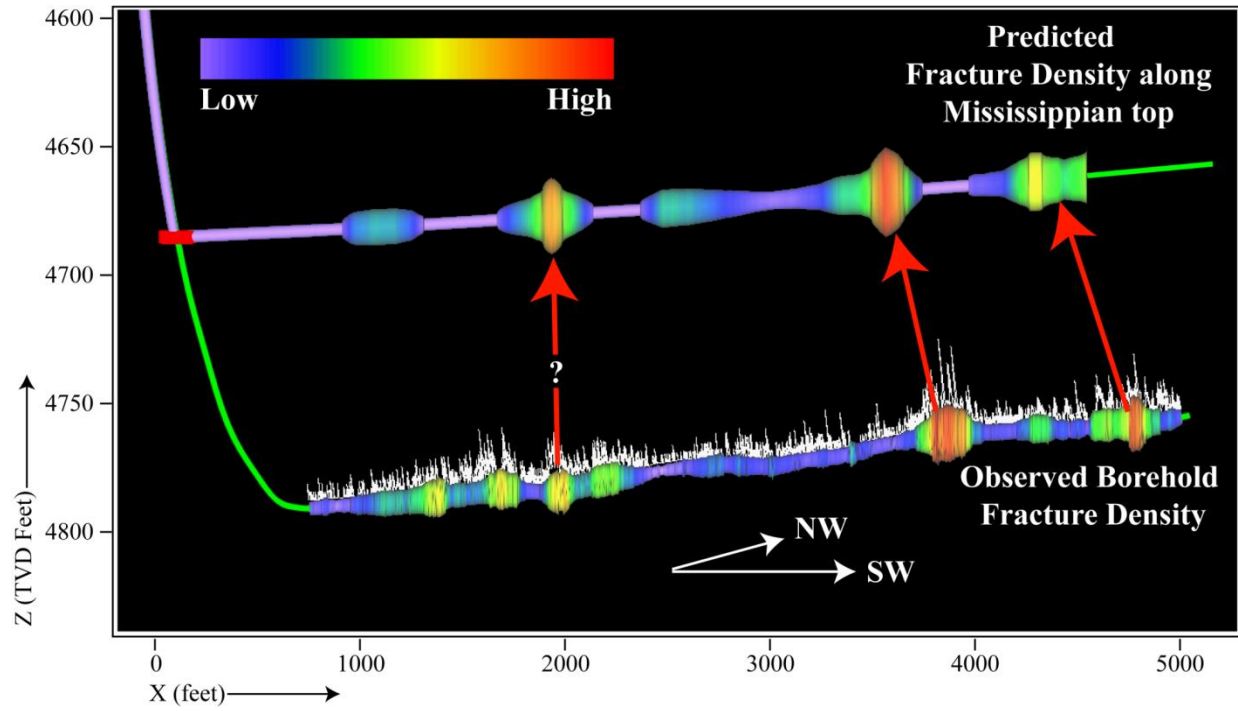


Figure 48: McMurtry 1-21H fracture density re-comparison: along-trajectory. Same as Figure 47 with projection direction of fractures from well-path to Mississippian top being along-dip.

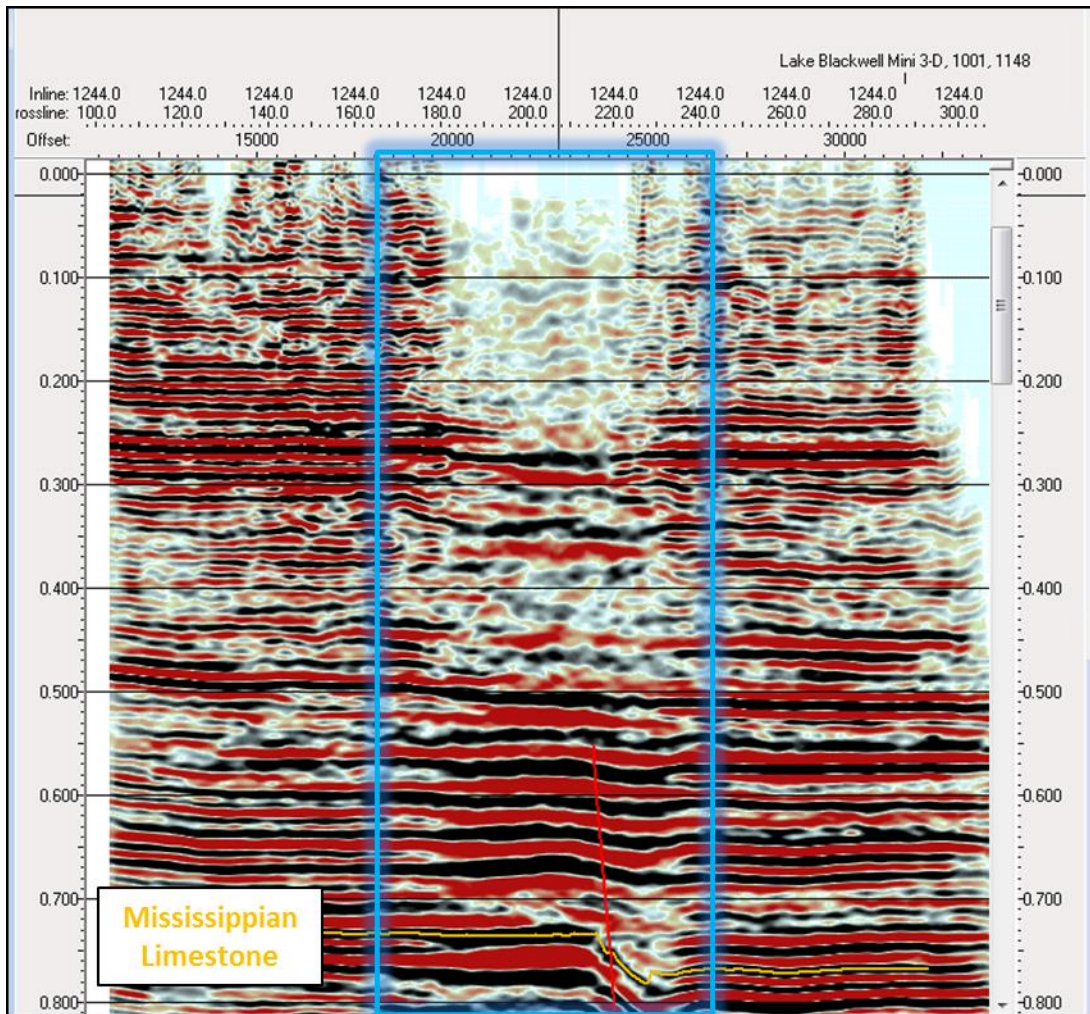


Figure 49: Seismic line across Lake Carl Blackwell shows a decrease in frequency, resulting in poorer data quality.

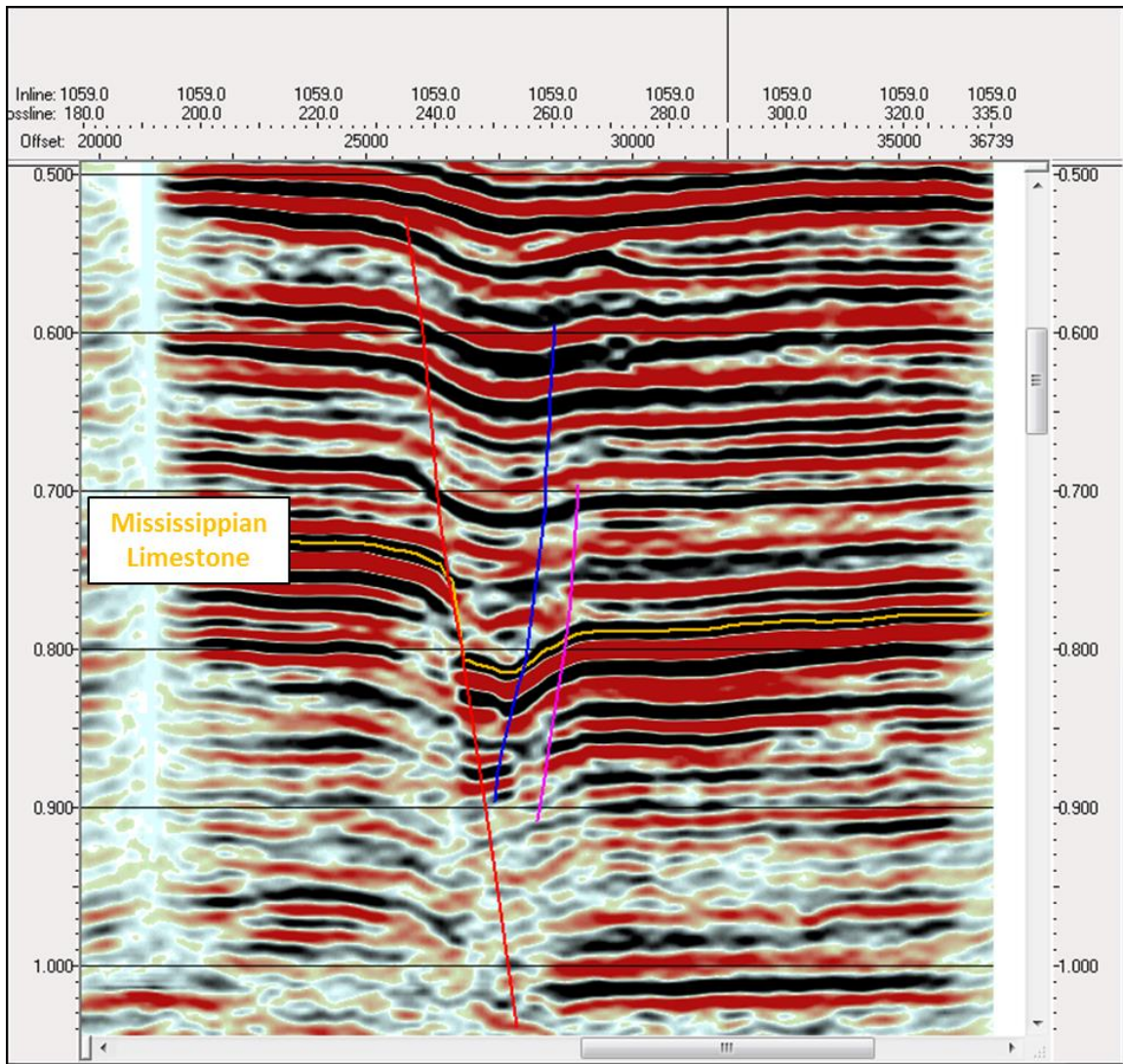


Figure 50: Seismic line at position  $x=1.5$  and  $y=5.5$  (Figure 29) shows similarities to structural sags observed in the Lady Fern trend.

## APPENDIX A

### SEISMIC ACQUISITION

With the need for advanced analysis of seismic data comes the necessity to understand potential short comings. Some of the limitations are created during the acquisition of the dataset. Seismic interpreters need to have an understanding of acquisition and processing parameters to make an accurate analysis of attributes. Dawson geophysical provided valuable information concerning the acquisition and processing of the LCB survey (section, 2.2.1).

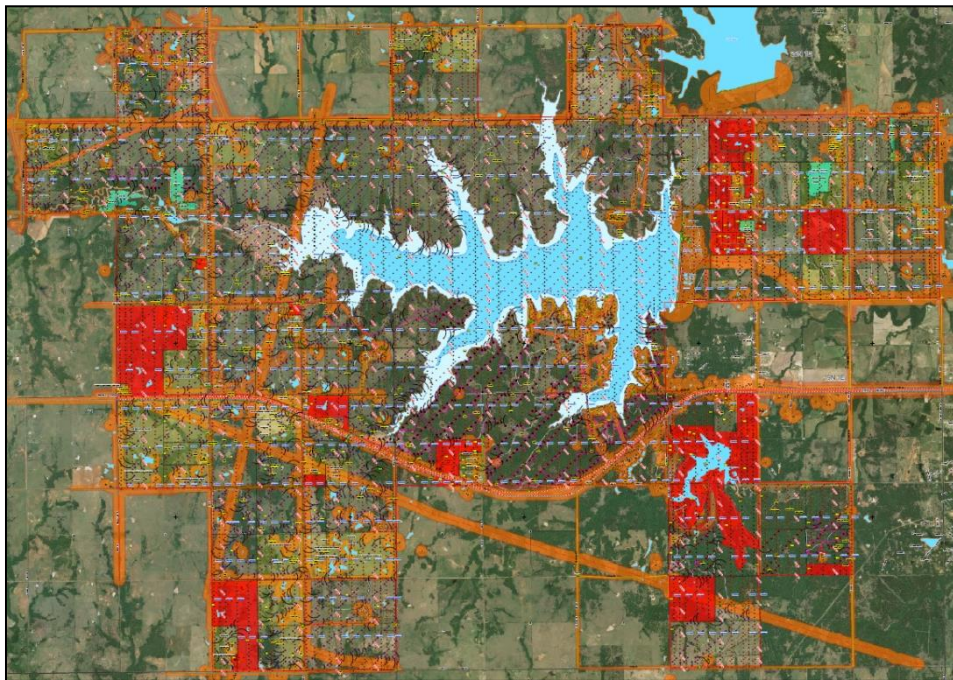


Figure A 1: LCB Acquisition setup. Map showing the shot and receiver locations for the LCB shoot. Receiver lines are N-S red dots and Sources lines are NE-SW black dots, with dots in the lake representing gun boat, regular dots as vibroseis, and bold dots dynamite locations. Red polygons

represent non-permitted zones, ie areas where no sources could be shot. Orange polygons represent additional hazards such as roads, wells, or pipeline.

The overarching goal is building a project for the lowest price with the highest quality. To do this acquisition projects need to be built with an end goal in mind such as structural analysis for geosteering or attribute work for facies identification. After the goal is defined, the initial set-up for the project is to maximize data quality to achieve this goal at the lowest price. Unfortunately, surface conditions and leasing constraints often inhibit the execution of the plan (Figure A 1). As a result plans are altered to mitigate problems which may negatively affect data quality.

Data processing will quickly show the problems introduced where areas of under sampled. Examination of CDP near offsets will show where data is sparse (Figure A 2). Near offsets approximately correspond to where source and receiver are closest and where the raypaths are nearly vertical. This highlights where shots were not taken, resulting in areas of lower fold.

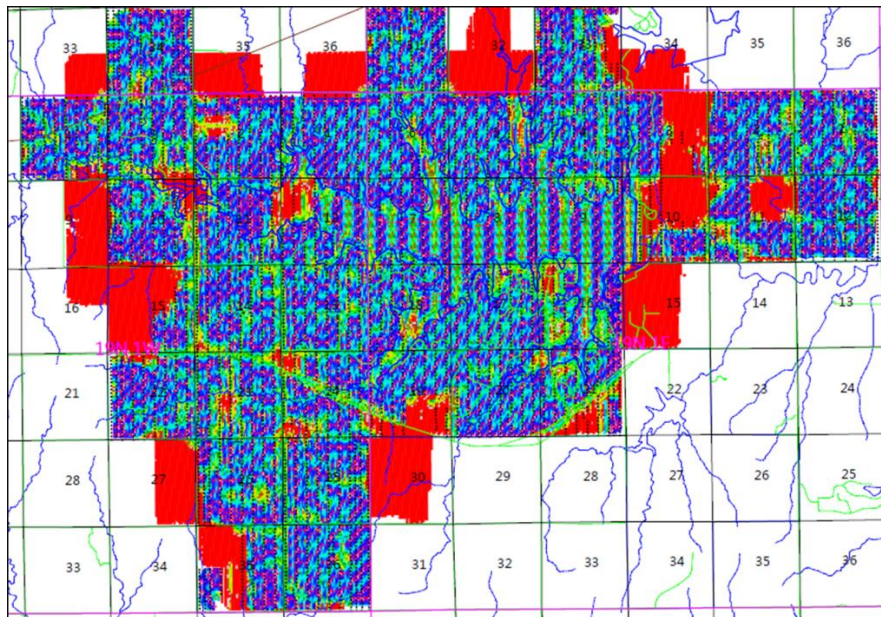


Figure A 2: LCB nearest offset map. The nearest offset map shows where shots were taken to create a nearly vertical raypath. Red shows where there are not immediate offset traces.



## APPENDIX B

### SURVEY MISTIES

The well used to tie from depth to time was the Ruark 1-29 SWD located within the boundaries of the LCBm survey. Unfortunately, the LCB and LMM survey did not have the necessary data to properly create a synthetic well tie. In absence of well information to identify key horizon the interpretation was extended by tying the surveys together where they overlapped with a mistie setting. Mistie tie settings are modifications added to the data so that seismic with different datums can be compared. This is done in three ways: bulk shifts, phase rotations and amplitude scaling. A bulk shift is to align the data vertically, so that horizons appear continuous. A phase rotation is applied so that the peak magnitudes of the traces are aligned. An amplitude scaling is done to balance the magnitudes of the traces.

The mistie of the LCB m to the LCB survey required a bulk shift of -.12 sec,  $-57.21^\circ$  phase rotation, and 1.34 change to properly balance the amplitudes (Figure B 1). All key horizons were identified and interpretation was extents from the LCBm to the LCB survey. The mistie of the LCBm to the LMM survey required a bulk shift -.12 sec,  $-121^\circ$  phase rotation, and .00029 change to properly balance the amplitudes (Figure B 2). The top of the Mississippian section and the Viola horizon were extended form the LCBm to the LMM survey. However, the two sub-horizons and Woodford did not have independent events. It is unclear why they were not identified, a greater understanding of acquisition and processing is necessary for a proper explanation.

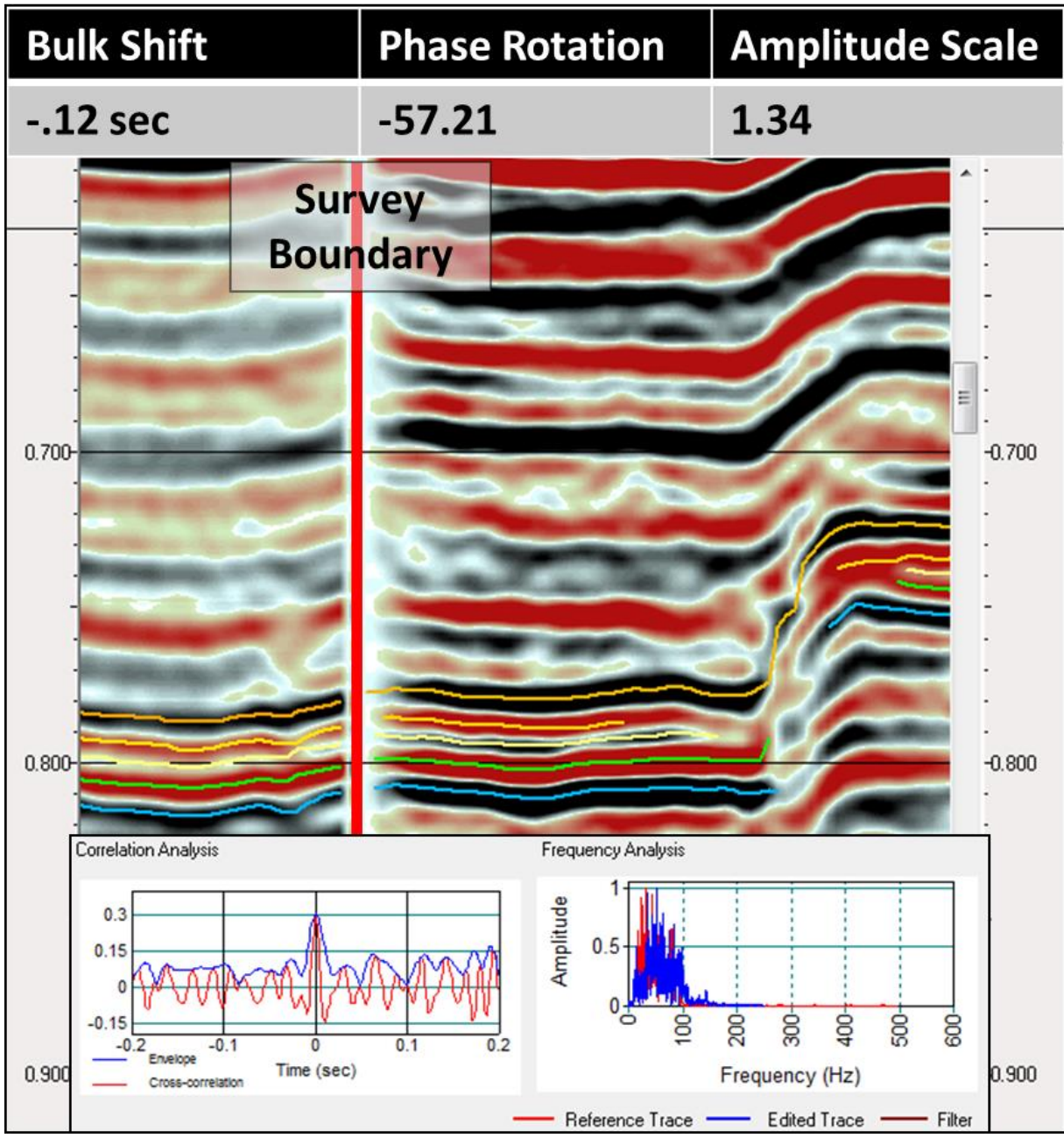


Figure B 1: Mistie analysis of the LCBm to LCB. Mistie analysis to extent the interpretation of the Mississippian horizon from the LCBm to LCB survey.

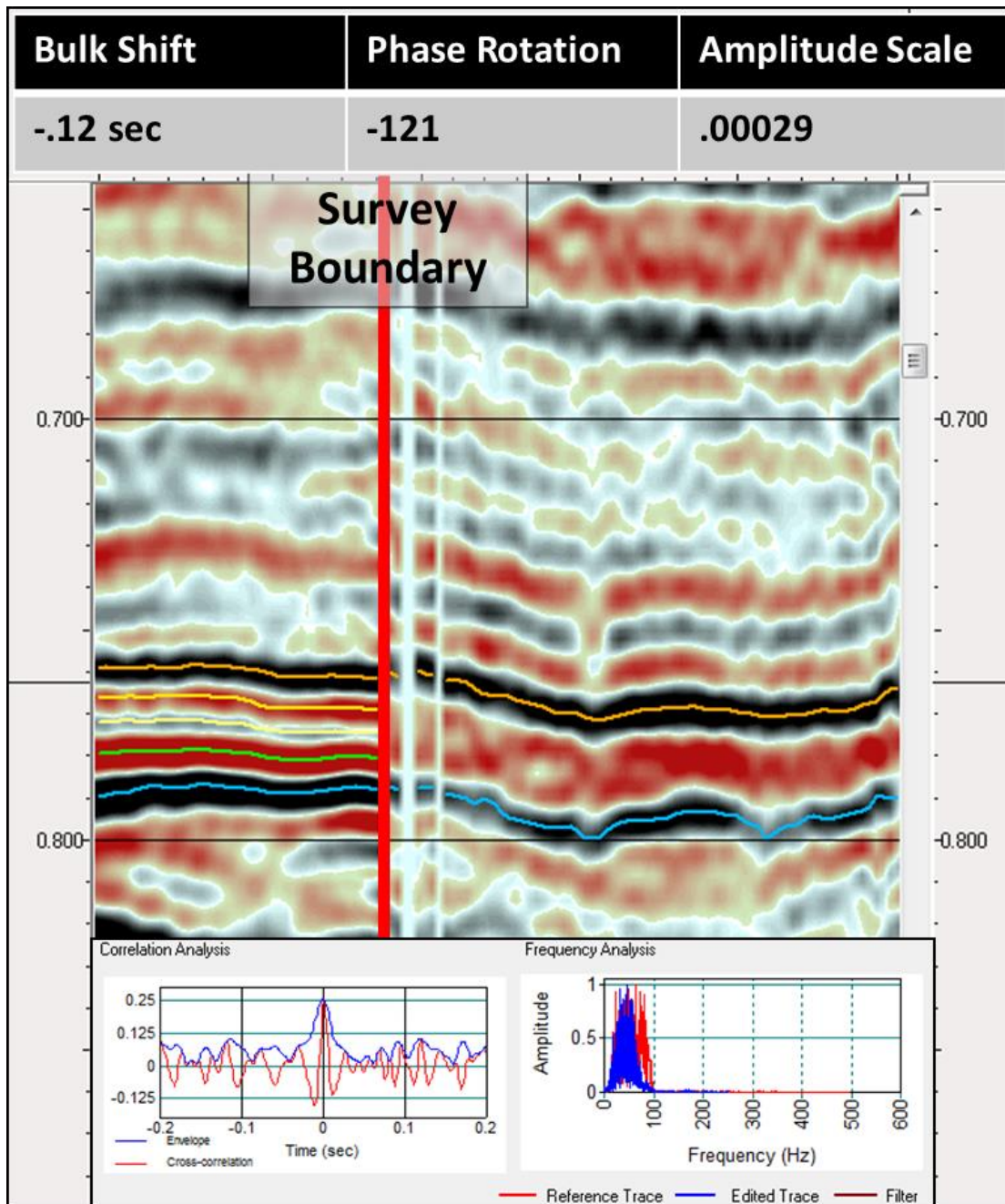


Figure B 2: Mistie analysis of the LCBm to LMM. Mistie analysis to extent the interpretation of the Mississippian horizon from the LCBm to LMM survey.

## APPENDIX C

### DETUNING AMPLITUDES

The seismic attribute, instantaneous amplitude is one of the more difficult to interpret because it is easily affected by inadequacies in the data such as tuning. Wedge modeling showed that there would be a 50% enhancement in the magnitude of the amplitude as the thickness of the Mississippian section decreased to about 90 ft (Figure 28b). As a result, amplitude information cannot be trusted to reflect characteristics of the reservoir when the thickness approaches 90 ft (Figure C 1). To mitigate this problem, a detuning workflow was proposed so that relative amplitudes could be interpreted.

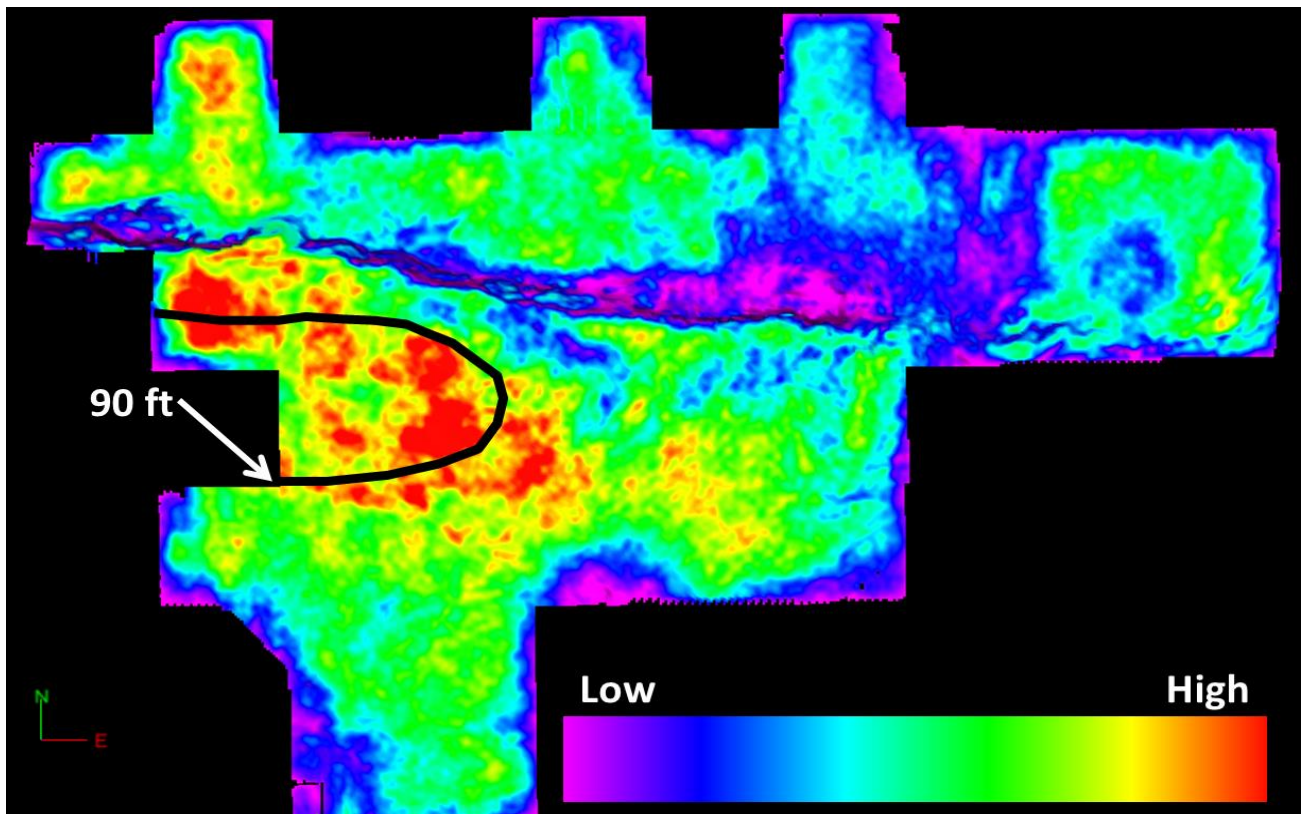
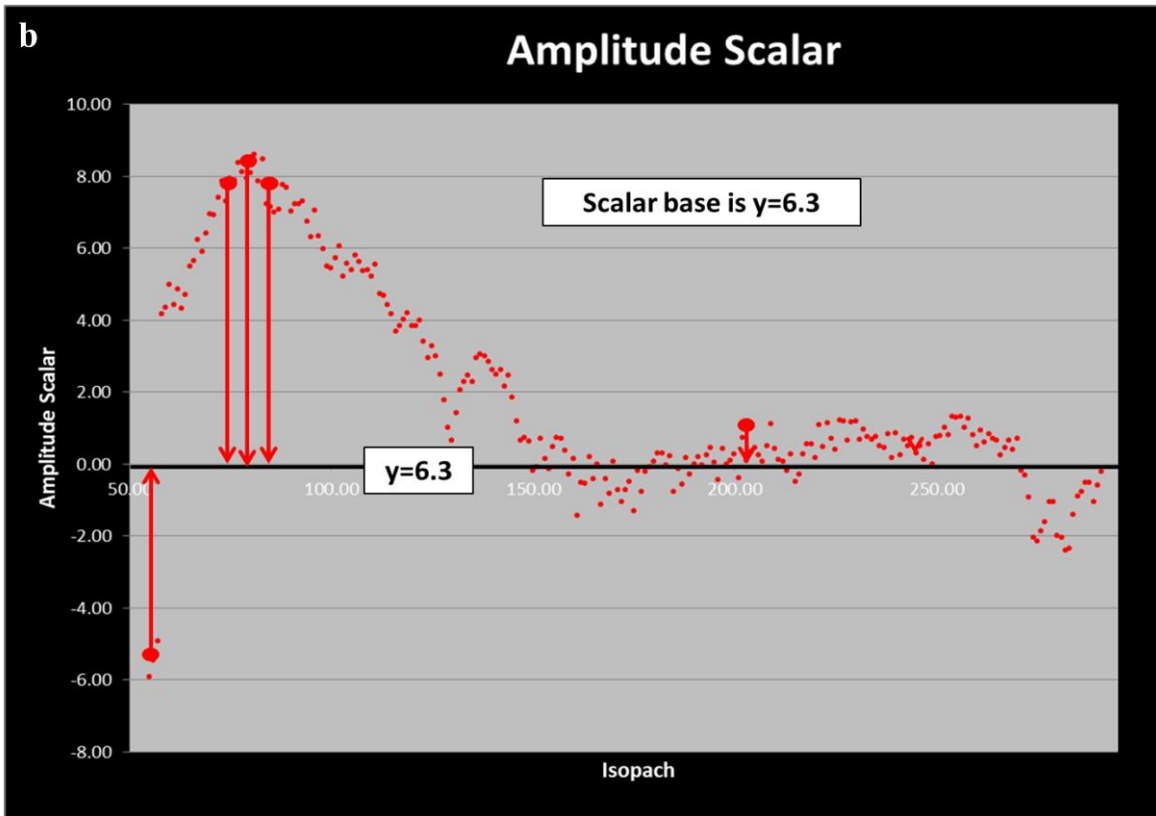
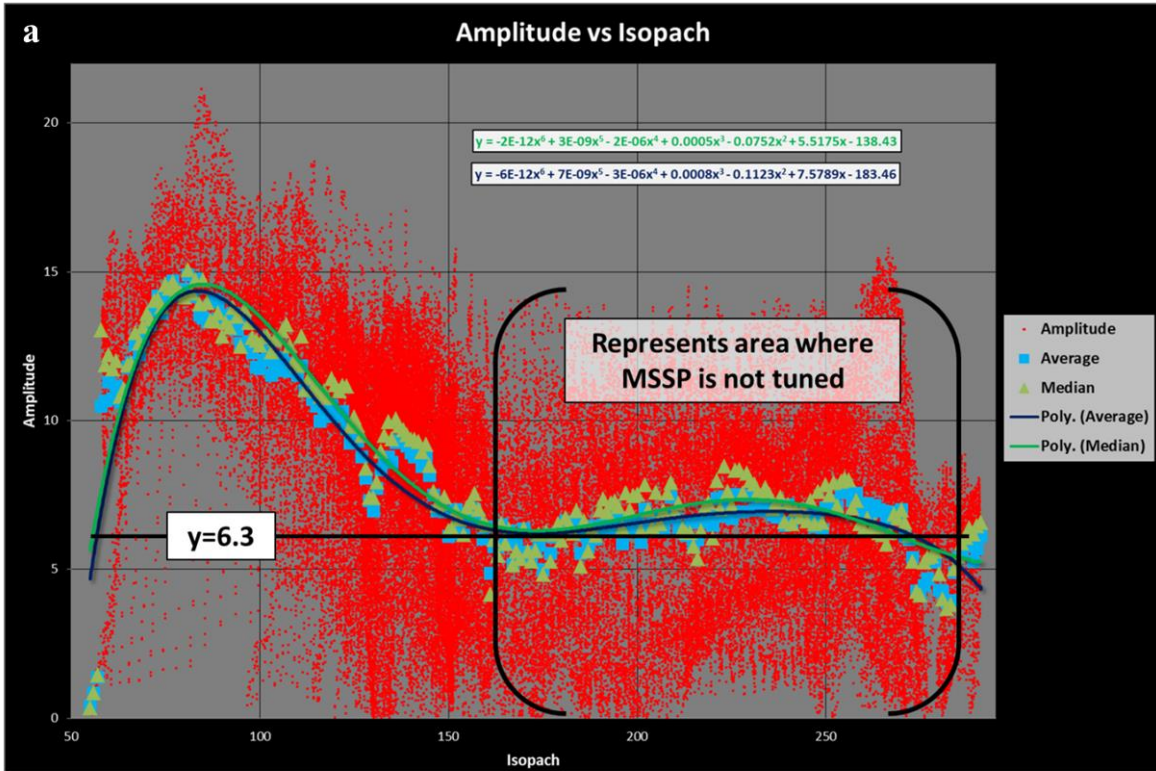


Figure C 1: LCB amplitude map. Enhanced amplitudes occur when the Mississippian thickness approaches 90 ft.

To accomplish this a first cross plot was created from the geostatistically generated isopach map and instantaneous amplitude to see if there is an enhanced amplitude response 50% greater than the base line amplitude (Figure C 2a). The correlation has a striking resemblance to that observed in the wedge model. Scatter in the data represent the variability in the reservoir that may display unique characteristics. This is the information that should be highlighted. However it is over printed by tuning (and unbalanced fold). To correct this, it was assumed that the mean amplitude response for the top of the Mississippian is approximately 6.3 (Figure C 2b). This base line is used to detune the data. The center of the of the point cloud was calculated using a polynomial equation. All points are then collapsed to the mean response while preserving scatter (Figure C 2c). As a result the tuned response is removed making a relative amplitude map which may show lateral characteristics of the reservoir. The concept of detuning data is beneficial for showing the relative spatial variation in amplitude (Figure C 3). However, in this attempt there is still the underlying problem of unregularized fold. If the effects of fold can be balanced, the detuned amplitude map could be interpreted with high confidence.



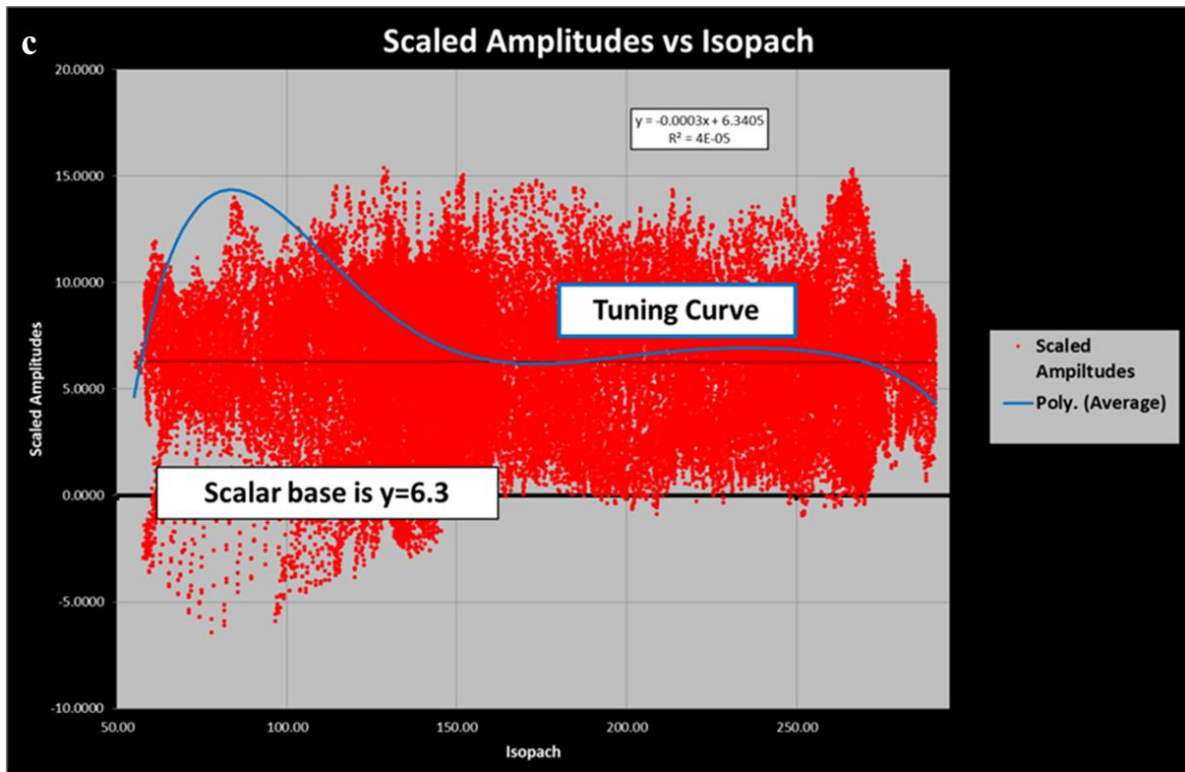


Figure C 2: Cross plot isopach and amplitude (a) Tuned, (b) Detuned method and (c) Detuned model.

Cross plot was created by comparing the geostatistically generated isopach and instantaneous amplitude grid. (a) The correlation has a striking resemblance the wedge model. (b) Baseline amplitude is 6.3, which is used to collapse the tuned response (c) creating an detuned model

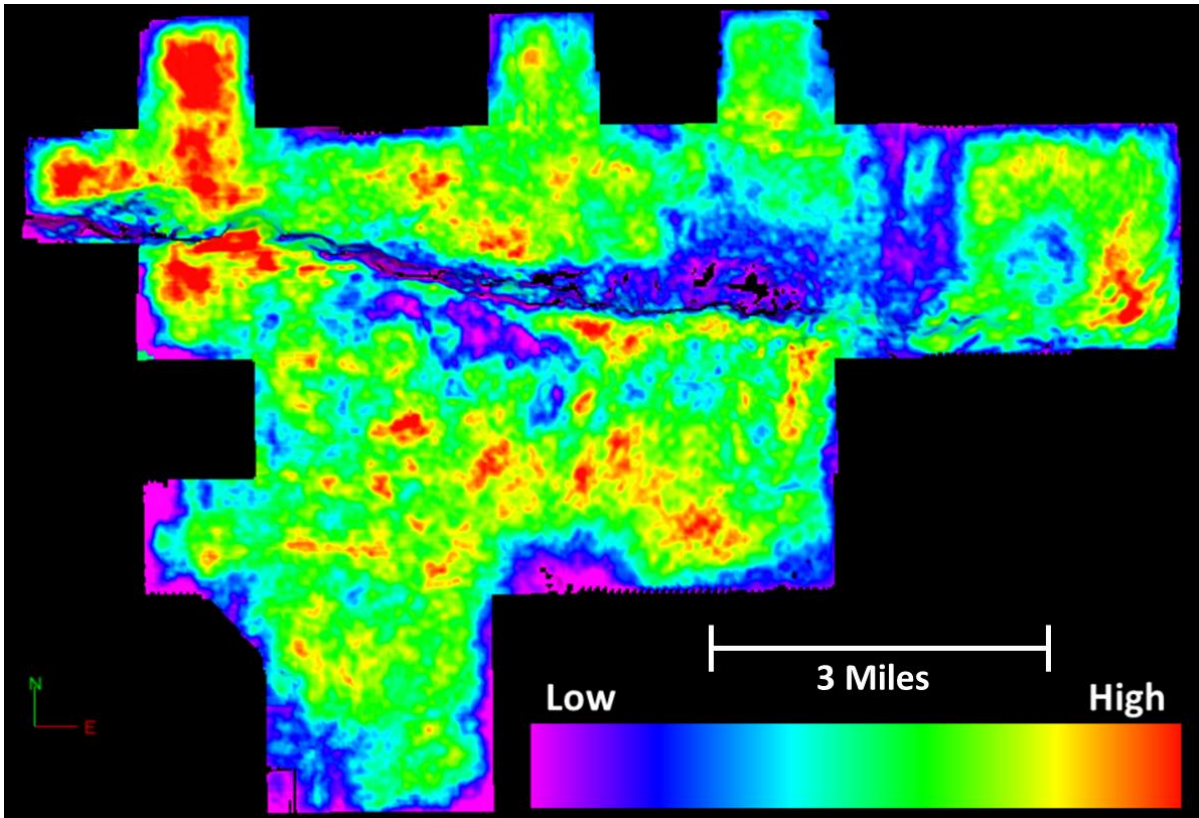


Figure C 3: Using the polynomial function, the amplitudes were detuned. The detuned amplitudes could reveal unique characteristics of the formation, however, they are still over printed by unregularized fold.



## APPENDIX D

### MCMURTRY 1-22H VALIDATION

Models are simplified representations of a system intended to promote understanding of the real system. They are built to understand a problem and to investigate possible solutions. To determine whether a model is correct or incorrect is a matter of judgment by the interpreter. While no model is absolutely correct, all models can be helpful by increasing our understanding of the system. As such, the fracture prediction algorithm is a model. The model had a good correlation when compared to the McMurtry 1-21H well (Figure 47). An additional FMI log was acquired in the McMurtry 1-22H. The correlation between the model and measured values was not apparent using the vertical or dip projected methods (Figure D 1; Figure D 2).

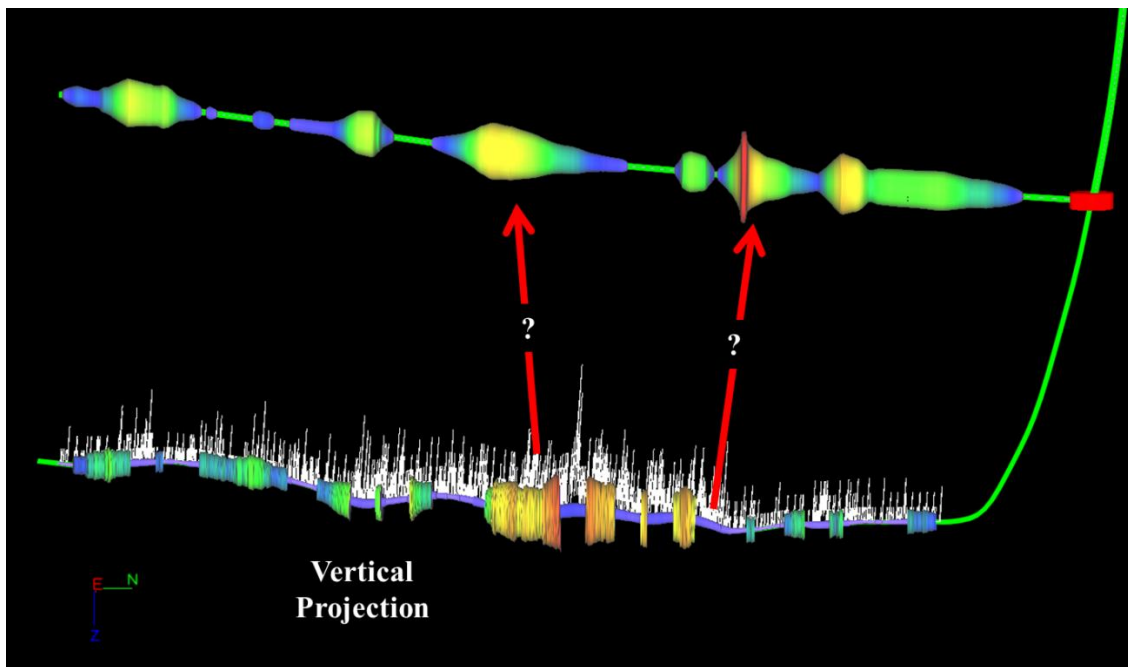


Figure D 1: McMurtry 1-22H fracture density comparison: along-trajectory. Observed fracture density is posted along the wellbore. Predicted fracture density is posted along the Mississippian Top surface. Colors represent fracture density with red and blue respectively implying higher and lower. Mississippian top geometry is from cokriging (Figure 12b). Projection direction of fractures from well-path to Mississippian top is vertical.

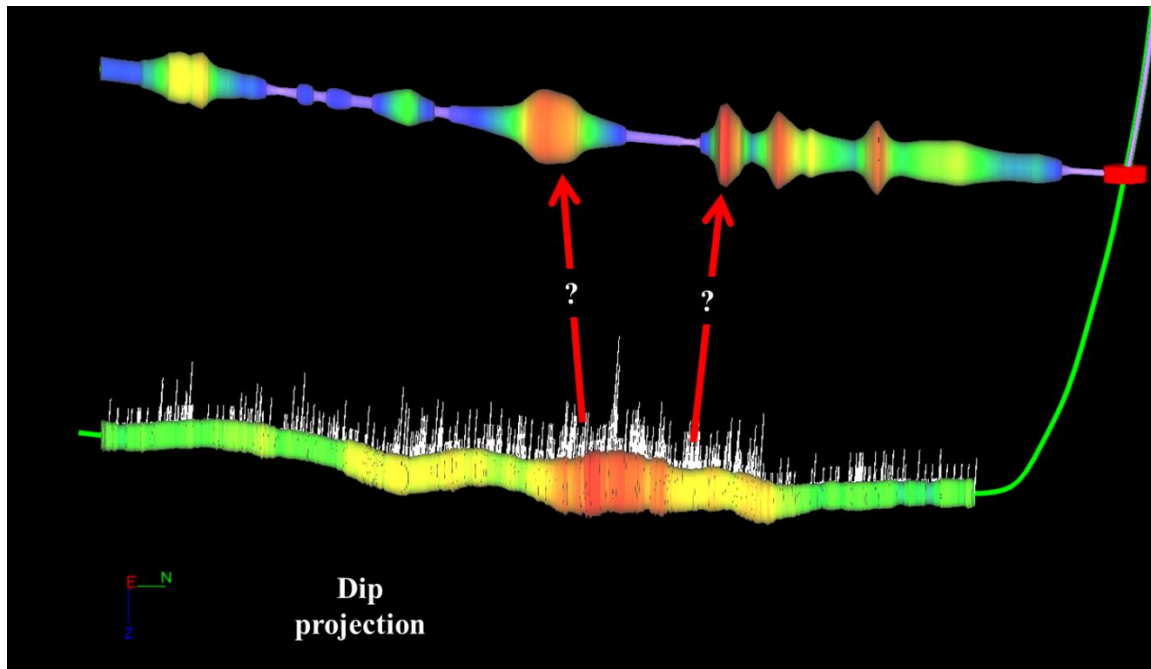


Figure D 2: McMurtry 1-22H fracture density re-comparison: along-trajectory. Same as Figure G2 with projection direction of fractures from well-path to Mississippian top being along-dip.

VITA

Robert Holman

Candidate for the Degree of

Master of Science

Thesis: SEISMIC CHARACTERIZATION OF FRACTURED ROCK FABRIC: MISSISSIPPIAN  
LIMESTONE, PAYNE COUNTY OKLAHOMA

Major Field: Geology

Biographical:

Education:

Completed the requirements for the Master of Science in Geology at Oklahoma State University,  
Stillwater, Oklahoma in December 2014

Completed the requirements for the Bachelor of Science in Geology at Brigham Young  
University- Idaho, Rexburg, Idaho in July 2011

Experience:

Chesapeake Energy, 3 years, Geophysical Technician